Single-Domain Antibodies as Tools to Perturb and Study RNA Viruses

Leo Hanke

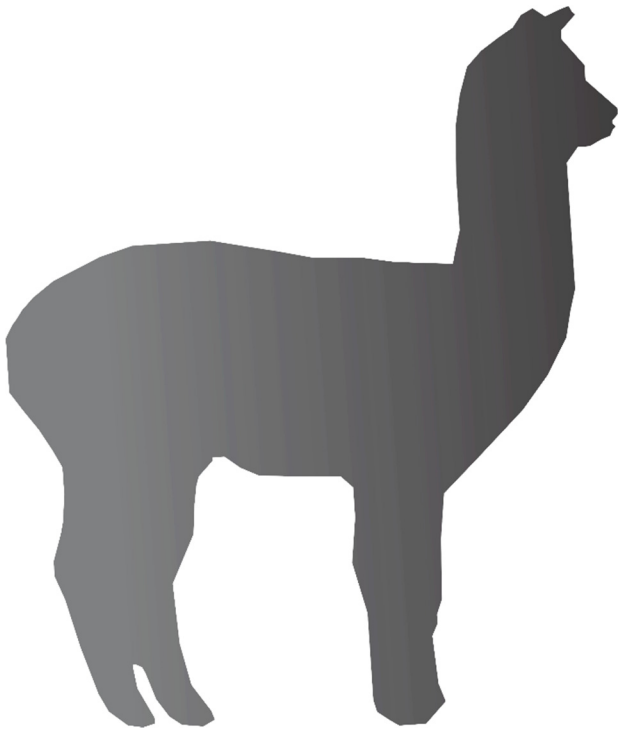

Single-Domain Antibodies as Tools to Perturb and Study RNA Viruses

Leo Hanke

Single-Domain Antibodies as Tools to Perturb and Study RNA Viruses

Single-Domain Antistoffen als Hulpmiddel bij de Bestudering van RNA Virussen

(met een samenvatting in het Nederlands)

Proefschrift

ter verkrijging van de graad van doctor aan de Universiteit Utrecht op gezag van de rector magnificus, prof.dr. G.J. van der Zwaan, ingevolge het besluit van het college voor promoties in het openbaar te verdedigen op maandag 24 april 2017 des middags te 12.45 uur

door

Leo Paul Hartmut Hanke

geboren op 16 oktober 1985
te Göttingen

Promotoren: Prof. dr. E.J.H.J Wiertz
Prof. dr. H.L. Ploegh

Other committee members:

Prof.dr. M.M. Maurice

Dr. T.R. Brummelkamp

Prof.dr. J. Borst

Prof.dr. J.A.G. van Strijp

Prof.dr. F.J.M. van Kuppeveld

The research described in this thesis was conducted at the Whitehead Institute for
Biomedical Research, Massachusetts Institute of Technology, Cambridge, MA, USA,
under the supervision of Prof. Dr. H.L. Ploegh.

Chapter 1

General Introduction

Viruses pose a significant burden on human health and contribute to serious morbidity in the human population (1). In contrast to other pathogens, viruses introduce only a small number of different proteins into the host organism and rely on a complex network of essential interactions with host proteins. Vaccines that elicit B-cell responses and yield circulating (neutralizing) antibodies have helped to eradicate dangerous viral pathogens, including smallpox and rinderpest. Other viruses are not so readily controlled by immunization. Alternative ways to interfere with their infection are therefore needed. To develop such approaches, a more detailed understanding of the viral life cycle is required, and potential vulnerabilities and drug target sites need to be identified and validated. Antibodies remain indispensable tools to probe, measure, or perturb viral proteins or associated biological pathways (2, 3). While full-sized antibodies are primarily limited to investigations of the extracellular space of living cells, the use of antibody fragments expressed in the cytosol extends their range to intracellular targets (4, 5). To accomplish this, full-sized antibodies are typically 'shrunk', in which their variable heavy and light domains (V_H and $V_{L,}$ respectively) are expressed as fusion proteins with a linker, and these fusions are referred to as single-chain variable fragments (scFvs). However, not all scFvs retain the specificity and affinity of the full-sized antibodies they are derived from. Also, scFvs are relatively unstable and have a tendency to form aggregates (6). Thus, despite much potential, the use of antibody fragments is complicated, which further makes it challenging to streamline their development and application.

In addition to traditional full-sized antibodies, the camelid immune system produces unusual antibodies composed of only heavy chains. The variable heavy chain fragment of a heavy chain-only antibody (VHH) is a single-domain that binds to its target with high specificity and affinity, comparable to a full-sized antibody (7). Therefore, VHHs represent an alternative to scFvs and can complement existing antibody applications. These fragments, also called nanobodies, are promising antiviral candidates and ideal tools to study virus replication and structure owing to a number of key features (8). Their small size (~15 kDa with physical dimensions of ~2x3.5 nm) allows VHHs to bind to epitopes not always accessible to conventional full-sized antibodies. Furthermore, due to an unusually long complementary determining region 3 (CDR3) loop, VHHs have a tendency to protrude into clefts created at protein domain-domain interfaces or at catalytic sites, and thus can recognize epitopes fundamentally different from those recognized by full-sized antibodies (9). As a natural single domain, VHHs are less hydrophobic and more soluble than scFvs that require the expression of a linker that connects the two domains which interact via hydrophobic residues. VHHs also often fold independently of intrachain disulfide bonds. These features allow for straightforward expression of VHHs in *E. coli* with high yields (up to 0.1 gram per liter of culture) as well as for expression in the cytosol of mammalian cells with full retention of their antigen binding

properties. VHHs are therefore ideal tools to perturb, neutralize, and study viruses both outside and inside living cells.

Viral proteins have evolved with optimized interactions to host proteins to efficiently exploit or counteract host-cell biosynthetic pathways and molecular machinery. A VHH that binds to a viral protein may occlude part of its surface and thus compromise the viral life cycle. VHHs generated against viral targets can be used to identify viral proteins and epitopes that are vulnerable to interference. Because of their ease of expression in target cells, including those infected with a virus, it is possible to evaluate the inhibitory properties of VHHs and collect evidence for the suitability of the viral antigen as an antiviral target. At the same time, the inhibited function will shed light on the precise role of the targeted viral protein, which will enhance our understanding of the viral life cycle. Such information can be leveraged for the generation of much needed novel antiviral therapeutics.

Figure 1 – Full-sized and single-domain antibody structures and fragments

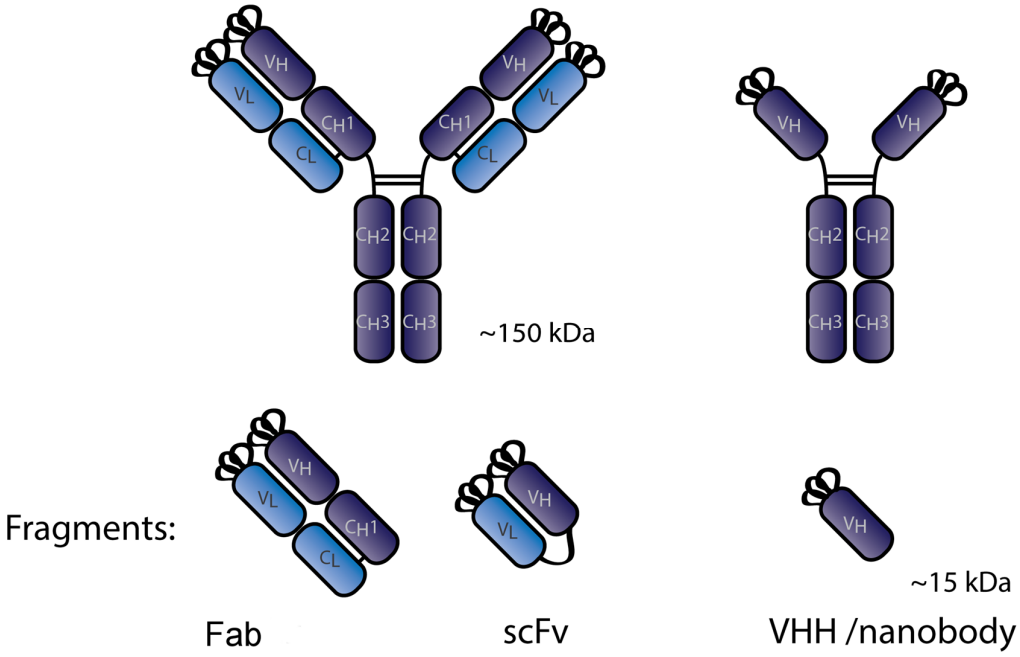

Generation and Functionalization of VHHs

Single-domain antibodies can be generated by immunization of a camelid (e.g. llama or alpaca) with (inactivated) virus or purified viral proteins of interest. The B cells of the immunized animal are then isolated and total RNA is extracted, reverse transcribed into cDNA, and cloned into plasmid vectors for an appropriate selection approach. The most common method of selecting for high-affinity VHHs is phage display, in which a library of phages that display

VHHs (and carry the corresponding VHH encoding sequence) are selected for on immobilized antigens (described in detail here (10)). Alternatively, functional screens based on phenotypes elicited by the (intra)cellular expression of the VHHs, such as survival of virus infection, can be used to identify antiviral VHH candidates. One recent example of this is described in detail in Chapter 5.

VHHs are versatile tools for research and clinical applications. Their relative ease of expression and stability also permits them to be modified for specific functions. The methods and techniques required to implement such modifications depend on the application. While genetic modifications can best be used for intracellularly expressed VHHs, purified VHHs also lend themselves to chemical or enzymatic modifications. Specifically, VHHs can be expressed intracellularly as genetic fusions with other proteins to elicit a specific function or modulate and direct the behavior of the VHH in a desired way. For example, VHHs can be fused to proteins with intracellular trafficking signals to direct them to different compartments within the cell, such as the nucleus, mitochondria, or lumen of the endoplasmic reticulum (ER) (11, 12). Other modifications include epitope tags that allow VHHs to be recognized by conventional antibodies or other VHHs for downstream applications, including flow cytometry-based quantification of VHH expression levels (13). VHHs can also be functionalized by fusing them to fluorescent proteins such as GFP or mCherry to observe their subcellular localization after target recognition in the course of a viral infection by fluorescent microscopy (14). VHH-protein fusions have also been used to reduce the levels of the VHH target by equipping the VHH with an Fbox domain. This fusion tags the VHH-antigen complex for proteasomal degradation (15). Genetically fused VHH homo- or hetero-dimers, connected via a serine/glycine linker, may be used to bring the two targeted moieties in close proximity to each other.

VHHs produced recombinantly in bacteria and used in extracellular applications similar to those of full-sized antibodies such as viral neutralization can likewise be genetically modified. Attractive fusions for such applications include the incorporation of an Fc region of conventional antibodies to enable antibody-like effector functions (16), or the inclusion of a toxin such as exotoxin A to specifically kill cells that express the target protein (17). Beyond genetic fusions, purified VHHs lend themselves to chemical or enzymatic modification. One attractive way to enzymatically modify VHHs is the use of sortase. The transpeptidase activity of sortase A allows it to modify any protein equipped with a sortase A recognition motif (LPETG) via direct covalent conjugation of a functionalizing element. Such an element could include a fluorophore for imaging, an epitope tag such as biotin for biochemical applications, or other proteins such as separately produced Fc fragments. The use of sortase in combination with click-chemistry even permits C-to-C terminal or N-to-N terminal fusion, for example to

generate VHH dimers (18). VHHs that are injected into the bloodstream are often rapidly cleared because of their small size. The use of a VHH dimer can effectively increase their time in circulation. Beside homodimers that remain longer in circulation just because of their increased size, VHH heterodimers whereby one VHH targets serum albumin have also been shown to significantly extend circulatory half-life (19). Homodimers expressed as mono-bivalent fusion variants targeting viral moieties have also been shown to significantly improve neutralization of the virus targeted (20, 21). The observed increase in neutralizing potency could be the result of increased avidity or of functional consequences, such as virion aggregation.

Extracellular Antiviral Applications of VHHs

Antibodies are critical components of the adaptive immune response and protect organisms from invading pathogens, including viruses. Host B cells produce antibodies upon exposure to antigens from the external environment ('non-self'). The B-cell response is a key element to clear infections or protect organisms from invading pathogens. This latter principle is extensively exploited in the clinic by vaccinations that render the host immune to future pathogenic exposures by inducing the production of antibodies that directly neutralize their targets. These neutralizing antibodies either cause virion aggregation or prevent their viral targets from binding to host cell receptors. Antibodies that neutralize viruses may also block internalization or uncoating of viral genomes. Alternatively, to clear established infections, antibodies function by stimulating and activating other parts of the immune system. The constant (C-terminal) region of an antibody mediates such effector functions, which include phagocyte recruitment, degranulation of neutrophils, and cytokine release by natural killer cells (22). Apart from vaccines that stimulate endogenous immune responses that result in long-lasting immunity, passive immunotherapy with monoclonal antibodies (mAb) can be an effective measure against acute diseases and be used for post-exposure prophylaxis. VHHs are well suited for this latter approach.

Since the discovery of single-domain antibodies in camelids, a sizable number of VHHs against a diverse set of viral targets have been developed (reviewed by Vanlandschot et al. (23)), and the number of targeted viruses and viral proteins continues to increase. The majority of antiviral VHHs target virion surface-exposed proteins that facilitate attachment to host cells and are often also the targets of neutralizing antibodies. Thus, VHHs can exhibit neutralizing activity, and have the potential to serve as therapeutic agents for passive immunization, as they lack an Fc region that may be recognized by the human immune system.VHHs in contrast show high homology to human V_H domains (24). However, to minimize immunogenicity for clinical

applications, VHHs can be humanized through introduction of only minor changes to the framework regions (25).

To date, VHHs have been generated that target rabies virus (21, 26), influenza A virus (IAV) (14, 27–31), hepatitis B virus (HBV) (12), herpes simplex virus (HSV) (17), human immunodeficiency virus (HIV) (32, 33), porcine reproductive and respiratory syndrome virus (PRRSV) (34, 35), respiratory syncytial (RSV) (30), poliovirus, and norovirus (36–39). VHHs represent a valuable addition to existing conventional antibodies for both neutralization and diagnostic purposes because of their ability to target distinct epitopes. Regions on viral surface proteins that are sterically inaccessible to conventional antibodies, including those that are involved in subunit-subunit interactions and hence may be more conserved, may still be accessible to VHHs, and thus represent especially interesting targets for VHH-based interventions. A good example of this is an HIV-1 gp120-specific VHH that neutralizes 96% of tested HIV-1 stains (33). Its potency was ascribed to its ability to bind deeply into the CD4 binding pocket of gp120 in a manner not possible for a full-sized antibodies or Fab fragments derived from it. Similarly, an IAV neuraminidase (NA)-specific VHH has been generated that binds to 8 out of 9 NA subtypes (40). VHHs with such broad neutralizing activity are not only promising for therapeutic applications, but may also help identify conserved epitopes. Identification of conserved epitopes and vulnerabilities can be important milestones to direct the production of therapeutic agents such as small molecule inhibitors.

Table 1 - List of antiviral VHHs

Virus	**Target**
Dengue virus (DENV)	NSI (41)
Food and mouth disease virus (FMDV)	Serotyp O (42)
Hantavirus	Nucleoprotein (43)
Hepatiitis B virus	HBcAg (44)
Hepatitis C virus	NS5B (45), helicase (46), protease (47)
Human immunodeficiency virus (HIV)	CXCR4 (48), gp120 (49), gp41 (32)
Herpes simplex virus 2 (HSV 2)	Glycoprotein D (17)
Influenza A virus (IAV)	M2 (28), NA (27), HA (31, 50), NP (14, 51)
Norovirus	P domain of Capsid protein (39)
Poliovirus	Capsid (36, 52, 53)
Porcine retrovirus (PERV)	p15 (54)
Porcine reproductive and respiratory syndrome (PRRSV)	Nsp4 (35) , Nsp9 (34)
Rabies virus	G protein (21)
Rotavirus	VP6 (16, 55–58)
Respiratory synsychal virus (RSV)	RSV fusion protein F (30, 59)
Vesicular stomatitis virus (VSV)	N protein (60)

For IAV, VHHs against all surface exposed proteins, hemagglutinin (HA), NA, and the ion channel M2 have been developed, and for each of these targets there exists at least one

neutralizing VHH candidate (20, 27, 28). These neutralizing VHHs have been administered to mice intranasally for those that target HA or NA, and intraperitoneally in the case of the M2-specific VHH, which protected them from IAV infection. Neutralizing VHHs have also been developed for rabies virus, which can be lethal in untreated infected un-vaccinated individuals. Apart from prophylactic immunization, the only effective countermeasure for rabies virus is post-exposure prophylaxis. This post-exposure approach utilizes both active and passive immunization and typically consists of an active vaccine together with serum-derived immunoglobulins as the passive component. The neutralizing VHHs that target the rabies G protein are a potential alternative to -very costly- immunoglobulins. The rabies-specific VHH has been shown to act synergistically with an anti-rabies vaccine, and protects mice from a lethal challenge with rabies virus (26). Similarly, rotavirus-neutralizing VHHs have been generated that protect piglets from rotavirus-induced diarrhea (57). This protective effect could be enhanced by fusing the VHH to an Fc domain (16). Other VHHs that are not directly neutralizing can be modified and equipped with functional proteins such as toxins. For example, Geoghegan et al. fused Pseudomonas exotoxin A to a VHH specific for the glycoprotein D of herpes simplex virus. Although this VHH did not neutralize the virus itself, the fusion protein specifically and potently killed HSV-2-infected cells, and therefore limited the propagation of the virus (17).

Intracellular Antiviral Applications of VHHs

Antibodies bind their targets with high affinity and specificity and can occlude a protein surface, which can modulate or inhibit its function. It is attractive to make use of these unparalleled binding characteristics, not only in extracellular space, but also inside living cells to target, modulate, or perturb proteins at the posttranslational level. The introduction or delivery of full-sized antibodies into living cells remains the most challenging part of this concept, especially in the context of an organism. Early attempts at using intracellular antibodies were dependent on microinjection of monoclonal antibodies into cultured cells. Using this method, it was shown that antibodies specific for the vesicular stomatitis virus (VSV) nucleoprotein protected cells from infection, which demonstrated that viral replication was dependent on the availability of free nucleoprotein (61). Although tedious, these experiments clearly indicated the power of intracellular antibodies, both as inhibitors and as tools to help understand the functions and characteristics of the different viral proteins. Later, variable fragments of conventional antibodies, most successfully used as scFvs, were constitutively expressed in living cells. An ER-targeted scFv specific for the HIV-1 envelope glycoprotein gp160 blocked the processing of the protein, and thus impaired viral maturation (62). A similar concept was then used to target HIV-1 integrase and matrix protein with scFvs to inhibit viral infection (4, 63). These

results demonstrated that antibodies or their fragments could inhibit intracellular protein functions, including those of viral proteins. Furthermore, this work highlighted the possibility to direct the localization of intracellular antibodies to different cellular compartments: untagged to reside in the cystosol, KDEL sequence-equipped to translocate to the ER, or expressed with a nuclear localization sequence (NLS) for nuclear accumulation. Nevertheless, the use of intracellularly expressed scFvs is inherently limited by poor expression levels in the reducing conditions of the cytosol, and the expression profile must be empirically determined and optimized for each candidate.

The use of intracellular VHHs circumvents many of the limitations that hinder expression of full-sized antibodies and their fragments inside cells, while maintaining high specificity and affinity, thus giving intracellular VHHs an unmatched advantage. Specifically, the size, solubility, and better expression of VHHs in the reducing conditions of the cytosol contribute to that. Analogous to methods used for scFvs, VHHs can be fused to target peptides to direct them to subcellular compartments such as the nucleus or the ER. While there are still many obstacles to overcome to make use of intracellularly expressed VHHs in therapeutic applications, they remain valuable tools in the laboratory. With regards to viral research, intracellularly expressed VHHs can help to identify new viral vulnerabilities, validate drug target sites, and determine the biological function of the viral protein or epitope recognized. Intracellularly expressed VHHs represent an alternative/addition to mutational analysis, which can disrupt the overall structure of larger protein complexes, and therefore may not always allow unambiguous conclusions of the functional contribution of the specific protein or (sub) domain.

Viral protein surfaces have evolved to optimally interact with specific host structures (lipids, carbohydrates, proteins, nucleic acids, etc.). Because of their complex and evolutionarily sculpted interactions, viral proteins are ideal targets for intervention using small antibodies. For instance, if a functionally important surface is occluded by a VHH, its binding is likely to have functional consequences on the life cycle of the virus. In contrast to viral proteins exposed on the surface of mature virions that are typically under strong selective pressure exerted by extracellular neutralizing antibodies, the intracellularly disposed viral proteins are much more conserved. An example of this is evident from a comparison of the amino acid sequences of IAV HA and nucleoprotein (NP). Surface-exposed HA is the major target of antibody-facilitated neutralization, and accordingly, exhibits a high degree of antigenic variation (64). In contrast, IAV NP is processed intracellularly and presented on major histocompatibility complex type I (MHCI) molecules for recognition by $CD8^+$ T cells and exhibits far less variability (Fig 1). While anti-IAV antibodies exhibit the highest neutralizing activity against the strain that elicited the antibodies, $CD8^+$ T cells specific for NP epitopes can limit infection

across different strains of IAV (65). Why these $CD8^+$ T cells do not readily yield mutant NP escape variants remains unknown. Perhaps inherent functional and structural constraints of NP limit its variability (66). Nevertheless, it makes NP and other intracellularly disposed viral proteins attractive candidates for antiviral intervention with intracellular VHHs.

Although the general suitability of intracellular antibodies for viral inhibition was demonstrated long ago, few examples of intracellularly expressed antiviral VHHs have been described to date. One of the first reported intracellularly expressed VHHs targeted the p15 matrix protein of porcine retrovirus, which blocked viral production, indicating the efficacy of intracellular VHHs for antiviral approaches (54). More recently, intracellularly expressed VHHs that target porcine reproductive respiratory syndrome virus (PRRSV) non-structural proteins 4 and 9 were reported to inhibit viral replication in MARC-145 cells *in vitro* (34, 35). *In vivo* inhibition of viral replication by intracellular VHHs was first shown by Serruys et al. in a mouse model for hepatitis B virus (HBV) infection (12). These VHHs were specific for the HBV S domain (HBsAg) and were targeted to the ER lumen. Using a hydrodynamics-based delivery method for both HBV and the VHHs, the VHHs potently reduced viral titers in mice compared to the HBV-only treated group.

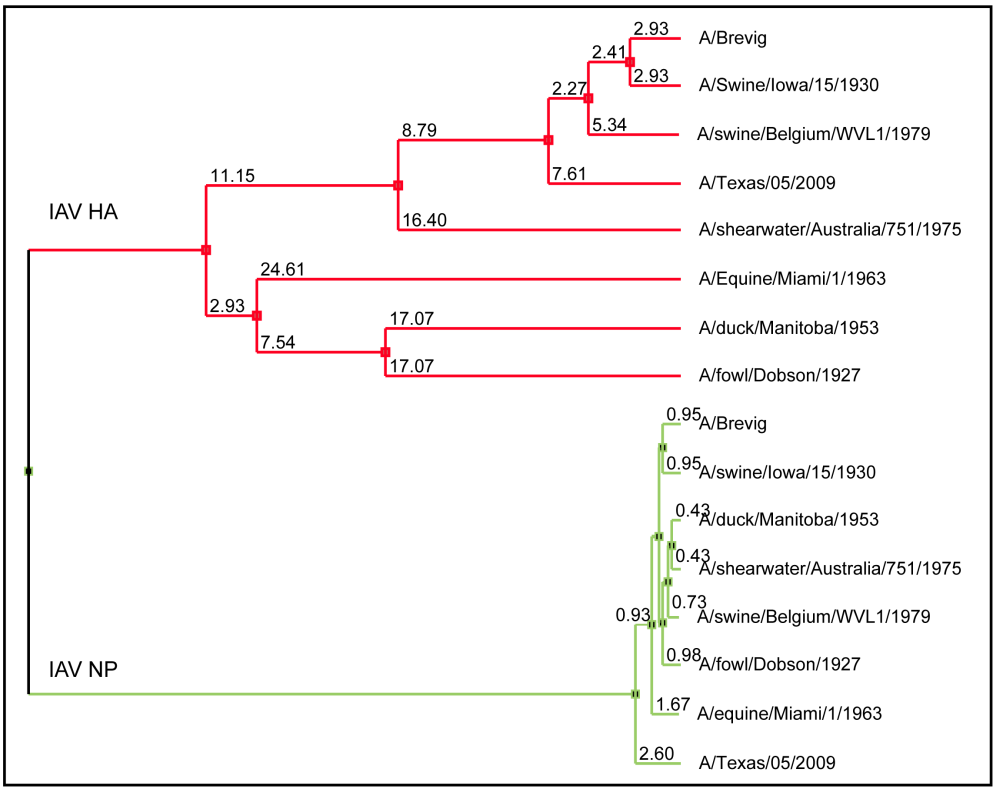

Figure 2 | Phylogenetic tree of hemagglutinin (HA) and nucleoprotein (NP) of influenza A virus (IAV). Eight IAV strains with the greatest diversity in their NP sequences were selected and are displayed. Note the disparity in the depth of the trees' branch points for HA and NP.

VHHs as Tools in Structural Studies

Determining the molecular structure of proteins and protein complexes is often essential to understand their biological functions. The main obstacle in X-ray crystallography, which allows for the determination of structures at atomic resolution, is the generation of diffraction-quality protein crystals (67). Many advances in structural biology were made possible or accelerated by using antibody fragments that act as crystallization chaperones. Specifically, antibody fragments can aid in crystal nucleation, promote co-complex dimer formation, and accelerate crystal growth (68). IAV N9 NA, for example, could only be crystallized in complex with Fab fragments of a monoclonal antibody (69). Similarly, Fab fragments have facilitated the crystallization of the HIV p24 capsid protein and the hepatitis B virus capsid (70–72). The molecular structure of a Fab fragment or VHH in complex with its target protein not only reveals the detailed binding site, but - together with functional data - may also uncover their mechanisms of action if they have functional (inhibitory or stimulatory) properties, and may help to determine the structure-function relationship of the targeted protein domain or surface (10, 73–76). There are many conceivable ways by which a VHH could interfere with the normal function of its target protein. In addition to direct occlusion of the binding site for an essential cofactor, VHHs have been observed to trap their targets in distinct conformations or alter their conformations upon binding. A prominent example of the first scenario is the structure of a G-protein-coupled receptor (GPCR) trapped in an active state by VHH binding (77). Similar mechanisms may apply to viral targets of VHHs. Strauss et al. provided examples of both concepts by high-resolution cryo-electron microscopy (cryo-EM) reconstructions of five neutralizing VHHs bound to the poliovirus capsid (36). While all five VHHs were shown to bind to the receptor binding site, one VHH resulted in extensive changes to the capsid structure. In addition to locking or inducing a specific target protein conformation, VHHs may help to identify clefts in the target protein that are bound by the long CDR3 loop, which may also be good binding clefts for small molecule inhibitors. Therefore, VHHs are valuable tools to aid crystallization, given their relative ease of expression, solubility, and thermal stability. Additionally, the structural data and defined binding sites gained from such studies may provide secondary information regarding the structure-function relationship of the targeted epitope, which may further aid in the understanding of the virus under investigation and could be leveraged for VHH-enabled small molecule drug discovery.

Thesis Abstract

In this thesis, I describe the generation and characterization of alpaca-derived, antiviral, single-domain antibody fragments (VHHs). The antiviral targets of the described VHHs are the nuclear proteins of influenza A virus (IAV) and vesicular stomatitis virus (VSV), and protect cells from infection when expressed in the cytosol. IAV is a segmented, negative-strand RNA virus and is the current focus of antiviral strategies because it causes reoccurring epidemics and pandemics in the human population. A broadly active, antiviral measure with high efficacy is therefore urgently needed. In contrast, VSV is a non-segmented, negative-strand RNA virus that is typically asymptomatic in humans, but is extensively studied as a prototypic non-segmented RNA virus. Data presented herein for both IAV and VSV highlight the advantages of VHHs as neutralizing agents and as tools to study viral structure and replication. I also demonstrate a robust cycle that: first, enables the production and selection of VHHs that impede viral growth; second, that the epitope recognized can be accurately defined in structural terms; and third, that the combination of both can explain the functional relevance of the targeted viral structure.

References

1. **Howard CR**, **Fletcher NF**. 2012. Emerging virus diseases: can we ever expect the unexpected? Emerg Microbes Infect **1**:e46.

2. **Lawson ADG**. 2012. Antibody-enabled small-molecule drug discovery. Nat Rev Drug Discov **11**:519–525.

3. **Marsden CJ**, **Eckersley S**, **Hebditch M**, **Kvist AJ**, **Milner R**, **Mitchell D**, **Warwicker J**, **Marley AE**. 2014. The Use of Antibodies in Small-Molecule Drug Discovery. J Biomol Screen **19**:829–838.

4. **Levy-Mintz P**, **Duan L**, **Zhang H**, **Hu B**, **Dornadula G**, **Zhu M**, **Kulkosky J**, **Bizub-Bender D**, **Skalka a M**, **Pomerantz RJ**. 1996. Intracellular expression of single-chain variable fragments to inhibit early stages of the viral life cycle by targeting human immunodeficiency virus type 1 integrase. J Virol **70**:8821–32.

5. **Lo ASY**, **Zhu Q**, **Marasco WA**. 2008. Intracellular antibodies (intrabodies) and their therapeutic potential. Handb Exp Pharmacol **181**:343–373.

6. **Wörn A**, **Maur AA Der**, **Honegger A**, **Barberis A**, **Plückthun A**, **Escher D**. 2000. PROTEIN CHEMISTRY AND STRUCTURE : Correlation between in Vitro Stability and in Vivo Performance of Anti-GCN4 Intrabodies as Cytoplasmic Inhibitors Correlation between in Vitro Stability and in Vivo Performance of Anti-GCN4 Intrabodies as Cytoplasmic Inhi **275**:2795–2803.

7. **Harmsen MM**, **De Haard HJ**. 2007. Properties, production, and applications of camelid single-domain antibody fragments. Appl Microbiol Biotechnol **77**:13–22.

8. **Wesolowski J**, **Alzogaray V**, **Reyelt J**, **Unger M**, **Juarez K**, **Urrutia M**, **Cauerhff A**, **Danquah W**, **Rissiek B**, **Scheuplein F**, **Schwarz N**, **Adriouch S**, **Boyer O**, **Seman M**, **Licea A**, **Serreze D V.**, **Goldbaum FA**, **Haag F**, **Koch-Nolte F**. 2009. Single domain antibodies: Promising experimental and therapeutic tools in infection and immunity.

Med Microbiol Immunol **198**:157–174.

9. **De Genst E**, **Silence K**, **Decanniere K**, **Conrath K**, **Loris R**, **Kinne J**, **Muyldermans S**, **Wyns L**. 2006. Molecular basis for the preferential cleft recognition by dromedary heavy-chain antibodies. Proc Natl Acad Sci U S A **103**:4586–91.

10. **Sosa BA**, **Demircioglu FE**, **Chen JZ**, **Ingram J**, **Ploegh HL**, **Schwartz TU**. 2014. How lamina-associated polypeptide 1 (LAP1) activates Torsin. Elife **3**:e03239.

11. **Van Den Abbeele A**, **De Clercq S**, **De Ganck A**, **De Corte V**, **Van Loo B**, **Soror SH**, **Srinivasan V**, **Steyaert J**, **Vandekerckhove J**, **Gettemans J**. 2010. A llama-derived gelsolin single-domain antibody blocks gelsolin-G-actin interaction. Cell Mol Life Sci **67**:1519–1535.

12. **Serruys B**, **van Houtte F**, **Verbrugghe P**, **Leroux-Roels G**, **Vanlandschoot P**. 2009. Llama-derived single-domain intrabodies inhibit secretion of hepatitis B virions in mice. Hepatology **49**:39–49.

13. **Schmidt FI**, **Lu A**, **Chen JW**, **Ruan J**, **Tang C**, **Wu H**, **Ploegh HL**. 2016. A single domain antibody fragment that recognizes the adaptor ASC defines the role of ASC domains in inflammasome assembly. J Exp Med **213**:771–90.

14. **Ashour J**, **Schmidt FI**, **Hanke L**, **Cragnolini J**, **Cavallari M**, **Altenburg A**, **Brewer R**, **Ingram J**, **Shoemaker C**, **Ploegh HL**. 2015. Intracellular Expression of Camelid Single-Domain Antibodies Specific for Influenza Virus Nucleoprotein Uncovers Distinct Features of Its Nuclear Localization. J Virol **89**:2792–2800.

15. **Caussinus E**, **Kanca O**, **Affolter M**. 2011. Fluorescent fusion protein knockout mediated by anti-GFP nanobody. Nat Struct Mol Biol **19**:117–121.

16. **Günaydın G**, **Yu S**, **Gräslund T**, **Hammarström L**, **Marcotte H**. 2016. Fusion of the mouse IgG1 Fc domain to the VHH fragment (ARP1) enhances protection in a mouse model of rotavirus. Sci Rep **6**:30171.

17. **Geoghegan EM**, **Zhang H**, **Desai PJ**, **Biragyn A**, **Markham RB**. 2015. Antiviral activity of a single-domain antibody immunotoxin binding to glycoprotein D of herpes simplex virus 2. Antimicrob Agents Chemother **59**:527–535.

18. **Witte MD**, **Cragnolini JJ**, **Dougan SK**, **Yoder NC**, **Popp MW**, **Ploegh HL**. 2012. Preparation of unnatural N-to-N and C-to-C protein fusions. Proc Natl Acad Sci U S A **109**:11993–8.

19. **Coppieters K**, **Dreier T**, **Silence K**, **de Haard H**, **Lauwereys M**, **Casteels P**, **Beirnaert E**, **Jonckheere H**, **Van de Wiele C**, **Staelens L**, **Hostens J**, **Revets H**, **Remaut E**, **Elewaut D**, **Rottiers P**. 2006. Formatted anti-tumor necrosis factor alpha VHH proteins derived from camelids show superior potency and targeting to inflamed joints in a murine model of collagen-induced arthritis. Arthritis Rheum **54**:1856–66.

20. **Ibañez LI**, **De Filette M**, **Hultberg A**, **Verrips T**, **Temperton N**, **Weiss RA**, **Vandevelde W**, **Schepens B**, **Vanlandschoot P**, **Saelens X**. 2011. Nanobodies with in vitro neutralizing activity protect mice against H5N1 influenza virus infection. J Infect Dis **203**:1063–1072.

21. **Terryn S**, **Francart A**, **Lamoral S**, **Hultberg A**, **Rommelaere H**, **Wittelsberger A**, **Callewaert F**, **Stohr T**, **Meerschaert K**, **Ottevaere I**, **Stortelers C**, **Vanlandschoot P**, **Kalai M**, **Van Gucht S**. 2014. Protective effect of different anti-rabies virus VHH constructs against rabies disease in mice. PLoS One **9**.

22. **Jiang X-R**, **Song A**, **Bergelson S**, **Arroll T**, **Parekh B**, **May K**, **Chung S**, **Strouse R**, **Mire-Sluis A**, **Schenerman M**. 2011. Advances in the assessment and control of the

effector functions of therapeutic antibodies. Nat Rev Drug Discov **10**:101–111.

23. **Vanlandschoot P**, **Stortelers C**, **Beirnaert E**, **Ibañez LI**, **Schepens B**, **Depla E**, **Saelens X**. 2011. Nanobodies: New ammunition to battle viruses. Antiviral Res **92**:389–407.

24. **Muyldermans S**, **Cambillau C**, **Wyns L**. 2001. Recognition of antigens by single-domain antibody fragments: The superfluous luxury of paired domains. Trends Biochem Sci **26**:230–235.

25. **Vincke C**, **Loris R**, **Saerens D**, **Martinez-Rodriguez S**, **Muyldermans S**, **Conrath K**. 2009. General strategy to humanize a camelid single-domain antibody and identification of a universal humanized nanobody scaffold. J Biol Chem **284**:3273–3284.

26. **Terryn S**, **Francart A**, **Rommelaere H**, **Stortelers C**, **Van Gucht S**. 2016. Post-exposure Treatment with Anti-rabies VHH and Vaccine Significantly Improves Protection of Mice from Lethal Rabies Infection. PLoS Negl Trop Dis **10**:e0004902.

27. **Cardoso FM**, **Ibañez LI**, **Van den Hoecke S**, **De Baets S**, **Smet A**, **Roose K**, **Schepens B**, **Descamps FJ**, **Fiers W**, **Muyldermans S**, **Depicker A**, **Saelens X**. 2014. Single-domain antibodies targeting neuraminidase protect against an H5N1 influenza virus challenge. J Virol **88**:8278–96.

28. **Wei G**, **Meng W**, **Guo H**, **Pan W**, **Liu J**, **Peng T**, **Chen L**, **Chen CY**. 2011. Potent neutralization of influenza a virus by a single-domain antibody blocking M2 ion channel protein. PLoS One **6**:e28309.

29. **Hufton SE**, **Risley P**, **Ball CR**, **Major D**, **Engelhardt OG**, **Poole S**. 2014. The breadth of cross sub-type neutralisation activity of a single domain antibody to influenza hemagglutinin can be increased by antibody valency. PLoS One **9**:e103294.

30. **Hultberg A**, **Temperton NJ**, **Rosseels V**, **Koenders M**, **Gonzalez-Pajuelo M**, **Schepens B**, **Ibañez LI**, **Vanlandschoot P**, **Schillemans J**, **Saunders M**, **Weiss RA**, **Saelens X**, **Melero JA**, **Verrips CT**, **van Gucht S**, **de Haard HJ**. 2011. Llama-derived single domain antibodies to build multivalent, superpotent and broadened neutralizing anti-viral molecules. PLoS One **6**:1–12.

31. **Ibañez LI**, **De Filette M**, **Hultberg A**, **Verrips T**, **Temperton N**, **Weiss RA**, **Vandevelde W**, **Schepens B**, **Vanlandschoot P**, **Saelens X**. 2011. Nanobodies with in vitro neutralizing activity protect mice against H5N1 influenza virus infection. J Infect Dis **203**:1063–1072.

32. **Lutje Hulsik D**, **Liu Y ying**, **Strokappe NM**, **Battella S**, **El Khattabi M**, **McCoy LE**, **Sabin C**, **Hinz A**, **Hock M**, **Macheboeuf P**, **Bonvin AMJJ**, **Langedijk JPM**, **Davis D**, **Forsman Quigley A**, **Aasa-Chapman MMI**, **Seaman MS**, **Ramos A**, **Poignard P**, **Favier A**, **Simorre JP**, **Weiss RA**, **Verrips CT**, **Weissenhorn W**, **Rutten L**. 2013. A gp41 MPER-specific Llama VHH Requires a Hydrophobic CDR3 for Neutralization but not for Antigen Recognition. PLoS Pathog **9**:20–23.

33. **McCoy LE**, **Quigley AF**, **Strokappe NM**, **Bulmer-Thomas B**, **Seaman MS**, **Mortier D**, **Rutten L**, **Chander N**, **Edwards CJ**, **Ketteler R**, **Davis D**, **Verrips T**, **Weiss RA**. 2012. Potent and broad neutralization of HIV-1 by a llama antibody elicited by immunization. J Exp Med **209**:1091–103.

34. **Liu H**, **Wang Y**, **Duan H**, **Zhang A**, **Liang C**, **Gao J**, **Zhang C**, **Huang B**, **Li Q**, **Li N**, **Xiao S**, **Zhou E-M**. 2015. An intracellularly expressed Nsp9-specific nanobody in MARC-145 cells inhibits porcine reproductive and respiratory syndrome virus replication. Vet Microbiol **181**:252–60.

35. **Liu H**, **Liang C**, **Duan H**, **Zhang X**, **Wang X**, **Xiao S**, **Zhou EM**. 2016. Intracellularly expressed nanobodies against non-structural protein 4 of porcine reproductive and respiratory syndrome virus inhibit virus replication. Biotechnol Lett **38**:1–8.

36. **Strauss M**, **Schotte L**, **Thys B**, **Filman DJ**, **Hogle JM**. 2016. Five of Five VHHs Neutralizing Poliovirus Bind the Receptor-Binding Site. J Virol **90**:3496–3505.

37. **Thys B**, **Schotte L**, **Muyldermans S**, **Wernery U**, **Hassanzadeh-Ghassabeh G**, **Rombaut B**. 2010. In vitro antiviral activity of single domain antibody fragments against poliovirus. Antiviral Res **87**:257–264.

38. **Schotte L**, **Thys B**, **Strauss M**, **Filman DJ**, **Rombaut B**, **Hogle JM**. 2015. Characterization of poliovirus neutralization escape mutants of single-domain antibody fragments (VHHs). Antimicrob Agents Chemother **59**:4695–4706.

39. **Koromyslova AD**, **Hansman GS**. 2015. Nanobody binding to a conserved epitope promotes norovirus particle disassembly. J Virol **89**:2718–30.

40. **Harmsen M**, **Blokker J**, **Pritz-Verschuren S**, **Bartelink W**, **van der Burg H**, **Koch G**. 2013. Isolation of Panels of Llama Single-Domain Antibody Fragments Binding All Nine Neuraminidase Subtypes of Influenza A Virus. Antibodies **2**:168–192.

41. **Fatima A**, **Wang H**, **Kang K**, **Xia L**, **Wang Y**, **Ye W**, **Wang J**, **Wang X**. 2014. Development of VHH antibodies against dengue virus type 2 NS1 and comparison with monoclonal antibodies for use in immunological diagnosis. PLoS One **9**:1–12.

42. **Wang D**, **Yang S**, **Yin S**, **Shang Y**, **Du P**, **Guo J**, **He J**, **Cai J**, **Liu X**. 2015. Characterization of single-domain antibodies against Foot and Mouth Disease Virus (FMDV) serotype O from a camelid and imaging of FMDV in baby hamster kidney-21 cells with single-domain antibody-quantum dots probes. BMC Vet Res **11**:120.

43. **Pereira SS**, **Moreira-Dill LS**, **Morais MSS**, **Prado NDR**, **Barros ML**, **Koishi AC**, **Mazarrotto GACA**, **Gonc¸alves GM**, **Zuliani JP**, **Calderon LA**, **Soares AM**, **Pereira Da Silva LH**, **Duarte Dos Santos CN**, **Fernandes CFC**, **Stabeli RG**. 2014. Novel camelid antibody fragments targeting recombinant nucleoprotein of Araucaria hantavirus: A prototype for an early diagnosis of hantavirus pulmonary syndrome. PLoS One **9**.

44. **Serruys B**, **Van Houtte F**, **Farhoudi-Moghadam A**, **Leroux-Roels G**, **Vanlandschoot P**. 2010. Production, characterization and in vitro testing of HBcAg-specific VHH intrabodies. J Gen Virol **91**:643–652.

45. **Thueng-in K**, **Thanongsaksrikul J**, **Srimanote P**, **Bangphoomi K**, **Poungpair O**, **Maneewatch S**, **Choowongkomon K**, **Chaicumpa W**. 2012. Cell Penetrable Humanized-VH/VHH That Inhibit RNA Dependent RNA Polymerase (NS5B) of HCV. PLoS One **7**.

46. **Phalaphol A**, **Thueng-in K**, **Thanongsaksrikul J**, **Poungpair O**, **Bangphoomi K**, **Sookrung N**, **Srimanote P**, **Chaicumpa W**. 2013. Humanized-VH/VHH that inhibit HCV replication by interfering with the virus helicase activity. J Virol Methods **194**:289–299.

47. **Jittavisutthikul S**, **Thanongsaksrikul J**, **Thueng-In K**, **Chulanetra M**, **Srimanote P**, **Seesuay W**, **Malik AA**, **Chaicumpa W**. 2015. Humanized-VHH transbodies that inhibit HCV protease and replication. Viruses **7**:2030–2056.

48. **Jähnichen S**, **Blanchetot C**, **Maussang D**, **Gonzalez-Pajuelo M**, **Chow KY**, **Bosch L**, **De Vrieze S**, **Serruys B**, **Ulrichts H**, **Vandevelde W**, **Saunders M**, **De Haard HJ**, **Schols D**, **Leurs R**, **Vanlandschoot P**, **Verrips T**, **Smit MJ**. 2010. CXCR4 nanobodies

(VHH-based single variable domains) potently inhibit chemotaxis and HIV-1 replication and mobilize stem cells. Proc Natl Acad Sci U S A **107**:20565–70.

49. **Forsman A**, **Beirnaert E**, **Aasa-Chapman MMI**, **Hoorelbeke B**, **Hijazi K**, **Koh W**, **Tack V**, **Szynol A**, **Kelly C**, **McKnight A**, **Verrips T**, **de Haard H**, **Weiss RA**. 2008. Llama antibody fragments with cross-subtype human immunodeficiency virus type 1 (HIV-1)-neutralizing properties and high affinity for HIV-1 gp120. J Virol **82**:12069–81.

50. **Gong X**, **Zhu M**, **Li G**, **Lu X**, **Wan Y**. 2016. Specific determination of influenza H7N2 virus based on biotinylated single-domain antibody from a phage-displayed library. Anal Biochem **500**:66–72.

51. **Schmidt FI**, **Hanke L**, **Morin B**, **Brewer R**, **Brusic V**, **Whelan SPJ**, **Ploegh HL**. 2016. Phenotypic lentivirus screens to identify functional single domain antibodies. Nat Microbiol **1**:16080.

52. **Thys B**, **Schotte L**, **Muyldermans S**, **Wernery U**, **Hassanzadeh-Ghassabeh G**, **Rombaut B**. 2010. In vitro antiviral activity of single domain antibody fragments against poliovirus. Antiviral Res **87**:257–264.

53. **Schotte L**, **Strauss M**, **Thys B**, **Halewyck H**, **Filman DJ**, **Bostina M**, **Hogle JM**, **Rombaut B**. 2014. Mechanism of action and capsid-stabilizing properties of VHHs with an in vitro antipolioviral activity. J Virol **88**:4403–13.

54. **Dekker S**, **Toussaint W**, **Panayotou G**, **de Wit T**, **Visser P**, **Grosveld F**, **Drabek D**. 2003. Intracellularly Expressed Single-Domain Antibody against p15 Matrix Protein Prevents the Production of Porcine Retroviruses. J Virol **77**:12132–12139.

55. **Garaicoechea L**, **Olichon A**, **Marcoppido G**, **Wigdorovitz A**, **Mozgovoj M**, **Saif L**, **Surrey T**, **Parreño V**. 2008. Llama-derived single-chain antibody fragments directed to rotavirus VP6 protein possess broad neutralizing activity in vitro and confer protection against diarrhea in mice. J Virol **82**:9753–64.

56. **Gómez-Sebastián S**, **Nuñez MC**, **Garaicoechea L**, **Alvarado C**, **Mozgovoj M**, **Lasa R**, **Kahl A**, **Wigdorovitz A**, **Parreño V**, **Escribano JM**. 2012. Rotavirus A-specific single-domain antibodies produced in baculovirus-infected insect larvae are protective in vivo. BMC Biotechnol **12**:59.

57. **Vega CG**, **Bok M**, **Vlasova AN**, **Chattha KS**, **Gómez-Sebastián S**, **Nuñez C**, **Alvarado C**, **Lasa R**, **Escribano JM**, **Garaicoechea LL**, **Fernandez F**, **Bok K**, **Wigdorovitz A**, **Saif LJ**, **Parreño V**. 2013. Recombinant Monovalent Llama-Derived Antibody Fragments (VHH) to Rotavirus VP6 Protect Neonatal Gnotobiotic Piglets against Human Rotavirus-Induced Diarrhea. PLoS Pathog **9**.

58. **Aladin F**, **Einerhand AWC**, **Bouma J**, **Bezemer S**, **Hermans P**, **Wolvers D**, **Bellamy K**, **Frenken LGJ**, **Gray J**, **Iturriza-Gómara M**. 2012. In vitro neutralisation of rotavirus infection by two broadly specific recombinant monovalent llama-derived antibody fragments. PLoS One **7**.

59. **Power UF**, **Stortelers C**, **Allosery K**, **Melero JA**. 2016. Generation and Characterization of ALX-0171 , a Potent Novel Therapeutic Nanobody for the Treatment of Respiratory Syncytial Virus Infection. Antimicrob Agents Chemother **60**:6–13.

60. **Schmidt FI**, **Hanke L**, **Morin B**, **Brewer R**, **Brusic V**, **Whelan SPJ**, **Ploegh HL**. 2016. Phenotypic lentivirus screens to identify functional single domain antibodies. Nat Microbiol **1**:16080.

61. **Arnheiter H**, **Davis NL**, **Wertz G**, **Schubert M**, **Lazzarini R a**. 1985. Role of the nucleocapsid protein in regulating vesicular stomatitis virus RNA synthesis. Cell **41**:259–267.

62. **Marasco W a**, **Haseltine W a**, **Chen SY**. 1993. Design, intracellular expression, and activity of a human anti-human immunodeficiency virus type 1 gp120 single-chain antibody. Proc Natl Acad Sci U S A **90**:7889–7893.

63. **Levin R**, **Mhashilkar AM**, **Dorfman T**, **Bukovsky A**, **Zani C**, **Bagley J**, **Hinkula J**, **Niedrig M**, **Albert J**, **Wahren B**, **Göttlinger HG**, **Marasco WA**. 1997. Inhibition of early and late events of the HIV-1 replication cycle by cytoplasmic Fab intrabodies against the matrix protein, p17. Mol Med **3**:96–110.

64. **Wong S-S**, **Webby RJ**. 2013. Traditional and new influenza vaccines. Clin Microbiol Rev **26**:476–92.

65. **Hayward AC**, **Wang L**, **Goonetilleke N**, **Fragaszy EB**, **Bermingham A**, **Copas A**, **Dukes O**, **Millett ERC**, **Nazareth I**, **Nguyen-Van-Tam JS**, **Watson JM**, **Zambon M**, **Johnson AM**, **McMichael AJ**. 2015. Natural T cell-mediated protection against seasonal and pandemic influenza: Results of the flu watch cohort study. Am J Respir Crit Care Med **191**:1422–1431.

66. **Berkhoff EGM**, **de Wit E**, **Geelhoed-Mieras MM**, **Boon a CM**, **Symons J**, **Fouchier R a M**, **Osterhaus a DME**, **Rimmelzwaan GF**, **Wit E De**. 2005. Functional constraints of influenza A virus epitopes limit escape from cytotoxic T lymphocytes. J Virol **79**:11239–11246.

67. **Yonath A**. 2011. X-ray crystallography at the heart of life science. Curr Opin Struct Biol **21**:622–626.

68. **Tereshko V**, **Uysal S**, **Koide A**, **Margalef K**, **Koide S**, **Kossiakoff AA**. 2008. Toward chaperone-assisted crystallography: protein engineering enhancement of crystal packing and X-ray phasing capabilities of a camelid single-domain antibody (VHH) scaffold. Protein Sci **17**:1175–87.

69. **Air GM**, **Webster RG**, **Colman PM**, **Laver WG**. 1987. Distribution of sequence differences in influenza N9 neuraminidase of tern and whale viruses and crystallization of the whale neuraminidase complexed with antibodies. Virology **160**.

70. **Prongay AJ**, **Smith TJ**, **Rossmann MG**, **Ehrlich LS**, **Carter CA**, **McClure J**. 1990. Preparation and crystallization of a human immunodeficiency virus p24-Fab complex. Proc Natl Acad Sci U S A **87**:9980–4.

71. **Momany C**, **Kovari LC**, **Prongay a J**, **Keller W**, **Gitti RK**, **Lee BM**, **Gorbalenya a E**, **Tong L**, **McClure J**, **Ehrlich LS**, **Summers MF**, **Carter C**, **Rossmann MG**. 1996. Crystal structure of dimeric HIV-1 capsid protein. Nat Struct Biol **3**:763–770.

72. **Dimattia MA**, **Watts NR**, **Stahl SJ**, **Grimes JM**, **Steven AC**, **Stuart DI**, **Wingfield PT**. 2013. Antigenic switching of hepatitis b virus by alternative dimerization of the capsid protein. Structure **21**:133–142.

73. **Li L**, **Park E**, **Ling J**, **Ingram J**, **Ploegh H**, **Rapoport TA**. 2016. Crystal structure of a substrate-engaged SecY protein-translocation channel. Nature **531**:395–399.

74. **Ingram JR**, **Knockenhauer KE**, **Markus BM**, **Mandelbaum J**, **Ramek A**, **Shan Y**, **Shaw DE**, **Schwartz TU**, **Ploegh HL**, **Lourido S**. 2015. Allosteric activation of apicomplexan calcium-dependent protein kinases. Proc Natl Acad Sci U S A **112**:201505914.

75. **Esra Demircioglu F**, **Sosa BA**, **Ingram J**, **Ploegh HL**, **Schwartz TU**. 2016. Structures

of torsinA and its disease-mutant complexed with an activator reveal the molecular basis for primary dystonia. Elife **5**:1–14.

76. **Burg JS**, **Ingram JR**, **Venkatakrishnan AJ**, **Jude KM**, **Dukkipati A**, **Feinberg EN**, **Angelini A**, **Waghray D**, **Dror RO**, **Ploegh HL**, **Garcia KC**. 2015. Structural basis for chemokine recognition and activation of a viral G protein–coupled receptor. Science (80-) **347**:1113–1117.

77. **Rasmussen SG**, **DeVree BT**, **Zou Y**, **Kruse AC**, **Chung KY**, **Kobilka TS**, **Thian FS**, **Chae PS**, **Pardon E**, **Calinski D**, **Mathiesen JM**, **Shah ST**, **Lyons JA**, **Caffrey M**, **Gellman SH**, **Steyaert J**, **Skiniotis G**, **Weis WI**, **Sunahara RK**, **Kobilka BK**. 2011. Crystal structure of the β2 adrenergic receptor-Gs protein complex. Nature **477**:549–55.

Chapter 2

Intracellular Expression of Camelid Single-Domain Antibodies Specific for Influenza Virus Nucleoprotein (NP) Uncovers Distinct Features of its Nuclear Localization.

Journal of Virology, March 2015

Joseph Ashour[1], Florian Schmidt[1], **Leo Hanke[1]**, Juanjo Cragnolini[1], Marco Cavallari[1], Arwen Altenburg[1], Rebeccah Brewer[1], Jessica Ingram[1], Charles Shoemaker[2], Hidde Ploegh[1]

[1]Whitehead Institute for Biomedical Research, Cambridge, Massachusetts, USA

[2]Tufts Cummings School of Veterinary Medicine, North Grafton, Massachusetts, USA

Abstract

Perturbation of protein-protein interactions relies mostly on genetic approaches or on chemical inhibition. Small RNA viruses, such as influenza A virus, do not easily lend themselves to the former approach, while chemical inhibition requires that the target protein be druggable. A lack of tools thus constrains the functional analysis of flu-encoded proteins. We generated a panel of camelid-derived single domain antibody fragments (VHHs) against influenza nucleoprotein (NP), a viral protein essential for nuclear trafficking and packaging of the influenza genome. We show that these VHHs can target NP in living cells and perturb NP's function during infection. Cytosolic expression of NP-specific VHHs (NP-VHHs) disrupts virus replication at an early stage of the life cycle. Based on their specificity, these VHHs fall into two distinct groups and both prevent nuclear import of the vRNP complex without disrupting nuclear import of NP alone. Different stages of the virus life cycle thus rely on distinct nuclear localization motifs of NP. Their molecular characterization may afford new means of intervention in the virus life cycle.

Importance

Many proteins encoded by RNA viruses are refractory to manipulation due to their essential role in replication. Thus, studying their function, and how to disrupt said function through pharmaceutical intervention, is difficult. We present a novel method based on single domain antibody technology that permits specific targeting and disruption of an essential flu protein in absence of genetic manipulation of the flu virus. Thorough characterization of the interaction should identify new targets for pharmaceutical intervention. This approach can be extended to study proteins encoded by other viral pathogens.

Introduction

The replication cycle of influenza A virus (IAV) is complex. The virus attaches to susceptible host cells via its hemagglutinin (HA), a homotrimeric type I membrane glycoprotein that recognizes sialoconjugates (1–3). The virus then enters the endocytic pathway and upon arrival in acidified late endosomes the HA trimer undergoes a conformational transition that renders it fusogenic. The M2 ion channel is responsible for acidification of the virus lumen, which results in dissociation of the eight vRNPs (comprised of PB1, PB2, PA, NP and genomic RNA) from the M1 protein and release of the vRNPs into the host cytosol (4–6). These vRNPs translocate into the nucleus via one of at least two nuclear localization sequences, NLS1 and NLS2, in NP (7–11) . Messenger RNA (mRNA) generated from vRNP-dependent synthesis of viral genomic RNA (vRNA) is exported from the nucleus and translated in the cytoplasm. Newly synthesized PB1, PB2, PA and NP translocate into the nucleus as monomers (NP and PB2) or dimers (PB1-PA), where they assemble with newly synthesized vRNA to yield the vRNP complex (12, 13). These vRNP complexes are exported from the nucleus for incorporation into budding virus particle (14).

In the course of a single replication cycle, influenza NP interacts with viral RNA and with viral proteins including PB1, PB2 and M1 (15, 16). Several host proteins also interact with NP, including importin-α BAT1, F-actin and CRM1 (17–20) . Mapping such interactions and assessing their relevance for virus replication remains a challenge because of their often essential role in the replication cycle. With rare exceptions, the influenza virus genome has resisted genetic manipulation, because many such changes cause a complete loss of a particular function and comprise viral fitness (21–23) .

The variable domains of heavy chain only antibodies (VHHs) isolated from camelids are small, ~15 kDa, and their ability to bind their cognate ligand is largely independent of modifications such as disulfide bonds and glycosylation (24, 25). These properties allow the VHHs to be expressed in the cytosol of eukaryotic cells with retention of the antigen binding capabilities. This in turn permits the specific targeting of host or viral proteins recognized by VHHs, thus enabling possible perturbation of target protein function (26–32) and reviewed in (33). VHHs are therefore unique tools for analysis of essential proteins encoded by RNA viruses in living cells.

We generated a VHH library against influenza virus and isolated VHHs specific for NP (NP-VHHs). Interaction of NP-VHHs with NP occurred when both proteins were coexpressed in the cytosol of mammalian cells. Expression of NP-VHHs during infection disrupted the replication cycle at an early stage and prevented nuclear import of vRNPs. This NP-VHH-dependent inhibition of import was specific for vRNPs, as nuclear import of NP alone was unperturbed,

as was infection with an unrelated pathogen, vesicular stomatitis virus (VSV). We conclude that influenza virus utilizes separate features of structure for import of NP and vRNPs.

Results

To generate VHHs specific for influenza virus, we immunized alpacas with an inactivated preparation of influenza A virus PR8, a mouse-adapted H1N1 strain of influenza virus. After five rounds of immunization, peripheral mononuclear cells were collected. VHH sequences were amplified from purified RNA, and cloned into an M13 phagemid vector. We used phage display to identify VHHs that bound virus immobilized on streptavidin beads via biotinylated HA (34) or recombinant HA-tagged influenza virus protein immobilized on anti-HA Sepharose beads. After two consecutive rounds of phage display and panning, we obtained four unique VHHs specific for influenza virus. Three additional VHHs specific for influenza virus were then obtained by selection using staphylococcal surface expression (35). All seven VHHs were equipped with a C-terminal sortase motif (36, 37) followed by a 6xHis-tag, expressed in bacteria and purified on a Ni-NTA affinity matrix followed by size exclusion chromatography. To determine the identity of their corresponding antigen(s), we immobilized the VHHs on Ni-NTA beads and immunoprecipitated the target antigen from lysates of influenza virus-infected MDCK cells metabolically labeled with [^{35}S]-cysteine/methionine for 2 h. The presence of HA, NP, M1, PB1, PB2, and PA proteins in the lysate was confirmed by immunoprecipitation using serum from influenza virus-infected mice (Fig. 1A lane 10). As a negative control we used MHCII VHH7, a single-domain antibody that recognizes murine class II MHC products (38) (Fig 1A, lane 9), which are absent from the MDCK lysate. Immunoprecipitation with six of the seven VHHs isolated from the influenza virus library yielded the influenza virus NP protein (Fig. 1A, lanes 2-7). These VHHs are referred to here as NP-VHH1, 2, 3, 4, 5 and 6. Interestingly, small amounts of HA coprecipitated with NP in the NP-VHH3 sample, the significance of which is not currently known. VHH F8 did not recover NP by immunoprecipitation (Fig. 1A, lane 8) and was used as an additional control in subsequent experiments.

To determine whether these NP-VHHs bind distinct epitopes on NP, we performed cross-competition assays, as follows. We tested the ability of biotinylated NP-VHH2 to retrieve recombinant NP equipped with a C-terminal 6x His tag (NP-His) preincubated with an excess of each of the individual VHHs. Recovery of VHH2 on streptavidin agarose would occur only if preincubation of NP with any of the other VHHs failed to occlude the epitope recognized by VHH2.

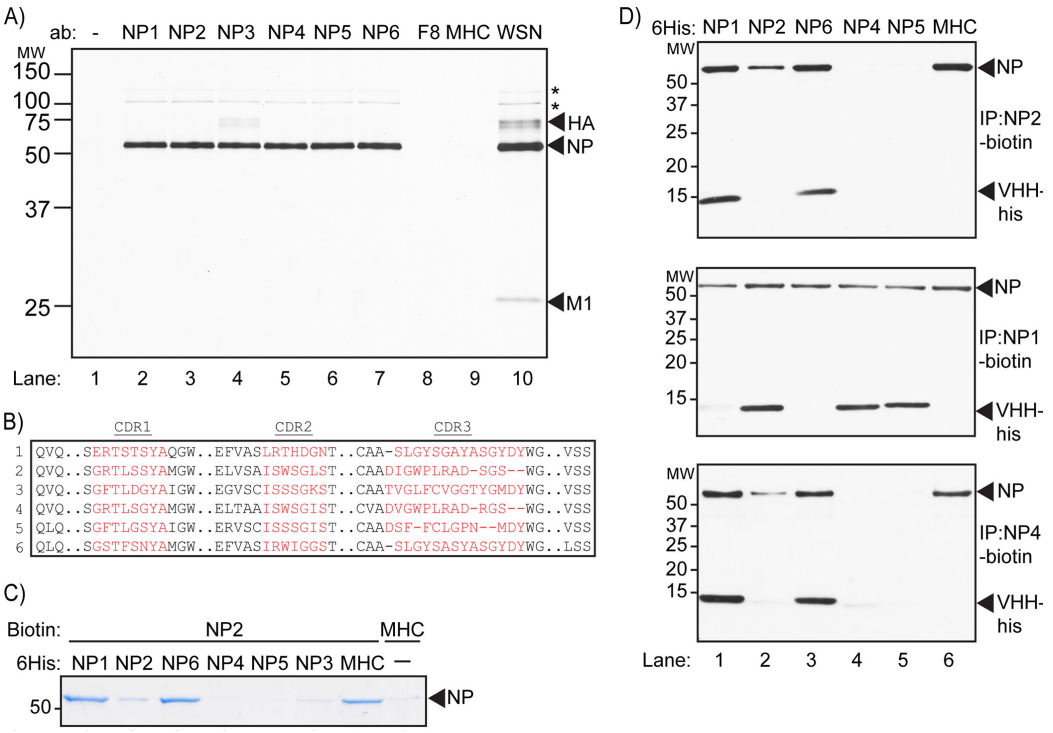

Figure 1 | VHHs isolated from the influenza VHH library are specific for NP. (A) Lysate from [^{35}S] labeled MDCK cells infected with influenza were subjected to immune-precipitation with purified VHH containing a C-terminal 6x His tag immobilized onto Ni-NTA beads. Samples were analyzed using SDS-PAGE and autoradiography. Asterisks denote expected mobility for PB2 (upper asterisk) and PB2/PA (lower asterisk). **(B)** ClustalW based alignment of NP-VHH CDR1, CDR2 and CDR3 amino acid sequence (in red). **(C)** His-tagged NP was incubated briefly with His-tagged versions of the given VHHs. Biotinylated NP-VHH2 immobilized onto streptavidin beads was then used to precipitate available NP-His. Precipitated NP-His was run on SDS-PAGE and visualized by Coomassie staining. **(D)** His-tagged NP was incubated briefly with His-tagged versions of the given VHHs. Biotinylated NP-VHH2 (top panel), VHH4 (middle panel) and VHH1 (bottom panel) immobilized on streptavidin beads were then used to pull-down NP-His. Precipitated protein was run on SDS-PAGE and detected via immune-blotting with His-HRP antibody.

Material recovered on streptavidin-agarose was analyzed by SDS-PAGE and Coomassie staining. As expected, recovery of NP was poor in samples preincubated with NP-VHH2 compared to than in an irrelevant control (Fig. 1C, lanes 2 and 6). We also observed competition upon pre-incubation of NP with NP-VHH3, -4 and -5 (Fig. 1C, lanes 4 to 6), suggesting that these VHHs occlude the epitope recognized by NP-VHH2. Pre-incubation with NP-VHH1 and -6 did not affect recovery of NP by NP-VHH2 (Fig. 1C, lanes 1 and 3), indicating that these two VHHs recognized an epitope(s) distinct from that recognized by NP-VHH2.

We next tested biotinylated NP-VHH-1 and 4 in a similar assay. Recovery of NP-His was detected by SDS-PAGE and immunoblotting using an anti-His antibody. NP-VHH2-biotin precipitated NP-His after preincubation with NP VHH1 and -6, but not -2, -4 or -5 (Fig. 1D top panel). Coprecipitation of NP-VHH1 and NP-VHH6 with NP-VHH2-biotin further confirms their recognition of distinct epitopes. A similar profile was observed with NP-VHH4-biotin

(Fig. 1D, bottom panel). In contrast, retrieval of NP-VHH1-biotin bound material showed recovery of NP-His from samples preincubated with NP-VHH1, -2, 4, 5 and 6. Neither NP-VHH1 nor NP VHH6 recognized NP in the presence of NP-VHH1-biotin, indicating that NP-VHH1 and -6 compete for the same epitope or similar epitopes. From these results, we conclude that the NP-VHHs in our panel comprise two groups, NP-VHH1 and -6 and NP-VHH2, -3, -4, and -5, each of which binds distinct nonoverlapping epitopes on NP. None of the NP-VHHs reacted with recombinant NP in immunoblots, suggesting that they recognize conformation-sensitive epitopes.

We next examined the anti-NP VHH panel for intracellular expression and manipulation of virus replication, in order to identify regions of NP essential for virus replication. As a first step, we confirmed that NP-VHHs interact with NP when expressed in the cytosol of mammalian cells in the absence of infection. We cotransfected MDCK cells with expression vectors that encode eGFP fusions of NP (NP-GFP) and mCherry fusions of NP-VHH1, -2 or -4 (NP-VHH-Ch). Since NP-VHH1, -2 and -4 represent both groups of NP-VHHs, we omitted NP-VHH3, 5 and 6 from this experiment and from the remainder of the study because of their comparatively poor expression in the cytosol (data not shown). Coexpressed fluorescent fusion proteins were visualized by live-cell imaging. In the absence of NP expression, mCherry and all VHH-mCherry fusions were diffusely expressed throughout the cell (Fig 2A). In the absence of NP-VHH expression, the NP-GFP fusion protein localized to the nucleus, indicative of the presence of a functional nuclear localization signal (NLS) (Fig. 2B, top two left panels). None of the NP-VHHs tested altered the nuclear localization of NP-GFP (Fig. 2B, lower three left panels). Furthermore, while VHH F8-mCherry or mCherry alone was observed throughout the cell, NP-VHH -1, -2 and -4 co-localized in the nucleus with NP-GFP, consistent with a specific interaction of NP-VHHs with NP inside the cell (Fig. 2B, panels in the middle column).

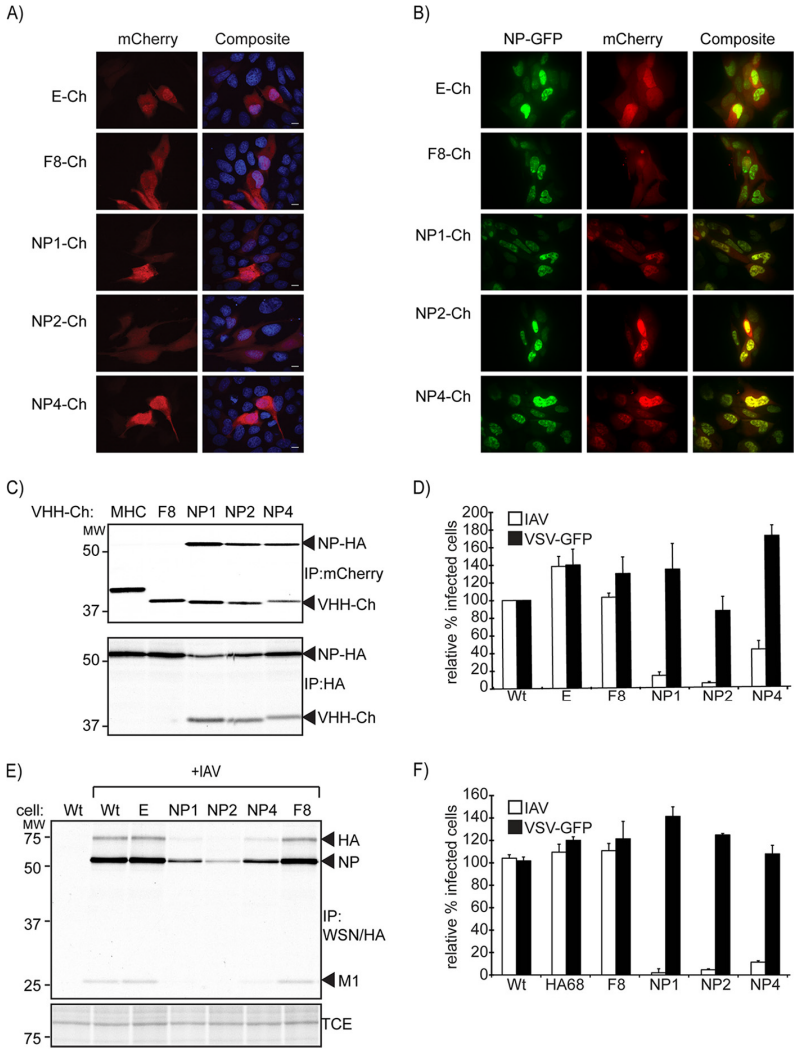

Figure 2 | NP-VHH-Ch and NP-GFP co-localize in the nucleus of transfected MDCK cells.
(A) Plasmids expressing NP-VHH-Ch and NP-GFP were co-transfected into MDCK cells. 24 hours post-transfection, cells were imaged using live confocal microscopy. B) NP and NP-VHH-Ch interact in the cytosol. 293T cells were transfected with expression plasmids for NP-VHH-Ch and NP-HA. 24 h post transfection, cells were metabolically labeled with ^{35}S-cysteine/methionine for 20 min and subsequently lysed in NP-40 containing lysis buffer. The lysate was split into two samples and subjected to immunoprecipitation using antibodies against HA or mCherry. Samples were analyzed via SDS-PAGE and autoradiography. **(C)** NP-VHH-Ch expression in the cytosol specifically inhibits influenza replication. MDCK cells constitutively expressing NP-VHH-Ch were challenged with influenza or VSV-GFP. 6 h post infection cells were fixed and IAV-infected cells stained with Alexa Fluor (AF) 647-coupled αNP-VHH1 under permeabilizing conditions. Levels of infection were quantified by flow cytometry and normalized to the Wt sample. Mean values ± s.e.m. from three independent experiments are shown. **(D)** Expression of NP-VHH-Ch in MDCK cells results in decreased influenza expression upon virus challenge. MDCK cells stably expressing VHH-Ch were challenged with influenza (MOI 1.0). 2 h post-infection cells were metabolically labeled with ^{35}S methionine for 20 min. Cells were lysed in NP-40 containing lysis buffer and the lysate was subsequently probed with WSN serum and FluB1 antibody. Samples were analyzed by SDS-PAGE and autoradiography. NP-VHH mediated inhibition is independent of cell type or mCherry fusion. A549 cells inducibly expressing NP-VHH-HA were treated with 1 µg/mL doxycycline for 24h or left untreated. Cells were challenged with influenza or VSV-GFP. 6 h post infection, cells were fixed and stained with AF 647-coupled αNP VHH1. Levels of infection were quantified by flow cytometry and infections obtained in induced samples were normalized to their un-induced counterpart. Mean values ± s.e.m. from three independent experiments are shown.

To confirm this interaction, we transiently expressed NP-VHH1-Ch, -2-Ch or -4-Ch with C-terminally HA-tagged NP (NP-HA) in 293T cells. As a negative control, we included MHCII-VHH7 fused to mCherry and VHH F8-mCherry. At 24 h after transfection, we metabolically labeled the cells with [^{35}S]-cysteine/methionine for 20 min and then lysed them in buffer containing NP-40. We performed immunoprecipitations with anti-mCherry or anti-HA antibody. Anti-mCherry coimmunoprecipitated NP only in lysates expressing an NP-VHH-mCherry fusion protein (Fig. 2C, top). Furthermore, the reciprocal immunoprecipitation using anti-HA co-immunoprecipitated only those VHHs specific for NP (Fig. 2C, bottom). Based on these results, we concluded that epitope recognition and binding of the NP-VHHs were retained when expressed in the cytosol.

Having demonstrated the ability of NP-VHHs to interact with NP in living cells, we wondered whether NP-VHHs can target and disrupt influenza virus replication. We generated MDCK cells that stably express NP-VHH-mCherry and measured virus replication using two independent methods. To quantify infection and expression of NP-VHHs by flow cytometry, MDCK cell lines were infected for 6 h, then stained for NP protein using Alexa Fluor 647-labeled NP-VHH1, and examined by flow cytometry. MDCK cells that express NP-VHH1, -2, and -4, supported influenza virus replication far worse than wild type (wt) MDCK cells or cell lines that express only mCherry or VHH F8-Cherry (Fig 2D).

We next infected wt MDCK cells or cells expressing NP-VHHs with influenza virus at an multiplicity (MOI) of 1.0. Two hours postinfection (hpi) cells were pulsed with [^{35}S]-cysteine/methionine for 10 min and then lysed in buffer containing NP-40. Viral antigens were immunoprecipitated from the lysates using a mixture of anti-WSN polyclonal mouse serum and a mouse monoclonal antibody (FluBI) which recognizes HA(39). Infection, as measured by the amount of newly synthesized NP, HA, and M1, was robust in wt cells and in cells that expressed mCherry or VHH F8-Cherry (Fig. 2E lanes 2, 3, and 7). In contrast, cells that expressed NP-VHH1, -2 and -4 produced substantially less viral antigen, indicating that infection was disrupted in these cells (Fig. 2E, lanes 4, 5, and 6).

To rule out the possibility that inhibition was cell type-specific or dependent on the relatively large mCherry fusion, we used lentiviral transduction to generate A549 cell lines with doxycyclineinducible expression of NP-VHHs. Instead of mCherry, the doxycycline-inducible NP-VHHs carry a C-terminal HA epitope tag. As an additional negative control for these experiments we included cells that express HA-VHH68 (39). Infection with influenza virus was assessed by flow cytometry as described above. Infection proceeded normally in the absence of NP-VHH expression (no doxycycline), but was essentially blocked in doxycycline-induced

cells (Fig. 2F). To demonstrate the selectivity of the NP-VHHs for influenza virus, we challenged the MDCK and A549 cell lines with a strain of vesicular stomatitis virus (VSV) that expresses eGFP (VSV-GFP) (40) and quantified infection by flow cytometry using the GFP signal as a proxy for infection. No difference in infection with VSV was observed in cell lines induced for expression of NP-VHHs compared to un-induced cells (Fig. 2S and F). The inhibition of infection imposed by NP-VHHs observed in influenza virus-challenged cells was therefore specific for influenza virus, and not for a virus-independent feature of the infected state.

In the course of infection, NP engages in a number of interactions with host proteins and viral components (41). Binding of NP-VHHs to NP could disrupt any one of them to account for the observed inhibition of virus replication. To explore how the NP-VHHs block virus replication, we established a mini-genome assay in 293T cells. In this assay, replication and transcription of a model vRNA segment is dependent on NP expression, nuclear import and association with RNA and the polymerase complex. Cells were transfected with expression plasmids for NP, PBI, PB2, and PA. The model vRNA segment encoding an HA-tagged version of influenza NA was transcribed from a co-transfected plasmid. Nuclear localization of NP-VHH-Ch (and by extension the NP ligand) was confirmed by confocal microscopy (data not shown). At 24 h after transfection, cells were lysed and NA protein levels were measured by SDS-PAGE and immunoblot analysis. Coexpression of neither VHH F8 nor MHCII VHH7 fused to mCherry inhibited expression of NA in the mini-genome assay (Fig. 3, lanes 6 and 7). For the three NP-VHHs tested, only NP-VHH1 inhibited NA protein expression, whereas NP-VHH2 and -4 were inactive fig. 3 lanes 3, 4 and 5). We thus conclude that expression of NP-VHH-1 inhibits genome replication, whereas NP-VHH -2 and -4 must block infection at a step upstream from replication.

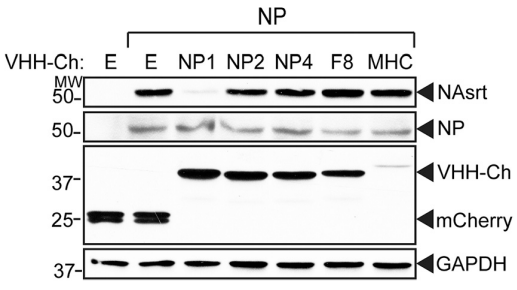

Figure 3 | NP-VHH 2 and 4 do not influence NP activity in a mini-genome assay. 293T cells were transfected with plasmids expressing influenza PB1, PB2, PA, NP, VHH-Ch and a plasmid transcribing a model genome segment encoding NAsrt (under control of the pPol1 promoter). 24 h post-transfection, cells were lysed in NP-40 containing lysis buffer. Samples were analyzed via western blot using antibody against HA epitope, NP, mCherry and GAPDH.

We next assayed nuclear import of vRNPs in MDCK cells that express NP-VHHs and challenged these cells with a high dose of influenza virus. We included the translation inhibitor cycloheximide to ensure that all NP (used here as a proxy for vRNPs) was derived from the input virus and not from newly synthesized protein. After 4 h of infection, cells were fixed and stained for NP to determine the extent of vRNP nuclear import. In WT cells, and in cells, expressing mCherry or VHH F8, input NP protein is localized predominantly in the nucleus (Fig. 4). In contrast, in cells that express NP-VHH1,2 and 4, the NP signal was mostly absent from the nucleus, indicating that nuclear import of the vRNPs was restricted. Thus, NP-VHH1 interferes with replication in the mini-genome assay and with nuclear import, whereas NP-VHH2 and -4 affect only nuclear import. Consequently, the segments of NP recognized by NP-VHH-1 and by NP-VHH2, and -4 not only are distinct epitopes but also participate in different aspects of its function in the course of infection.

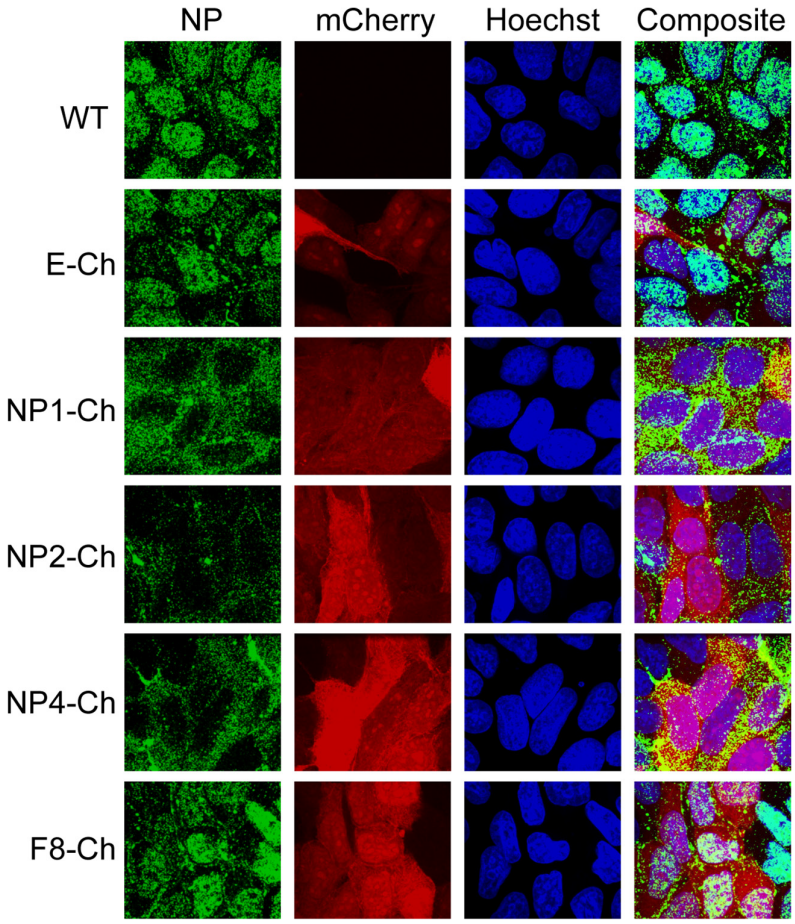

Figure 4 | NP-VHH-Ch inhibits nuclear import of the incoming vRNP complex.
MDCK cells stably expressing VHH-Ch were infected with influenza (MOI 500) in the presence of cycloheximide. Four hours after infection, cells were fixed and permeabilized with 4% paraformaldehyde and 0.5% NP-40. Staining was performed with Hoechst (blue) and anti-NP (green) before visualization by confocal microscopy.

Discussion

We exploited the unique properties of single domain antibodies that target influenza virus NP in the cytosol of influenza virus-infected cells and studied their impact on influenza virus replication. The NP-VHHs expressed in this fashion interacted with influenza virus NP in intact cells, consistent with the fact that epitope recognition is independent of lumen-associated posttranslational modifications of the VHHs, such as glycosylation and disulfide bond formation (modifications not present in the bacterial system used for phage display). Interactions between NP-VHHs and NP in the course of infection disrupted influenza virus replication at an early step. The primary mechanism by which this occurs is a halt in nuclear import of the incoming vRNPs. The NP-VHH1 recognizes an epitope distinct from that recognized by NP-VHH2 and -4 and had an additional inhibitory activity at the level of genome replication. None of the NP-VHHs tested interfered with nuclear localization of NP when it was expressed on its own. Thus, we conclude that the inhibitory activity of NP-VHHs results from interference with the nuclear import pathway utilized specifically by influenza virus vRNPs, and not by NP alone, consistent with separate functions for the two nuclear localization signals identified for NP (7, 42).

Analysis of the NLS motifs in NP has resisted identification of separable functions for these motifs in the course of infection. The complexity of interactions of NP with host and viral proteins, and the lack of tools available to analyze essential gene function have surely contributed to this state of affairs (8–10) . Mutational inactivation of either or both motifs failed to inhibit nuclear import of NP when it was expressed alone, leading to the suggestion that the protein contains a third NLS (43). Likewise, import of purified vRNPs in a digitonin permeabilized cell system was partially inhibited by preincubation with conventional antibodies specific for NLS1 and NLS2 (44). In the latter case, nuclear import was assessed by immunocytochemistry with an anti-NP antibody, and vRNP-independent import of NP may have confounded these results. Our panel of NP-VHHs allowed us to perturb nuclear import of vRNPs in living cells. This critical step in the virus life cycle could thus be analyzed under physiological conditions, i.e., during an infection.

Could an influenza virus infected cell avoid nuclear reimport of vRNPs recently exported from the nucleus and destined for incorporation into budding virions? In a similar vein, what determines nuclear import of incoming vRNPs? Our data, along with the model proposed by Wu and Pante (42), suggest that directionality of transport for vRNPs may be accomplished by regulating access to NLS1 and NLS2 sites on NP. Thus, RNA-associated NP, as found on the incoming vRNPs, might be available for the nuclear import machinery via NLS2, while NLS1 remains masked in vRNPs. An additional modification(s) to NP would have to occur to prevent

reimport of newly exported vRNPs via NLS2 in the course of infection. How this occurs is unclear but likely involves interactions with influenza virus M1 and nuclear export protein (NEP) (45). Further manipulation of this pathway using the NP-VHHs in hand should improve our understanding of the virus life cycle. For example, cocrystallization studies of NP-VHHs and NP should allow the molecular identification of the precise regions of NP recognized by NP-VHHs and thus the features of structure of NP essential for vRNP import.

Nuclear import is an essential step that must occur at least twice during the life cycle of the virus: once during nuclear entry of vRNPs, so that the incoming virus can establish a foothold, and then to enable assembly of newly replicated RNA with newly synthesized NP in the course of producing progeny virions. Given the essential nature of these steps and the relatively conserved nature of NP across different strains of influenza virus, nuclear import may be a promising target for development of broad-spectrum antivirals. A recent screen for small molecules capable of inhibiting influenza virus replication identified nucleozin as a potent inhibitor of NP nuclear import (46). Nucleozin treatment does not specifically affect nuclear import of vRNPs, indicating that it must target a different aspect of NP function different from that blocked by our NP-VHHs.

A detailed examination of the function of influenza virus NP protein in replication beyond its identification as an essential protein has been challenging. Excepting some temperature sensitive influenza virus strains, efforts to generate viable influenza virus with mutant versions of NP displaying complete loss of function in, for example nuclear import or nuclear localization, have so far proven unsuccessful (7, 47, 48). In addition, only a few small molecules to date have been identified that targets NP function (46, 49–53) . The use of intracellularly expressed single-domain antibodies represents an alternative for studying the function of essential proteins encoded by RNA viruses. The specificity of VHHs and their high affinity and ease of expression in both prokaryotic and eukaryotic cells, paired with their suitability as crystallization chaperones (54), make them attractive tools to unlock aspects of the influenza virus life cycle that have been difficult to access by other means.

Materials and methods

Antibodies and plasmids.

GAPDH-HRP (horseradish peroxidase) conjugated antibody was purchased from Abcam (ab105428). Anti-mCherry antibody was purchased from Abcam (ab167453). Anti-HA antibody was purchased from Sigma (HA-7). Protein-G agarose was purchased from Roche Diagnostics. Nickel-nitrilotriacetic acid (NTA) beads were purchased from Qiagen. FluB1 antibody was purified from FluBI hybridoma cells using published methods (55). Anti-WSN

serum was obtained from mice immunized with the A/WSN/33 strain of influenza. Expression of NP-HA, NP-GFP, all VHH-Ch and mCherry constructs were achieved by cloning into pCAGGs. Expression vectors encoding PB1, PB2, PA, and NP were a kind gift from Adolfo Garcia-Sastre. Anti-NP antibody was a kind gift from Ari Helenius.

Virus

VSV GFP was propagated and titrated over Vero cells. A/WSN/33 strain of influenza virus was propagated and titrated over MDCK cells. All infections, unless otherwise noted, were performed as follows: cells were washed in PBS and then incubated with virus resuspended in PBS (0.2% BSA). After 1 hour at room temperature the inoculum was replaced with DMEM (0.2% BSA) and cells were shifted to 37ºC with 5% CO2.

Cells

Stable integration of mCherry or VHH-Ch constructs in MDCK cells was achieved by co-transfection of pCAGGS expressing vectors and a plasmid expressing the Zeocin resistance cassette with subsequent selection for Zeocin resistance. Thereafter, cells were maintained in DMEM (10% FBS). A549 cells were cultivated in DMEM with 10% FBS. A549 cell lines inducibly expressing HA-tagged VHHs were generated using lentivirus produced with derivatives of pInducer20 (56) and selected in the presence of 500 µg/mL G418.

VHH library generation

To obtain VHHs specific for influenza virus, two alpacas underwent five rounds of immunization with alcohol fixed influenza virus PR8. Peripheral blood cells were collected from both alpacas and total RNA was isolated from each sample using a Qiagen RNeasy Plus minikit (Qiagen). Purified RNA was then used for cDNA synthesis using random hexamers, oligo-(dT) and primers specific for the constant region of the alpaca heavy chain gene. cDNA was then used as a template with primers specific to the VHH region (57) . PCR products from both alpacas were pooled, digested with NotI-HF and AscI (NEB), gel purified, ligated into a M13 phagemid vector (pJSC), and transformed via electroporation into TG1 bacteria for phage display-based panning. Three separate methods of panning were utilized to isolate influenza virus specific VHHs. The first method used intact biotinylated HAsrt virus (34) immobilized on streptavidin beads. The second method utilized recombinant influenza virus protein with a C-terminal sortase motif expressed in 293T cells, biotinylated, and immobilized on streptavidin beads. A third method utilized a *Staphylococcus aureus* display platform, based on a strategy developed for *Staphylococcus carnosus* (35) , which will be described in detail elsewhere.

Recombinant protein expression and purification.

NP from influenza virus A/WSN/33 was cloned with a C-terminal His-tag into pET30b expression vector. Transformed E. coli BL21 (DE3) were cultured in Terrific Broth at 37ºC

before the temperature was reduced to 25ºC at OD600=0.5. Protein expression was induced with 1 mM IPTG at OD600=0.6 and cells were grown for additional 3 h. The resulting pellet was resuspended in 25 mM TRIS pH 7.5, 1 M NaCl, 0.2% NP-40, 10 units/ml Benzonase and 0.1 mg/ml lysozyme. Cells were lysed by sonication and NP was purified on Ni-NTA agarose, cation exchange and Superdex 200 gel filtration columns.

Recombinant VHHs were cloned with a C-terminal sortase recognition site (LPETG) followed by a 6x His-tag into pHEN6 expression vector for periplasmic expression and transformed into *E.coli* strain WK6. Protein expression was induced by addition of 1 mM IPTG at OD600=0.6 and cells were grown overnight at 30ºC. The periplasm fraction was harvested by osmotic shock and VHHs purified by Ni-NTA affinity and size exclusion chromatography using a Superdex 75 column.

Sortase modification of recombinant proteins.

Sortase A pentamutant of *S. aureus* (5 uM final concentration) and probe (GGG-biotin, 250 mM final concentration) were added to the VHH (30 μM final concentration) in sortase buffer (50 mM Tris pH 7.5, 150 mM NaCl, 10 mM CaCl2). The mixture was incubated at 4ºC overnight. The His-tagged sortase and unreacted VHH were removed by passing over a Ni-NTA column and the biotinylated VHH was purified on a Superdex 75 size exclusion column and analyzed by gel electrophoresis.

Competition assay.

Immunoprecipitations for competition assays were performed with 2 μg of biotinylated VHH bound to streptavidin magnetic beads (MyOne Dynabeads, Invitrogen) and 7.5 μg of recombinant NP. Before addition to the beads, NP was "blocked' with 50 μg of the individual His-tagged VHHs from the panel of NP-specific (VHH1-6) and control VHHs, VHH7 and F8. Bound NP was eluted in 0.2 M glycine, pH=2.2 and analyzed by SDS-PAGE and immunoblotting with anti-His-HRP.

Metabolic labeling and immunoprecipitation.

Pulse chase experiments were performed as described in reference (58) and (59). Briefly, MDCK cells (~1 x 10^7/ sample) were trypsinized and incubated at 37ºC in starvation medium (methionine/cysteine free DMEM supplemented with 10% dialyzed fetal calf serum) for 30 min. Metabolic labeling was performed at 37ºC using starvation medium plus 10mCi/ml [35S]methionine/cysteine (PerkinElmer). Cell pellets were lysed in NP-40 containing lysis buffer and precleared with protein-G agarose beads for 1 h at 4ºC. Immunoprecipitations were performed for 1 h at 4ºC with gentle agitation. Samples were eluted by boiling in reducing sample buffer, run on SDS-PAGE and visualized by autoradiography.

Flow cytometry-based infection assays.

To quantify infection by flow cytometry, MDCK or A549 cells were seeded in 24-well plates 16 or 40 h before infection ($3 \cdot 10^4$ cells/well). A549 cells were treated with 1 µg/mL doxycycline 24 h before infection to induce VHH expression or left untreated. Cells were infected with appropriate amounts of IAV (in 0.2%BSA/DMEM) or VSV-GFP (in DMEM) to infect ca. 20% of wild-type cells. At 30 min postinfection, inoccula were removed, and cells were cultivated for 5.5 h in DMEM (10% serum). Cells were trypsinized, fixed in 4% formaldehyde, PBS, and stained in the presence of 0.05% saponin with 1 µg/mL AlexaFluor (AF) 647-coupled anti-NP VHH1 or 2 (IAV-infected cells), and/or mouse anti-HA and goat anti-mouse AF 488/AF 647 (A549-based cell lines), all under permeabilizing conditions. Levels of infection were normalized to the WT sample (for MDCK cells) or the noninduced sample (for A549 samples). Fluorescence was quantified using a BD Biosciences LSRFortessa flow cytometer and the FlowJo software package.

References

1. **Gottschalk A**, **Fezekas De St Groth S**. 1960. On the relationship between the indicator profile and prosthetic group of mucoproteins inhibitory for influenza virus haemagglutinin. J Gen Microbiol **22**:690–697.
2. **Graham E**, **Gottschalk A**. 1960. Studies on mucoproteins. I. The structure of the prosthetic group of ovine submaxillary gland mucoprotein. Biochim Biophys Acta **38**:513–24.
3. **Hirst G**. 1948. The nature of the virus receptors of red cells; evidence on the chemical nature of the virus receptors of red cells and of the existence of a closely analogous substance in normal serum. J Exp Med 301–314.
4. **Matlin KS**, **Reggio H**, **Helenius A**, **Simons K**. 1981. Infectious entry pathway of influenza virus in a canine kidney cell line. J Cell Biol **91**:601–613.
5. **Doms RW**, **Helenius A**, **White J**. 1985. Membrane fusion activity of the influenza virus hemagglutinin. The low pH-induced conformational change. J Biol Chem **260**:2973–2981.
6. **Martin K**, **Helenius a.** 1991. Nuclear transport of influenza virus ribonucleoproteins: The viral matrix protein (M1) promotes export and inhibits import. Cell **67**:117–130.
7. **Ozawa M**, **Fujii K**, **Muramoto Y**, **Yamada S**, **Yamayoshi S**, **Takada A**, **Goto H**, **Horimoto T**, **Kawaoka Y**. 2007. Contributions of two nuclear localization signals of influenza A virus nucleoprotein to viral replication. J Virol **81**:30–41.
8. **Cros JF**, **García-Sastre A**, **Palese P**. 2005. An unconventional NLS is critical for the nuclear import of the influenza A virus nucleoprotein and ribonucleoprotein. Traffic **6**:205–213.
9. **Weber F**, **Kochs G**, **Gruber S**, **Haller O**. 1998. A classical bipartite nuclear localization signal on Thogoto and influenza A virus nucleoproteins. Virology **250**:9–18.
10. **Neumann G**, **Castrucci MR**, **Kawaoka Y**. 1997. Nuclear import and export of

influenza virus nucleoprotein. J Virol **71**:9690–700.

11. **O'Neill RE**, **Jaskunas R**, **Blobel G**, **Palese P**, **Moroianu J**. 1995. Nuclear import of influenza virus RNA can be mediated by viral nucleoprotein and transport factors required for protein import. J Biol Chem **270**:22701–22704.

12. **Huet S**, **Avilov S V**, **Ferbitz L**, **Daigle N**, **Cusack S**, **Ellenberg J**. 2010. Nuclear import and assembly of influenza A virus RNA polymerase studied in live cells by fluorescence cross-correlation spectroscopy. J Virol **84**:1254–1264.

13. **Tarendeau F**, **Boudet J**, **Guilligay D**, **Mas PJ**, **Bougault CM**, **Boulo S**, **Baudin F**, **Ruigrok RWH**, **Daigle N**, **Ellenberg J**, **Cusack S**, **Simorre J-P**, **Hart DJ**. 2007. Structure and nuclear import function of the C-terminal domain of influenza virus polymerase PB2 subunit. Nat Struct Mol Biol **14**:229–33.

14. **Chou Y ying**, **Heaton NS**, **Gao Q**, **Palese P**, **Singer R**, **Lionnet T**. 2013. Colocalization of Different Influenza Viral RNA Segments in the Cytoplasm before Viral Budding as Shown by Single-molecule Sensitivity FISH Analysis. PLoS Pathog **9**.

15. **Biswas SK**, **Boutz PL**, **Nayak DP**. 1998. Influenza virus nucleoprotein interacts with influenza virus polymerase proteins. J Virol **72**:5493–5501.

16. **Poole EL**, **Medcalf L**, **Elton D**, **Digard P**. 2007. Evidence that the C-terminal PB2-binding region of the influenza A virus PB1 protein is a discrete ??-helical domain. FEBS Lett **581**:5300–5306.

17. **Elton D**, **Simpson-holley M**, **Archer K**, **Hallam R**, **Mccauley J**, **Digard P**, **Medcalf LIZ**, **Cauley JMC**. 2001. Interaction of the Influenza Virus Nucleoprotein with the Cellular CRM1-Mediated Nuclear Export Pathway Interaction of the Influenza Virus Nucleoprotein with the Cellular CRM1-Mediated Nuclear Export Pathway. J Virol **75**:408–419.

18. **Digard P**, **Elton D**, **Bishop K**, **Medcalf E**, **Weeds a**, **Pope B**. 1999. Modulation of nuclear localization of the influenza virus nucleoprotein through interaction with actin filaments. J Virol **73**:2222–31.

19. **O'Neill RE**, **Palese P**. 1995. NPI-1, the human homolog of SRP-1, Interacts with influenza virus nucleoprotein. Virology **206**:116–125.

20. **Momose F**, **Basler CF**, **Neill REO**, **Iwamatsu A**, **Palese P**, **Nagata K**. 2001. Cellular Splicing Factor RAF-2p48 / NPI-5 / BAT1 / UAP56 Interacts with the Influenza Virus Nucleoprotein and Enhances Viral RNA Synthesis. J Virol **75**:1899–1908.

21. **Mackenzie JS**, **Dimmock NJ**. 1973. A preliminary study of physiological characteristics of temperature-sensitive mutants of influenza virus. J Gen Virol **19**:51–63.

22. **Palese P**, **Tobita K**, **Ueda M**, **Compans RW**. 1974. Characterization of temperature sensitive influenza virus mutants defective in neuraminidase. Virology **61**:397–410.

23. **Garcia-Sastre A**, **Egorov A**, **Matassov D**, **Brandt S**, **Levy DE**, **Durbin JE**, **Palese P**, **Muster T**. 1998. RAPID COMMUNICATION Influenza A Virus Lacking the NS1 Gene Replicates in Interferon-Deficient Systems **330**:324–330.

24. **Hamers-Casterman C**, **Atarhouch T**, **Muyldermans S**, **Robinson G**, **Hamers C**, **Songa EB**, **Bendahman N**, **Hamers R**. 1993. Naturally occurring antibodies devoid of light chains. Nature **363**:446–8.

25. **Holliger P**, **Hudson PJ**. 2005. Engineered antibody fragments and the rise of single domains. Nat Biotechnol **23**:1126–1136.

26. **Cardoso FM**, **Ibañez LI**, **Van den Hoecke S**, **De Baets S**, **Smet A**, **Roose K**, **Schepens B**, **Descamps FJ**, **Fiers W**, **Muyldermans S**, **Depicker A**, **Saelens X**. 2014. Single-domain antibodies targeting neuraminidase protect against an H5N1 influenza virus challenge. J Virol **88**:8278–96.

27. **Ibañez LI**, **De Filette M**, **Hultberg A**, **Verrips T**, **Temperton N**, **Weiss RA**, **Vandevelde W**, **Schepens B**, **Vanlandschoot P**, **Saelens X**. 2011. Nanobodies with in vitro neutralizing activity protect mice against H5N1 influenza virus infection. J Infect Dis **203**:1063–1072.

28. **Acharya P**, **Luongo TS**, **Georgiev IS**, **Matz J**, **Schmidt SD**, **Louder MK**, **Kessler P**, **Yang Y**, **McKee K**, **O'Dell S**, **Chen L**, **Baty D**, **Chames P**, **Martin L**, **Mascola JR**, **Kwong PD**. 2013. Heavy Chain-Only IgG2b Llama Antibody Effects Near-Pan HIV-1 Neutralization by Recognizing a CD4-Induced Epitope That Includes Elements of Coreceptor- and CD4-Binding Sites. J Virol **87**:10173–10181.

29. **Vercruysse T**, **Pardon E**, **Vanstreels E**, **Steyaert J**, **Daelemans D**. 2010. An intrabody based on a llama single-domain antibody targeting the N-terminal ??-helical multimerization domain of HIV-1 Rev prevents viral production. J Biol Chem **285**:21768–21780.

30. **Rothbauer U**, **Zolghadr K**, **Tillib S**, **Nowak D**, **Schermelleh L**, **Gahl A**, **Backmann N**, **Conrath K**, **Muyldermans S**, **Cardoso MC**, **Leonhardt H**. 2006. Targeting and tracing antigens in live cells with fluorescent nanobodies. Nat Methods **3**:887–9.

31. **Kirchhofer A**, **Helma J**, **Schmidthals K**, **Frauer C**, **Cui S**, **Karcher A**, **Pellis M**, **Muyldermans S**, **Casas-Delucchi CS**, **Cardoso MC**, **Leonhardt H**, **Hopfner K-P**, **Rothbauer U**. 2010. Modulation of protein properties in living cells using nanobodies. Nat Struct Mol Biol **17**:133–8.

32. **Caussinus E**, **Kanca O**, **Affolter M**. 2011. Fluorescent fusion protein knockout mediated by anti-GFP nanobody. Nat Struct Mol Biol **19**:117–121.

33. **Vanlandschoot P**, **Stortelers C**, **Beirnaert E**, **Ibañez LI**, **Schepens B**, **Depla E**, **Saelens X**. 2011. Nanobodies??: New ammunition to battle viruses. Antiviral Res **92**:389–407.

34. **Popp MWL**, **Karssemeijer RA**, **Ploegh HL**. 2012. Chemoenzymatic site-specific labeling of influenza glycoproteins as a tool to observe virus budding in real time. PLoS Pathog **8**:1–16.

35. **Fleetwood F**, **Devoogdt N**, **Pellis M**, **Wernery U**, **Muyldermans S**, **Ståhl S**, **Löfblom J**. 2013. Surface display of a single-domain antibody library on Gram-positive bacteria. Cell Mol Life Sci **70**:1081–1093.

36. **Popp MW**, **Antos JM**, **Grotenbreg GM**, **Spooner E**, **Ploegh HL**. 2007. Sortagging: a versatile method for protein labeling. Nat Chem Biol **3**:707–8.

37. **Popp MW-L**, **Antos JM**, **Ploegh HL**. 2009. Site-Specific Protein Labeling via Sortase-Mediated Transpeptidation. Curr Protoc Protein Sci 1–9.

38. **Witte MD**, **Cragnolini JJ**, **Dougan SK**, **Yoder NC**, **Popp MW**, **Ploegh HL**. 2012. Preparation of unnatural N-to-N and C-to-C protein fusions. Proc Natl Acad Sci U S A **109**:11993–8.

39. **Dougan SK**, **Ashour J**, **Karssemeijer R a**, **Popp MW**, **Avalos AM**, **Barisa M**, **Altenburg AF**, **Ingram JR**, **Cragnolini JJ**, **Guo C**, **Alt FW**, **Jaenisch R**, **Ploegh HL**. 2013. Antigen-specific B-cell receptor sensitizes B cells to infection by influenza virus. Nature **503**:406–9.

40. **Stojdl DF**, **Lichty BD**, **TenOever BR**, **Paterson JM**, **Power AT**, **Knowles S**, **Marius R**, **Reynard J**, **Poliquin L**, **Atkins H**, **Brown EG**, **Durbin RK**, **Durbin JE**, **Hiscott J**, **Bell JC**. 2003. VSV strains with defects in their ability to shutdown innate immunity are potent systemic anti-cancer agents. Cancer Cell **4**:263–275.

41. **Watanabe T**, **Watanabe S**, **Kawaoka Y**. 2010. Cellular networks involved in the influenza virus life cycle. Cell Host Microbe **7**:427–439.

42. **Wu WW**, **Panté N**. 2009. The directionality of the nuclear transport of the influenza A genome is driven by selective exposure of nuclear localization sequences on nucleoprotein. Virol J **6**:68.

43. **Bullido R**, **Gómez-Puertas P**, **Albo C**, **Portela A**. 2000. Several protein regions contribute to determine the nuclear and cytoplasmic localization of the influenza A virus nucleoprotein. J Gen Virol **81**:135–42.

44. **Wu WWH**, **Sun Y-HB**, **Panté N**. 2007. Nuclear import of influenza A viral ribonucleoprotein complexes is mediated by two nuclear localization sequences on viral nucleoprotein. Virol J **4**:49.

45. **Shimizu T**, **Takizawa N**, **Watanabe K**, **Nagata K**, **Kobayashi N**. 2011. Crucial role of the influenza virus NS2 (NEP) C-terminal domain in M1 binding and nuclear export of vRNP. FEBS Lett **585**:41–46.

46. **Kao RY**, **Yang D**, **Lau L-S**, **Tsui WHW**, **Hu L**, **Dai J**, **Chan M-P**, **Chan C-M**, **Wang P**, **Zheng B-J**, **Sun J**, **Huang J-D**, **Madar J**, **Chen G**, **Chen H**, **Guan Y**, **Yuen K-Y**. 2010. Identification of influenza A nucleoprotein as an antiviral target. Nat Biotechnol **28**:600–5.

47. **Noton SL**, **Simpson-Holley M**, **Medcalf E**, **Wise HM**, **Hutchinson EC**, **Mccauley JW**, **Digard P**. 2009. Studies of an Influenza A Virus Temperature-Sensitive Mutant Identify a Late Role for NP in the Formation of Infectious Virions. J Virol **83**:562–571.

48. **Li Z**, **Watanabe T**, **Hatta M**, **Watanabe S**, **Nanbo A**, **Ozawa M**, **Kakugawa S**, **Shimojima M**, **Yamada S**, **Neumann G**, **Kawaoka Y**. 2009. Mutational analysis of conserved amino acids in the influenza A virus nucleoprotein. J Virol **83**:4153–4162.

49. **Hagiwara K**, **Kondoh Y**, **Ueda A**, **Yamada K**, **Goto H**, **Watanabe T**, **Nakata T**, **Osada H**, **Aida Y**. 2010. Discovery of novel antiviral agents directed against the influenza A virus nucleoprotein using photo-cross-linked chemical arrays. Biochem Biophys Res Commun **394**:721–727.

50. **Shen Y-F**, **Chen Y-H**, **Chu S-Y**, **Lin M-I**, **Hsu H-T**, **Wu P-Y**, **Wu C-J**, **Liu H-W**, **Lin F-Y**, **Lin G**, **Hsu P-H**, **Yang A-S**, **Cheng Y-SE**, **Wu Y-T**, **Wong C-H**, **Tsai M-D**. 2011. E339…R416 salt bridge of nucleoprotein as a feasible target for influenza virus inhibitors. Proc Natl Acad Sci **108**:16515–16520.

51. **Su CY**, **Cheng TJ**, **Lin MI**, **Wang SY**, **Huang WI**, **Lin-Chu SY**, **Chen YH**, **Wu CY**, **Lai MM**, **Cheng WC**, **Wu YT**, **Tsai MD**, **Cheng YS**, **Wong CH**. 2010. High-throughput identification of compounds targeting influenza RNA-dependent RNA polymerase activity. Proc Natl Acad Sci U S A **107**:19151–19156.

52. **Gerritz SW**, **Cianci C**, **Kim S**, **Pearce BC**, **Deminie C**, **Discotto L**, **McAuliffe B**, **Minassian BF**, **Shi S**, **Zhu S**, **Zhai W**, **Pendri A**, **Li G**, **Poss MA**, **Edavettal S**, **McDonnell PA**, **Lewis HA**, **Maskos K**, **Mörtl M**, **Kiefersauer R**, **Steinbacher S**, **Baldwin ET**, **Metzler W**, **Bryson J**, **Healy MD**, **Philip T**, **Zoeckler M**, **Schartman R**, **Sinz M**, **Leyva-Grado VH**, **Hoffmann H-H**, **Langley DR**, **Meanwell NA**, **Krystal M**. 2011. Inhibition of influenza virus replication via small molecules that induce the formation of higher-order nucleoprotein oligomers. Proc Natl Acad Sci U S A

108:15366–71.

53. **Lejal N**, **Tarus B**, **Bouguyon E**, **Chenavas S**, **Bertho N**, **Delmas B**, **Ruigrok RWH**, **Di Primo C**, **Slama-Schwok A**. 2013. Structure-based discovery of the novel antiviral properties of naproxen against the nucleoprotein of influenza a virus. Antimicrob Agents Chemother **57**:2231–2242.

54. **Tereshko V**, **Uysal S**, **Koide A**, **Margalef K**, **Koide S**, **Kossiakoff AA**. 2008. Toward chaperone-assisted crystallography: protein engineering enhancement of crystal packing and X-ray phasing capabilities of a camelid single-domain antibody (VHH) scaffold. Protein Sci **17**:1175–87.

55. **Avalos AM**, **Bilate AM**, **Witte MD**, **Tai AK**, **He J**, **Frushicheva MP**, **Thill PD**, **Meyer-Wentrup F**, **Theile CS**, **Chakraborty AK**, **Zhuang X**, **Ploegh HL**. 2014. Monovalent engagement of the BCR activates ovalbumin-specific transnuclear B cells. J Exp Med **211**:365–79.

56. **Meerbrey KL**, **Hu G**, **Kessler JD**, **Roarty K**, **Li MZ**, **Fang JE**, **Herschkowitz JI**, **Burrows AE**, **Ciccia A**, **Sun T**, **Schmitt EM**, **Bernardi RJ**, **Fu X**, **Bland CS**, **Cooper TA**, **Schiff R**, **Rosen JM**, **Westbrook TF**, **Elledge SJ**. 2011. The pINDUCER lentiviral toolkit for inducible RNA interference in vitro and in vivo. Proc Natl Acad Sci U S A **108**:3665–70.

57. **Maass DR**, **Sepulveda J**, **Pernthaner A**, **Shoemaker CB**. 2007. Alpaca (Lama pacos) as a convenient source of recombinant camelid heavy chain antibodies (VHHs). J Immunol Methods **324**:13–25.

58. **Claessen JHL**, **Mueller B**, **Spooner E**, **Pivorunas VL**, **Ploegh HL**. 2010. The transmembrane segment of a tail-anchored protein determines its degradative fate through dislocation from the endoplasmic reticulum. J Biol Chem **285**:20732–20739.

59. **Wiertz EJ**, **Tortorella D**, **Bogyo M**, **Yu J**, **Mothes W**, **Jones TR**, **Rapoport TA**, **Ploegh HL**. 1996. Sec61-mediated transfer of a membrane protein from the endoplasmic reticulum to the proteasome for destruction. Nature **384**:432–8.

Chapter 3

The Antiviral Mechanism of an Influenza A Nucleoprotein-specific Single-Domain Antibody Fragment

MBio, December 2016

Leo Hanke[1], Kevin E. Knockenhauer[2] , Rebeccah Brewer[1], Eline van Diest[1], Florian I. Schmidt[1], Thomas U. Schwartz[2] and Hidde L. Ploegh[1,2]

[1]Whitehead Institute for Biomedical Research, Cambridge, Massachusetts, USA

[2]Department of Biology, Massachusetts Institute of Technology, Cambridge, Massachusetts, USA

Abstract

Alpaca-derived single domain antibody fragments (VHHs) that target the influenza A nucleoprotein (NP) can protect cells from infection when expressed in the cytosol. We found that one such VHH, αNP-VHH1, exhibits similar antiviral activity as Mx proteins by blocking nuclear import of incoming vRNPs and viral transcription and replication in the nucleus. We determined a 3.2 Å crystal structure of αNP-VHH1 in complex with influenza A NP. The VHH binds to a non-conserved region on the body domain of NP, which has been associated with binding to host factors and serves as a determinant of host range. Several of the NP:VHH interface residues determine sensitivity of NP to antiviral Mx GTPases. The structure of the NP:αNP-VHH1 complex affords a plausible explanation for the inhibitory properties of the VHH and suggests a rationale for the antiviral properties of Mx proteins. Such knowledge can be leveraged for much needed novel antiviral strategies.

Importance

Influenza strains can rapidly escape from protection afforded by seasonal vaccines, or acquire resistance to available drugs. Additional ways to interfere with the virus life cycle are therefore urgently needed. The influenza nucleoprotein is one promising target for antiviral interventions. We have previously isolated alpaca derived single-domain antibody fragments (VHHs) that protect cells from influenza infection if expressed intracellularly. We show here that one such VHH exhibits antiviral activities similar to proteins of the cellular antiviral defense (Mx proteins). We determined the three dimensional structure of this VHH in complex with the influenza nucleoprotein and identified the interaction site, which overlaps with regions that determine sensitivity of the virus to Mx proteins. Our data defines a new vulnerability of influenza virus, helps to better understand the cellular antiviral mechanisms, and provides a well characterized tool to further study them.

Introduction

Seasonal human influenza A virus (IAV) epidemics and occasional pandemics cause significant morbidity and continue to pose a large economic burden. Influenza A is a segmented, negative stranded RNA virus and belongs to the family of *orthomyxoviridae*. To infect a cell, virus particles must fuse with the host cell membrane to release the viral ribonucleoprotein (vRNP) complexes into the cytosol. vRNPs must then cross the nuclear membrane, to enter the nucleus, where viral transcription and replication take place.

vRNPs contain a negative-stranded RNA genome segment decorated by many copies of the nucleoprotein NP. NP bound to viral RNA (vRNA) assembles into two helical, anti-parallel strands that form a loop at one end. At the other end, the heterotrimeric polymerase, comprised of PA, PB1 and PB2, is positioned and binds to the base-paired, conserved ends of the vRNA as well as to NP.

The major vRNP protein component, NP, is a basic, ~56 kDa protein consisting of a head and body domain and a tail loop (aa 402-428). In the context of a vRNP, the tail loop protrudes into adjacent NP molecules and mediates oligomerization (1). Besides binding and condensing vRNA, the diverse functions of NP include nuclear import, export, and RNA synthesis. NP interacts with the viral proteins M1 and PB2 and a variety of host proteins (2–6). Because of its complex interactions, NP is a key determinant of host specificity, such that IAV strains with NP sequences of avian origin are much less virulent in human cells (7, 8).

Nuclear import of vRNPs through nuclear pores is mediated by importin-α/β. At least two nuclear localization sequences (NLS) that are recognized by the different importin-α isoforms are present on NP, including a nonconventional NLS (NLS1, NP residue 3-13), and NLS2 comprising residues 198 – 216 (9, 10). NP is dispensable for transcription of short (<100 nucleotides) vRNA-like templates, but is essential for transcription and replication of full-length viral genome segments. NP thus serves as a crucial factor for transcript elongation (11). Newly synthesized NP exists as monomers and small oligomers (trimers) and is imported into the nucleus to assemble new vRNPs (12). Later in infection, the progeny vRNPs are exported to the cytosol with the aid of the viral nuclear export protein (NEP), M1 and the host CRM1 export machinery for delivery to the budding site (5, 13).

Anti-influenza drugs and vaccines have traditionally targeted the surface-exposed viral hemagglutinin (HA), neuraminidase (NA), or the ion channel M2. The selective pressure exerted by drugs, antibodies and T cells confers a selective advantage to those viruses with mutations in their surface proteins as a means of escape (antigenic drift). Strain-dependent

sequence variation in other influenza proteins, such as NP, exists, but is far less prominent than the antigenic drift seen for HA, NA and M2 variants.

Alternative approaches to traditional interventions must therefore target the more conserved proteins of the viral RNP complex to prevent them from entering the nucleus or to inhibit the associated activity of the RNA-dependent RNA polymerase, a vulnerability of the virus that is also exploited by host, antiviral Mx proteins. Mx GTPases are interferon-induced effectors of the cell-autonomous antiviral immune response, with broad specificity against a number of RNA viruses. Although molecular details of how Mx proteins exert their antiviral activity are unknown, we do know the stages in the viral life cycle that are perturbed by Mx proteins (14). The human MxA protein is localized in the cytosol and prevents nuclear import of incoming vRNPs (15). In contrast, mouse Mx1, a close homolog, is localized in the nucleus and interferes with viral transcription and replication (14).

To better relate specific contributions of different NP surface regions to their function, and to identify new vulnerabilities that perturb the viral life cycle, we have used intracellularly expressed variable domains of alpaca heavy chain-only antibodies (VHHs) that target IAV NP. In contrast to conventional antibodies or their fragments, camelid heavy chain-only antibodies recognize their target with a single variable binding domain. As fragments, these ~15 kDa antibody domains can bind with high affinity and specificity, are soluble and mostly independent of stabilization by disulfide bonds. This allows expression of VHHs in the cytosol of mammalian cells with retention of their binding properties. Intracellular expression of the anti-NP VHHs during IAV infection disrupts the viral replication cycle at an early stage by preventing essential nuclear import of incoming vRNPs, but not of NP alone (16, 17). We can thus target a specific NP surface and examine the consequences for virus replication.

We found that one of our NP specific VHHs, αNP-VHH1, blocks vRNP nuclear import, viral transcription and replication in similar fashion as do interferon-induced, antiviral Mx proteins. We used VHHs as crystallization chaperones to grow crystals of recombinant NP in complex with αNP-VHH1. The 3.2 Å crystal structure reveals that the VHH binding site overlaps with a region associated with viral sensitivity to Mx proteins. According to one of the proposed vRNP structures, VHH binding occludes access to NLS2 on the adjacent NP molecule, thus providing a plausible mechanistic explanation for the antiviral activity of αNP-VHH1 and Mx proteins.

Results

αNP-VHH1 inhibits virus replication after nuclear import of vRNPs

We reported the identification of several VHHs that target influenza NP (16, 17). When expressed in the cytosol, almost all identified VHHs block nuclear import of incoming vRNPs. Due to the multiple roles of NP in the viral life cycle, it is likely that VHHs interfere with virus replication at multiple steps. We tested the effect of αNP-VHH1 in the course of an influenza infection in A549 cell derivatives in which VHH expression is doxycycline-inducible. Since αNP-VHH1 inhibits the initial nuclear import of vRNPs, we infected with influenza virus and induced expression of αNP-VHH1 in the cytosol at different time points from 16 hours (h) before to 5 h after infection. We expected that induction of VHH expression after infection permits vRNP import into the nucleus, to then be able to examine the effects of αNP-VHH1 after this step. We assessed expression levels of NP and HA-tagged αNP-VHH1 by flow cytometry 6 h post infection (p.i.), using αNP-VHH2 AlexaFluor647 (another NP-specific VHH) and an AlexaFluor488-labeled monoclonal anti-HA antibody, respectively (Fig 1A). VHH levels were lower when their expression was induced at later time points, while the fraction of NP positive cells and thus infection was higher. When expression was induced 3 or 4 h p.i., VHH levels were barely detectable, which we attribute to influenza-mediated shut down of host protein synthesis (18). Induction of VHH expression as early as 1 h prior to infection was sufficient to prevent most *de novo* NP production, likely by limiting access of vRNPs to the nucleus. A substantial fraction of cells still expressed NP when doxycycline was added simultaneously with or 2 h p.i.. This leaves a narrow window to allow VHH expression in infected cells to study VHH perturbation after nuclear import. To evaluate the effect of the small quantities of VHH induced at 0 and 2 h p.i., we used the same experimental setup as before, but instead quantified virus titers in the supernatants (Fig 1B). Time points that allowed both VHH production and NP synthesis (0 and 2 h p.i.) yielded drastically reduced virus titers. This suggests that αNP-VHH1 impairs viral replication in ways other than its interference with nuclear import of incoming vRNPs.

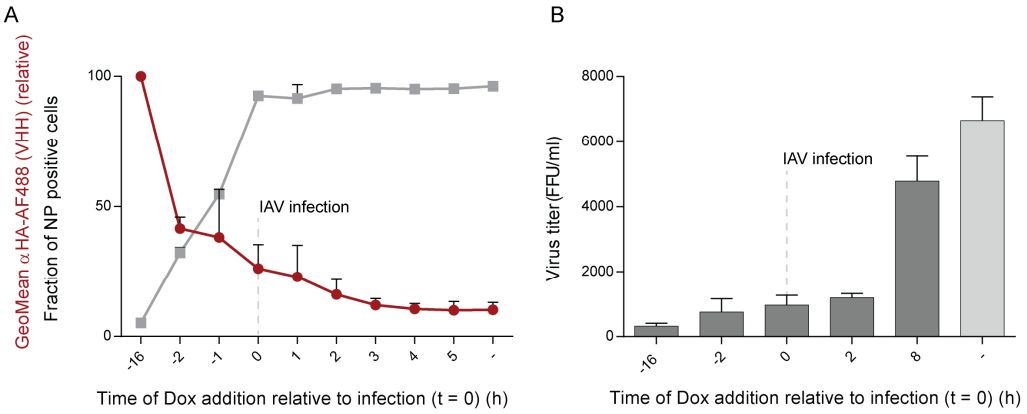

Figure 1 | αNP-VHH1 impairs influenza A virus replication at early and late time points. A549 cells expressing αNP-VHH1-HA in a doxycycline (Dox)-inducible manner were seeded 24 h before influenza A virus (IAV) infection. VHH expression was induced at the indicated time points relative to infection; cells were infected with IAV at an MOI of 1 at t = 0 h. **(A)** Cells were harvested 6 h post infection (p.i.), stained for HA and NP, and analyzed by flow cytometry. Geometric mean of αHA-AlexaFluor488 (VHH expression level, red) and fraction of infected cells (NP positive, gray) are shown. Mean values ± standard deviation (SD) from technical duplicates are displayed.
(B) Supernatants were collected 24 h.p.i and titered on MDCK cells. 24 h p.i., NP in infected MDCK cells (nuclei) was stained with αNP-VHH2-TAMRA, and infected cells were quantified by CellProfiler. Data from three independent experiments (±s.e.m.) is shown.

αNP-VHH1 inhibits replication/transcription of long RNA segments

Nuclear import of vRNPs is followed by transcription and replication of viral genome segments. We have previously analyzed polymerase activity in the presence of NP-specific VHHs using a transfection-based polymerase reconstitution assay in 293T cells, bypassing natural infection and nuclear import of vRNPs. We found that αNP-VHH1 fused to mCherry blocked the synthesis of the template genome encoding the viral NA (16), but HA-tagged αNP-VHH1 did not affect transcription of an artificial genome segment encoding EGFP in independent experiments (17). We excluded the possibility that the size of the VHH fusions contributed to this discrepancy (data not shown). Since the template genome segments we used differ in their length, we speculated that the VHH may interfere with the role of NP in transcript elongation. An interference with elongation that is dependent on the length of the viral genome segment is also seen for antiviral Mx proteins located in the nucleus (14). Initiation and synthesis of primary viral transcripts for M1 and NS2 are barely affected by Mx1, but Mx1 interferes with the synthesis of the longer transcripts encoding NP, HA, PA, PB2 or PB1 (14). To test whether the inhibitory effect of αNP-VHH1 during transcription and replication is dependent on the length of the transcript, we designed two artificial genome segments: one encoding EGFP on a 720 nucleotide (nt) transcript, the other mCherry-T2A-EGFP on a 1500 nt transcript. This approach enabled us to compare templates of different lengths in a polymerase reconstitution assay, while measuring the same fluorescent molecule as a readout (EGFP). We co-transfected

a control VHH (VHH7, α-murine-MHCII), αNP-VHH1, human MxA or murine Mx1 and quantified EGFP positive cells 24 h post transfection (Fig 2). The fraction of EGFP-positive cells in the presence of all tested proteins was unaffected for the short 720 nt template, at least at the co-transfected amounts of plasmid DNA. The 1500 nt genome segment showed reduced overall expression compared to the 720 nt genome segment in the absence of any perturbants. Co-transfection of Mx1 or αNP-VHH1 clearly reduced EGFP positive cells and thus polymerase efficiency on the 1500 nt transcript, while the control VHH and MxA did not affect EGFP expression. We thus show that, similar to Mx proteins in the nucleus, αNP-VHH1 interacts with NP in a manner that does not block initiation of polymerase activity, but rather hinders NP in its role as a factor for transcript elongation by the RNA-dependent polymerase. This also explains the reduced virus titers in the presence of αNP-VHH1, although we cannot exclude that additional stages of the replication cycle, such as nuclear export, transport to the budding site and virion assembly, are impaired by the VHH as well.

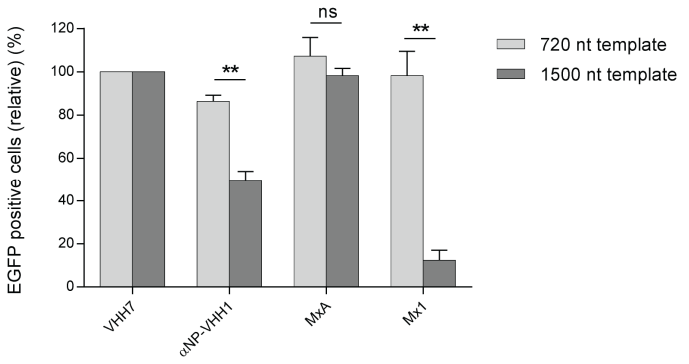

Figure 2 | Inhibition of polymerase activity by αNP-VHH1 and Mx1 is dependent on transcript length. 293T cells were transfected with expression vectors for influenza A/WSN/33 PA, PB1, PB2, NP, as well as the indicated VHHs or Mx proteins. In addition, we co-transfected plasmid pPolI-RT, from which a synthetic genome segment was transcribed, that either encoded EGFP (720 nt) or mCherry-T2A-EGFP (1500 nt). 24 h post transfection, EGFP positive cells were quantified by flow cytometry. Since reduced EGFP levels were expressed from the mCherry-T2A-EGFP construct, values were normalized to EGFP positive cells expressing VHH7 (control). Data from three independent experiments is shown (±s.e.m.). Statistical significance was assessed by Student's t test (**, P<0.01, ns = not significant).

αNP-VHH1 binds to the NP body domain

To define the molecular binding site of αNP-VHH1 on NP as a means of obtaining mechanistic insight into its inhibitory properties, we determined the binding site by X-ray crystallography. To produce the NP:αNP-VHH1 complex, we expressed and purified both proteins individually. We then combined the proteins in a 1:3, NP:αNP-VHH1 molar ratio and purified the complex by size exclusion chromatography. In the absence of RNA, purified NP exists as monomers or trimers, and the oligomerization state can be influenced by salt concentration (19). As in vRNPs, the NP:NP interaction in trimers is facilitated by the NP tail loop that protrudes into an

adjacent NP molecule (20). In the size exclusion elution profile, both monomeric and trimeric peaks shift after addition of the VHH, indicating that binding of the VHH does not affect NP oligomerization and that αNP-VHH1 can interact with both species (Fig 3A).

We obtained co-crystals of the complex that diffracted to 3.2 Å (Table 1) and solved the structure by molecular replacement (MR) using the available structures of NP (2IQH) and a VHH (4KRL) as reference models (1, 21). Our model was refined to a final R_{work} of 20.3% and R_{free} of 26.1%. The NP:αNP-VHH1 complex resembles previously characterized NP structures, forming a trimer with the tail loops projecting into the adjacent NP molecule (Fig 3B) (1, 22). αNP-VHH1 binds to the body domain at the end opposite to the tail loop of each NP monomer (Figs 3B and 3C), underlining that it does not interfere with oligomerization of NP. Despite being a potent inhibitor of vRNP nuclear import, the VHH binding site is distant from the known NLS1 and NLS2 (Figs 3C and 3D). It is also not in the proximity of the RNA binding cleft (Fig 3C), and thus likely does not alter binding of NP to RNA.

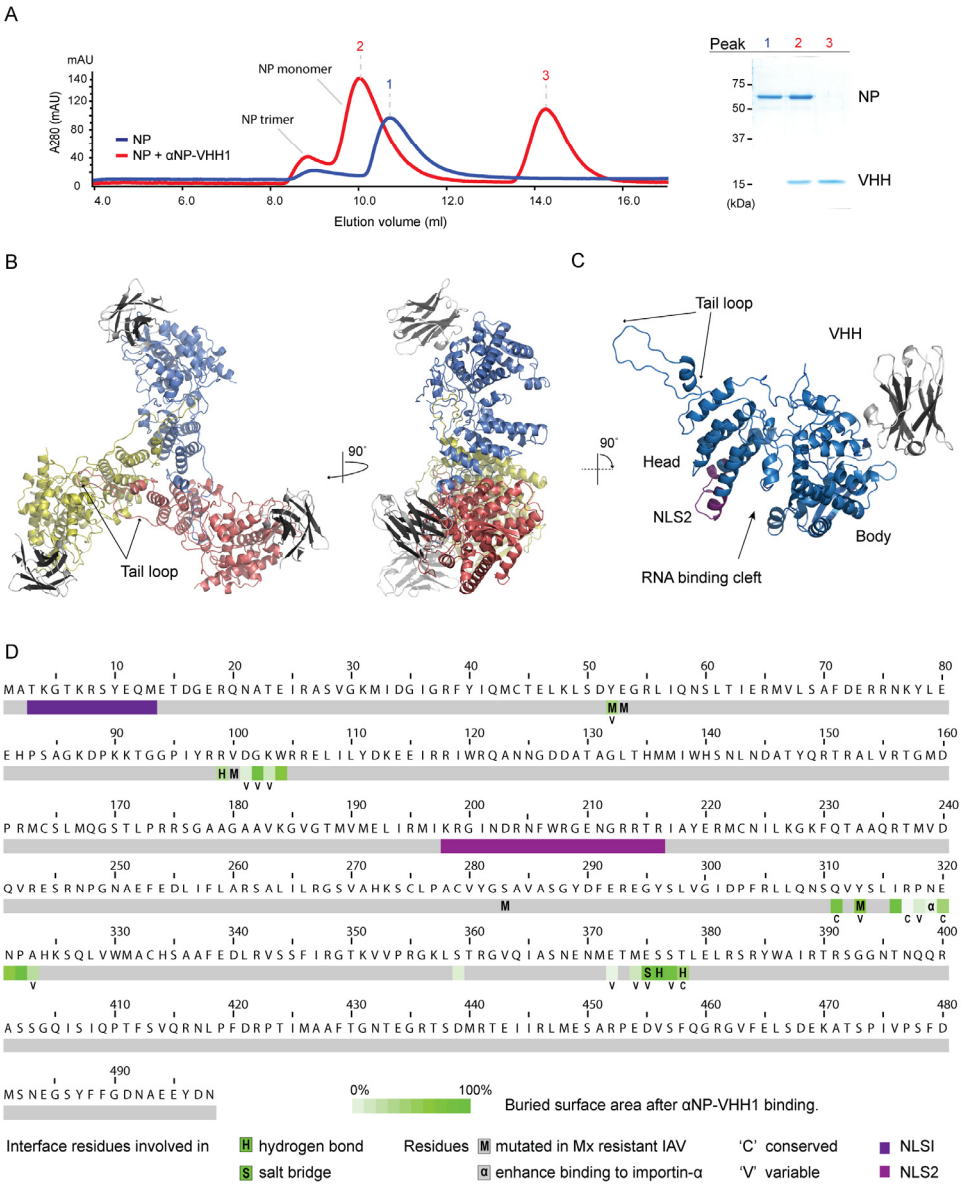

Figure 3 | αNP-VHH1 binds to the body domain of NP. **(A)** NP alone (blue), or preincubated with an excess of αNP-VHH1 (red), was subjected to size exclusion chromatography with a Superdex 200 column. Absorbance at 280 nm of the elution profile is displayed (left). Samples of the peak fractions 1, 2, and 3 were analyzed by SDS-PAGE and Coomassie staining (right). **(B,C)** Ribbon re-presentation of αNP-VHH1 in complex with NP. **(B)** The three assembled NP molecules that form the trimer are shown in yellow, red and blue, the VHH (gray) is bound opposite to the tail loop. **(C)** NP monomer bound by αNP-VHH1. NP subdomains, RNA binding cleft and NLS2 are indicated. NLS1 is disordered in the electron density maps and not shown. All illustrations were generated in PyMOL. **(D)** Sequence of influenza A/WSN/33 NP. The NP:αNP-VHH1 interface residues are shown in green. 'H' labels residues involved in hydrogen bonds and 'S' labels residues engaged in salt bridge at the αNP-VHH1 interface. Conserved interface residues are marked with a 'C' (conservation grades 8-9), variable interface residues with a 'V' (conservation grades 1-3) according to Kukol et al. (24). Unlabeled interface residues exhibit average conservation grades. The two nuclear localization sequences (NLS) of NP are shown in purple and magenta. Residues associated with sensitivity of influenza A to Mx proteins are indicated with an 'M' (31–33); residues enhancing importin-α binding with 'α' (25).

Table 1. Data collection and refinement statistics

Protein	Influenza A NP, αNP-VHH1 native
Organism	*Influenza A, Vicugna pacos*
PDB ID	5TJW
Data collection	
Space group	$P2_13$
a, b, c (Å)	137.548, 137.548, 137.548
α, β, γ (°)	90.0, 90.0, 90.0
Wavelength (Å)	0.9778
Resolution range (Å)	97.26 – 3.22 (3.34-3.22)*
Total reflections	132024
Unique reflections	14205
Completeness (%)	99.9 (100.0)
Redundancy	9.3 (7.9)
R_{sym} (%)	17.8 (100.0)
$R_{p.i.m.}$ (%)	6.6 (44.2)
I/σ	15.4 (2.1)
$CC_{1/2}$ (%)	99.6 (68.7)
Refinement	
Resolution range (Å)	97.26 – 3.23
R_{work} (%)	20.44
R_{free} (%)	26.16
Coordinate error (Å)	0.38
Number of Reflections	
Total	14189
R_{free} reflections	1419
Number of non-hydrogen atoms	4579
Protein atoms	4579
R.m.s. deviations	
Bond lengths (Å)	0.005
Bond angles (°)	0.633
Average B factors (Å^2)	
Protein	74.65
Ramachandran (%)	
Favored (%)	96.4
Allowed (%)	3.43
Outlier (%)	0.17
Clashscore	9.53
Molprobity score	1.74
Molprobity percentile	100th

*Values in brackets are for the highest resolution shell.

αNP-VHH1 binds a variable surface on NP associated with host adaptation

We identified the residues involved of the NP:αNP-VHH1 binding interface using PDBePISA (23). The VHH uses residues from all of its three complementary determining regions (CDRs) to interact with NP. On NP, αNP-VHH1 buries a total of 23 residues and an interface of 542 Å^2 (Fig 4A). The manner in which the VHH binds NP suggests that it exerts its antiviral properties due to the steric exclusion of potential NP binding partners, including viral or host proteins. The NP binding interface is dispersed over discontinuous elements of secondary structure, which explains why the VHH only binds to correctly folded, but not to denatured NP, for

example in immunoblots (data not shown). To validate that αNP-VHH1 engages NP at the determined binding site, we generated an E375R mutant of NP, showed that is expressed to wildtype levels, and confirmed that this mutation in the binding site results in a loss of αNP-VHH1 binding (Fig S1).

To analyze the possible extent of structural conservation of NP at the VHH binding interface, we evaluated conservation grades of the interface residues acquired by large-scale surveys of NP sequences (24). Kukol et al. determined conservation grade scores of NP residues using the ConSurf algorithm, which takes into account evolutionary relationships between protein sequences. None of interface residues are strictly conserved, only 17% were considered conserved, 43% variable and 39% received scores for an average degree of conservation. Part of the binding interface represents the largest cluster of variable residues on the otherwise rather conserved NP (Fig 4D). Despite binding to a variable region on NP, we confirmed binding of αNP-VHH1 to the commonly used laboratory strains WSN and PR8 (Fig S2).

Functional properties of NP are often investigated by mutagenesis or by analysis of naturally occurring, adaptive mutations. In agreement with their variable character, several of the 23 interface residues have been examined in the context of interspecies adaptation. These residues include Asn319, that enhances importin-α affinity (Fig 4C) and residues Tyr52, Asn101, Tyr313, Glu375 and Ser377, which undergo convergent changes in the process of adaptation from avian to human hosts (8, 25–30). In agreement with the similarity of viral inhibition between αNP-VHH1 and Mx proteins, the αNP-VHH1 binding interface overlaps with a cluster of residues (Tyr52, Glu53, Val100, Ser283, and Tyr313) (Fig 4B), whose mutation allows escape from Mx proteins (31–33).

Efforts to screen for small molecule antivirals that perturb the viral replication cycle have yielded a handful of inhibitors that target NP (34, 35). One of them, nucleozin, promotes cytosolic accumulation of incoming vRNPs. Two independent binding sites have been identified for nucleozin (35). One of the two binding sites, at residue Tyr52, overlaps with the αNP-VHH1 binding site (Fig 4E). The second nucleozin binding site, Try289/Asn309, is in close proximity of Tyr52 but is not masked by αNP-VHH1 and should therefore be accessible to the drug in the presence of αNP-VHH1. However, the proximity highlights the susceptibility of this NP surface to interference, and αNP-VHH1 may thus also help to better understand the inhibitory properties of nucleozin and its derivates.

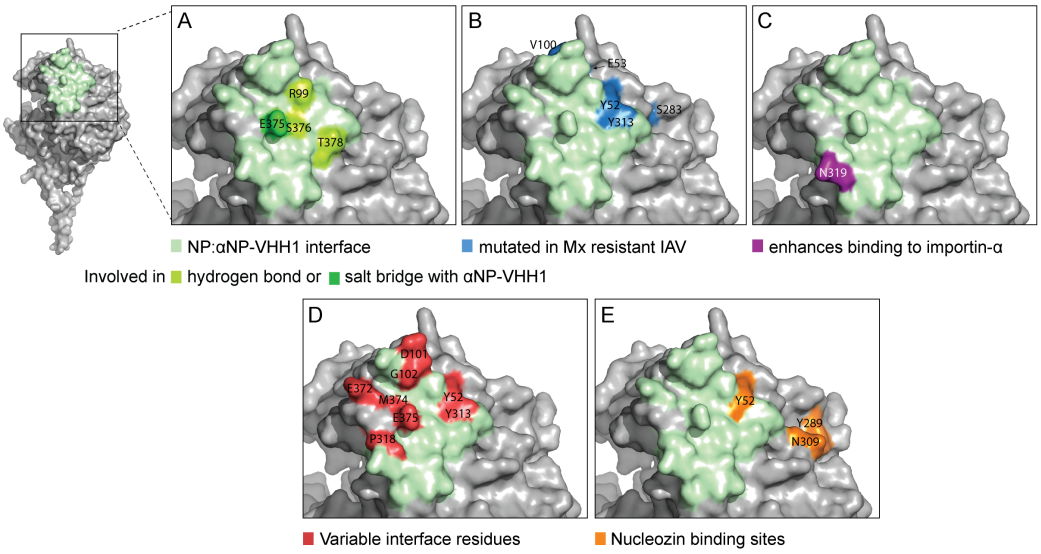

Figure 4 | The binding interface of NP and αNP-VHH1. Surface representation of an NP monomer with magnified view of the NP:αNP-VHH1 interface. **(A)** Residues involved in the interaction that are at least partially occluded upon VHH binding are shown in green. **(B)** Residues associated with sensitivity of influenza A to Mx proteins are shown in blue. **(C)** Residue that enhances binding to importin-α is shown in purple. **(D)** Variable interface residues that are part of the largest cluster of variable residues of NP according to Kukol et al. (24) are shown in red. **(E)** The two independent nucleozin binding sites are displayed in orange (34, 50).

The effects of αNP-VHH1 on vRNP integrity and nuclear import

None of the two characterized NLSs are in proximity of the αNP-VHH1 binding site (Figs 3C and 3D). Nuclear import of NP alone is unaffected by αNP-VHH1, whilenuclear import of incoming vRNPs is strongly inhibited (16, 17). Thus, the structure of the vRNP complex must be important for αNP-VHH1 to elicit its inhibitory function. To evaluate the general effect of αNP-VHH1 binding to vRNPs, we purified vRNPs from virions, added an excess of αNP-VHH1 or a control VHH, and analyzed the appearance of vRNPs by negative stain electron microscopy (EM). We did not detect gross differences between vRNPs complexed with αNP-VHH1, indicating that αNP-VHH1 does not disrupt the overall structure of the complex (Fig 5A). A typical VHH is 2 x 3.5 nm in size (36). Assuming that the VHH binds to the periphery of the vRNP, one would expect a slight increase of vRNP width. However, vRNPs examined in the presence of αNP-VHH1 exhibit a slightly reduced width (Fig 5B). Purified vRNPs often adopted a slightly curved shape. Upon addition of αNP-VHH1 we noted a trend for vRNPs to adopt curved shapes less frequently, but were unable to validate this tendency statistically.

To analyze the possible impact of αNP-VHH1 binding to vRNPs on a structural level, we examined the two available cryo-EM models of vRNPs (37, 38). While overall similar, both models differ in NP orientation and handedness. The binding interface for αNP-VHH1 is exposed in both models and should thus allow VHH binding. The right-handed helical model

of Moeller et al. is based on vRNPs purified from transiently transfected cells transcribing influenza genome segments and expressing NP and polymerase subunits (38). When superimposing our structure on this model, αNP-VHH1 blocks the major groove of the vRNP complex (Fig 5C), which would reduce the accessible surface of the vRNP and thus limit interactions of the vRNP with other viral and host proteins.

The vRNPs that were used for the left-handed helical model of Arranz et al. derive from purified virions and therefore more likely represent the incoming vRNPs encountered by αNP-VHH1 in the cytosol. Modeled onto this structure, αNP-VHH1 is positioned on the edge of the major groove without blocking it (Fig 5D). Instead, αNP-VHH1 slightly clashes with the head domain of the adjoining NP molecule. Considering the inherent structural flexibility of the NP tail loop and thus of vRNPs, this clash may not be all that detrimental. However, the necessary structural compensation might explain the slightly thinner vRNPs observed by EM and why some vRNPs appear less curved. Importantly, according to this model, αNP-VHH1 masks NLS2 of the adjacent NP protomer, providing a plausible explanation for the inhibition of vRNP nuclear import.

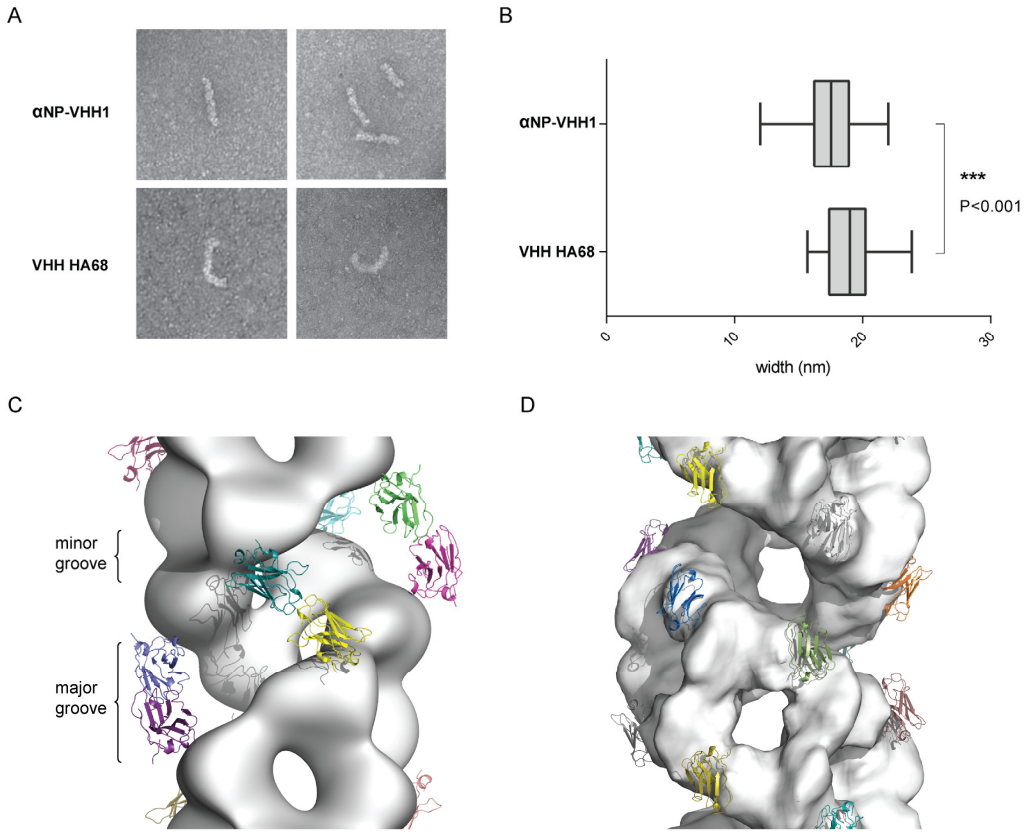

Figure 5 | αNP-VHH1 binding to vRNPs. (A) vRNPs purified from influenza A/PR/8/34 virions were treated with an excess of αNP-VHH1 or a control VHH (VHH HA68 against IAV HA (51)) and visualized by negative stain electron microscopy. **(B)** The width of vRNPs (n=28) was measured at two

positions using ImageJ. A two-tailed Student's t-test was performed to evaluate statistical significance. **(C,D)** Superposition of the NP:αNP-VHH1 structure on vRNP models from **(C)** Moeller et al. (PDB ID: 2YMN) and **(D)** Arranz et al. (PDB ID: 4BBL). Electron density is shown for both models and colored VHHs are located according to the NP orientation in the model.

Discussion

To identify new vulnerabilities in the life cycle of influenza A virus, we used cytosolically expressed single domain antibodies, also called VHHs, that target the nucleoprotein NP. To relate the inhibitory properties of αNP-VHH1 to the structural features it recognizes on NP, we determined its crystal structure of the VHH in complex with NP. The binding site of αNP-VHH1 overlaps with evolutionarily variable residues implicated in interactions with host proteins, including both a supporting (importin-α) and an antagonizing (Mx proteins) host factor. αNP-VHH1 exploits a surprisingly similar vulnerability as do the host's antiviral, interferon-induced Mx proteins.

The antiviral activity of Mx GTPases has long been recognized, first described as a restriction factor for influenza A virus (39). While there is consensus on the general antiviral activity of MxA/Mx1 as an entity that targets both the viral PB2 and NP, their exact mode of action has remained elusive. Several residues on NP alter viral susceptibility to Mx1 proteins, some of which are occluded by αNP-VHH1. Whether these residues directly alter affinity to Mx proteins has so far not been shown and no structure of an Mx protein in complex with NP has been reported. Because of possible alternative binding sites and affinities of Mx to momomeric NP versus NP assembled in vRNPs, these interactions might be difficult to show unambiguously. Our data show that occluding this surface on the NP body domain is sufficient to mimic the antiviral activity of Mx GTPases, suggesting that a direct interaction of Mx proteins with this surface is likely. The involvement of (an) additional, unknown factor(s) that contribute(s) to Mx activity cannot be excluded. However, we can conclude that targeting NP alone, and not PB2, is sufficient to mimic the effect of Mx proteins. Because of the structurally defined αNP-VHH1 binding site on NP, it is the ideal model protein to investigate possible antiviral mechanisms of Mx proteins.

Antiviral effects of Mx are dependent on GTPase activity in most settings (40). Mx proteins are known to form ring-like structures that -in the case of MxA- are thought to clasp around the incoming vRNPs to prevent nuclear import (41). Our VHHs lack any enzymatic activity and do not oligomerize, suggesting that high affinity binding may be sufficient for antiviral activity. Oligomerization and the resulting avidity effects may allow the same antiviral mechanism at lower affinity interactions between NP and Mx proteins. In the light of evolution, this may be advantageous for two reasons: (I) it allows a single Mx homolog to act as a potent broad-

spectrum effector that binds to multiple virus families with lower affinity. (II) if low affinity binding is sufficient for antiviral activity then it would be more difficult to escape from all Mx activity by antigenic drift.

Superposition of αNP-VHH1 on EM-based vRNP models showed that αNP-VHH1 could mask the NLS2 on adjoining NP molecules. Mx proteins might function in similar fashion and prevent vRNP interactions with host factors, including those important for nuclear import. Indeed, a crucial residue for host specificity that enhances binding to importin-α, Asn319, is found in the interface with αNP-VHH1. In addition, escape from Mx proteins with mutations in residues Val100, Ser283 and Tyr313 occurs at the expense of nuclear import efficiency (32).

Why this surface is important for nuclear import of vRNPs is unknown. Modeled on the vRNP structure from Arranz et al., our data showed the proximity of αNP-VHH1 to the NLS2 on an adjoining NP molecule, suggesting that VHH binding to vRNPs prevents importin binding to NLS2. It is conceivable that importin-α, when bound specifically to one NLS of NP, is stabilized by residues of the αNP-VHH1 interface, including Val100, Ser283, Tyr313 and Tyr319. However, the inherent flexibility and heterogeneity of the vRNP complexes presents a major challenge to prove this contention by structural means. Higher resolution structures of the vRNP complex, ideally complexed with host factors, are needed. The structure of αNP-VHH1 with NP might be of use in determining the exact orientation of NP and handedness of the helix in such higher order complexes by yielding more static templates for analysis.

The strength of intracellular VHHs as specific perturbants of protein function is their ability to mask specific structurally defined NP epitopes without prior manipulation of the virus by mutation. This approach is inherently limited by the ability of the virus to shut down host protein synthesis, including that of inhibitory VHHs. While we were able to circumvent these limitations using inducible VHH expression to some extent, cell-penetrating VHHs or other means of permeabilization that allow efficient delivery from extracellular space could also find application (42, 43). Such an approach would allow an evaluation of the importance of the blocked surface at later stages of infection and importantly, transform VHHs into discovery tools for antiviral agents suitable for therapeutic intervention.

Given the continued relevance of influenza virus as a serious health threat and its ability to rapidly acquire resistance against drugs or escape from immune responses that target HA, NA and M2, the more conserved influenza proteins including NP, may prove to be alternative targets for intervention. So far, we have developed more than 20 IAV NP specific VHHs that bind to at least four unique binding sites on NP (16, 17). Continued efforts in this direction might help to map more precisely the contributions of different NP surfaces to the influenza life cycle and inspire the development of novel antivirals. In conclusion, the crystal structure

of an inhibitory VHH in complex with NP uncovers a new vulnerability in the virus life cycle and may phenocopy mechanisms of actions of the cellular antiviral defense. The ease of expression and the capability of binding to common laboratory-adapted influenza strains, combined with our detailed molecular characterization of the binding site, make αNP-VHH1 a versatile tool to identify the specific contributions of this NP surface and of host factors that potentially compete with αNP-VHH1 for binding.

Supplementary Figures

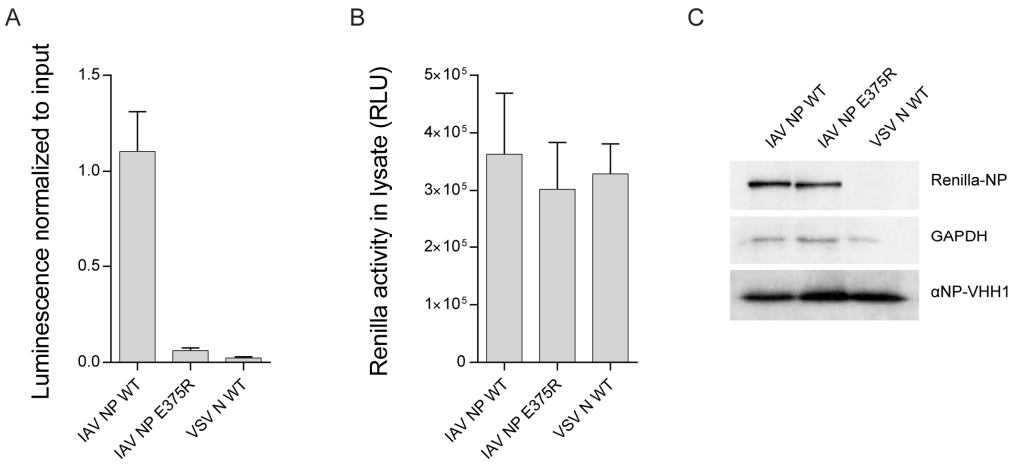

Figure S1 | NP mutation E375R abolishes αNP-VHH1 binding. αNP-VHH1 and Renilla luciferase fusions of influenza A/WSN/33 NP wild type (WT) or E375R, or vesicular stomatitis virus N, were transiently co-expressed in 293T cells. Cell lysates were incubated in 96-well plates coated with anti-HA antibody to capture the VHHs. **(A)** Activity of the co-purified luciferase was measured. Emitted light was normalized to luciferase activity in the lysate. **(B)** Renilla activity of the Renilla-NP/N fusion proteins in cell lysates shown as relative light units (RLU) emitted. Data in **(A)** and **(B)** are from three independent experiments (±s.e.m.). **(C)** Lysates from cells transfected as above were subjected to immunoblot analysis using αNP, αGAPDH and αHA-tag (VHH-HA) antibodies.

Figure S2 | αNP-VHH1 stains NP in cells infected with WSN and PR8 strains. A549 cells were infected with influenza A/WSN/33 or A/PR/8/34 and harvested 6 hours post infection. Cell were fixed, permeabilized, stained with αNP-VHH1-AlexaFlour647 and analyzed by flow cytometry.

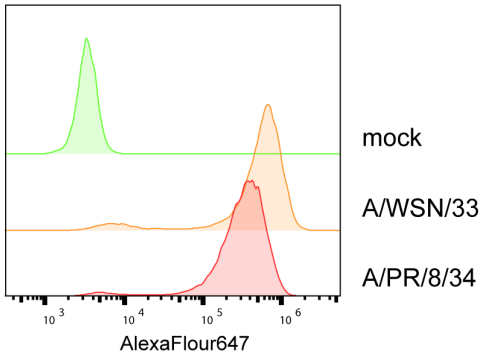

Material and Methods

Virus

Influenza A/WSN/33 used for infection experiments was propagated and titrated on MDCK cells. Infections were performed in DMEM with 0.3% BSA for 1 h at 37° C. vRNPs were purified from influenza A/PR/8/34 virions purchased from Charles River Laboratories.

Cell lines

Human HEK 293T cells and dog MDCK cells were obtained from ATCC and grown in DME with 10% FBS. The A549 cell line inducible expressing αNP-VHH1-HA, derived from A549 cells obtained from ATCC, was described earlier (16), and was cultivated in DME with 10% FBS and 500 µg/ml G418.

Reagents

Doxycycline hyclate (Dox) was purchased from Sigma Aldrich. Nickel-nitrilotriacetic acid (NTA) beads were purchased from Qiagen. Mouse anti-HA.11 (clone 16B12) coupled to Alexa Fluor (AF) 488 was purchased from Life Technologies. Mouse anti-HA.11 (clone 16B12) was acquired from BioLegend. VHHs either coupled to Alexa Fluor (AF) 647 or 5-carboxytetramethylrhodamine (TAMRA) were generated using sortase A as described earlier (44). Hybridoma cells secreting mouse monoclonal anti-IAV NP (clone H16-L10-4R5 ATCC HB-65) were obtained from ATTC and antibodies in the supernatant were purified using a protein G column.

Infection Assay

To analyze the effect of αNP-VHH1 expressed at different times during infection, A549 cells inducibly expressing the VHH were infected with A/WSN/33 at an MOI of 1. VHH expression was induced at the indicated time points relative to infection with 1 µg/ml doxycycline (final concentration). 6 hours post infection, cells were trypsinized, fixed in 4% PFA, permeabilized with 0.1% saponin and stained with anti-HA-AF488 and αNP-VHH2-AF647. Fraction of infected cells (NP) and geometric mean fluorescence intensity (VHH-HA) were quantified by flow cytometry using a BD Accuri and the FlowJo software package.

Titration of released virus

To quantify release of progeny virus from cells expressing αNP-VHH1, A549 cells inducibly expressing the VHH were infected with A/WSN/33 at an MOI of 1 in the presence of TPCK trypsin. VHH expression was induced at the indicated time points relative to infection with 1 µg/ml doxycycline (final concentration). 24 hours post infection, supernatants were collected, filtered, diluted in a 2-fold dilution series, and used to infect MDCK cells for 1 hour at 37° C. The inoculum was replaced with DME, 0.35% BSA and 1.5% carboxymethyl cellulose in the

absence of trypsin to avoid spreading of the virus. After 24 hours, cells were fixed in 4% PFA, permeabilized with 0.1% saponin in PBS, 2% BSA and stained with DAPI and αNP-VHH2-TAMRA. Fluorescence images of the MDCK monolayer were acquired using a Cytation 3 Cell Imaging Multi-Mode Reader (BioTek); infected cells (nuclei) were quantified using CellProfiler (45).

Influenza polymerase reconstitution assay

To assess influenza polymerase activity, 293T cells were transiently transfected with 200 ng of pCAGGS NP and 50 ng of pCAGGS PB1, pCAGGS PB2 and pCAGGS PA. To provide an artificial genome segment, 50 ng of pPolI-RT plasmid was co-transfected, from which an artificial genome segment was transcribed that contained the NA untranslated regions and encoded either for EGFP or mCherry-2TA-EGFP. 150 ng of pCAGGS vector encoding for αNP-VHH1, VHH7 (α-murine-MHCII) or pCDNA3.1 encoding for MxA or Mx1 were additionally co-transfected where indicated. All transfections were performed using Lipofectamine 2000. 24 hours post transfection, cells were trypsinized and the fraction of EGFP positive cells was quantified by flow cytometry using a BD Accuri.

Protein expression and purification

The sequence encoding αNP-VHH1 with a C-terminal sortase recognition site (LPETG) followed by a His-tag was cloned into a pHEN6 expression vector for periplasmic expression. *E.coli* WK6 bacteria were transformed with the vector and expression was induced with 1 mM IPTG at OD600=0.6; cells were grown overnight at 30° C. The VHH was retrieved from the periplasm by osmotic shock and purified by Ni-NTA affinity purification and size-exclusion chromatography on a Superdex 75 column.

NP from influenza virus A/WSN/33 with a C-terminal His-tag was cloned into the pET30 expression vector. *E. coli* BL21 (DE3) bacteria were transformed and grown in Terrific Broth at 37° C until OD600=0.5 and at 25° C until OD600=0.6. Protein expression was induced with 1 mM IPTG at OD600=0.6 and cells were grown for an additional 3 h at 25° C. Bacteria pellet were resuspended in 25 mM Tris/HCl pH 7.5, 1 M NaCl, 0.2% NP-40, 10 units/ml benzonase and 0.1 mg/ml lysozyme. Cells were lysed by sonication and NP was purified on Ni-NTA agarose, Mono S ion exchange and Superdex 200 size-exclusion columns.

Crystallization

For co-crystallization, purified αNP-VHH1 was mixed in a 3:1 molar ratio with recombinant NP and purified by size-exclusion on a Superdex 200 column. Both, tri- and monomeric peaks were collected and VHH binding was confirmed by SDS-PAGE and Coomassie staining. The complex was concentrated to 4 mg/ml in 20 mM Tris/HCl pH 7.5, 200 mM NaCl buffer using a protein concentrator. Initial crystal growth was observed in 0.1 M sodium acetate, 1.5 M

ammonium sulfate in a vapor diffusion experiment in a 96-well sitting drop setup (Procomplex, Qiagen) at 18° C. Crystal growth was optimized with 0.025% (v/v) dichloromethane and diffraction quality crystals were grown in a 24-well vapor diffusion hanging drop set up. Crystals were cryoprotected in 20% glycerol and flash frozen in liquid nitrogen.

Data processing and structure determination

Datasets were collected at the Advanced Photon Source user end station 24-IDC. Data reduction was performed in HKL2000(46). Molecular replacement (MR) was performed in the PHENIX suite using *PhaserMR* (47). As a MR model for NP we used PDB ID: 2IQH (NP) (1) and PDB ID: 4KRL (VHH) (21). Refinement was performed using *phenix.refine* and the model was built in *coot* (48).

Purification of vRNPs and electron microscopy

vRNPs were isolated and purified from IAV PR8 virions as described elsewhere (49). In brief, influenza A/PR/8/34 was concentrated and virions where lysed in 100 mM KCl, 5 mM $MgCl_2$, 5% (w/v) glycerol, 50 mM octylglucoside, 10 mg/ml lysolecithin, 1.5 mM dithiothreitol, 100 mM MES pH 5.5. vRNPs were then separated from other viral proteins on a glycerol gradient and concentrated. vRNPs were treated with an excess αNP-VHH1 or the control VHH in 50 mM Tris/HCl pH 7.5, 150 mM NaCl, and subsequently stained with 2% uranyl acetate. Electron micrographs were recorded with a FEI Tecnai Spirit Bio-Twin and images were analyzed with imageJ.

LUMIER assay

To analyze binding of VHHs to wildtype and mutant versions of IAV NP, we applied LUMIER assays as described in detail before (17). 293T cells were co-transfected with pCAGGS αNP-VHH1-HA and wildtype or mutant E375R pEXPR NP-Renilla (derived from NP of influenza A/WSN/33) or pEXPR VSV-N-Renilla using Lipofectamine 2000. 24 h post transfection, cells were lysed and incubated in LUMITRAC 600 96-well plates (Greiner) coated with anti-HA.11 antibody to capture the VHH. Activity of the co-purified luciferase was quantified by addition of coelenterazine-containing Renilla luciferase substrate mix (BioLux Gaussia Luciferase Assay Kit, New England BioLabs) and light emission measured using a SpectraMax M3 microplate reader (Molecular Devices).

References

1. **Ye Q**, **Krug RM**, **Tao YJ**. 2006. The mechanism by which influenza A virus nucleoprotein forms oligomers and binds RNA. Nature **444**:1078–1082.
2. **Noton SL**, **Medcalf E**, **Fisher D**, **Mullin AE**, **Elton D**, **Digard P**. 2007. Identification of the domains of the influenza A virus M1 matrix protein required for NP binding, oligomerization and incorporation into virions. J Gen Virol **88**:2280–2290.

3. **Biswas SK**, **Boutz PL**, **Nayak DP**. 1998. Influenza virus nucleoprotein interacts with influenza virus polymerase proteins. J Virol **72**:5493–5501.

4. **Nakada R**, **Hirano H**, **Matsuura Y**. 2015. Structure of importin-alpha bound to a non-classical nuclear localization signal of the influenza A virus nucleoprotein. Sci Rep **5**:15055.

5. **Elton D**, **Simpson-holley M**, **Archer K**, **Hallam R**, **Mccauley J**, **Digard P**, **Medcalf LIZ**, **Cauley JMC**. 2001. Interaction of the Influenza Virus Nucleoprotein with the Cellular CRM1-Mediated Nuclear Export Pathway Interaction of the Influenza Virus Nucleoprotein with the Cellular CRM1-Mediated Nuclear Export Pathway. J Virol **75**:408–419.

6. **Momose F**, **Basler CF**, **Neill REO**, **Iwamatsu A**, **Palese P**, **Nagata K**. 2001. Cellular Splicing Factor RAF-2p48 / NPI-5 / BAT1 / UAP56 Interacts with the Influenza Virus Nucleoprotein and Enhances Viral RNA Synthesis. J Virol **75**:1899–1908.

7. **Zimmermann P**, **Manz B**, **Haller O**, **Schwemmle M**, **Kochs G**. 2011. The viral nucleoprotein determines Mx sensitivity of influenza A viruses. J Virol **85**:8133–8140.

8. **Gabriel G**, **Klingel K**, **Otte A**, **Thiele S**, **Hudjetz B**, **Arman-Kalcek G**, **Sauter M**, **Shmidt T**, **Rother F**, **Baumgarte S**, **Keiner B**, **Hartmann E**, **Bader M**, **Brownlee GG**, **Fodor E**, **Klenk H-D**. 2011. Differential use of importin-α isoforms governs cell tropism and host adaptation of influenza virus. Nat Commun **2**:156.

9. **Wang P**, **Palese P**, **O'Neill RE**. 1997. The NPI-1/NPI-3 (karyopherin alpha) binding site on the influenza a virus nucleoprotein NP is a nonconventional nuclear localization signal. J Virol **71**:1850–6.

10. **Weber F**, **Kochs G**, **Gruber S**, **Haller O**. 1998. A classical bipartite nuclear localization signal on Thogoto and influenza A virus nucleoproteins. Virology **250**:9–18.

11. **Turrell L**, **Lyall JW**, **Tiley LS**, **Fodor E**, **Vreede FT**. 2013. The role and assembly mechanism of nucleoprotein in influenza A virus ribonucleoprotein complexes. Nat Commun **4**:1591.

12. **Ye Q**, **Guu TSY**, **Mata DA**, **Kuo RL**, **Smith B**, **Krug RM**, **Tao YJ**. 2013. Biochemical and structural evidence in support of a coherent model for the formation of the double-helical influenza a virus ribonucleoprotein. MBio **4**:e00467-12.

13. **Martin K**, **Helenius a.** 1991. Nuclear transport of influenza virus ribonucleoproteins: The viral matrix protein (M1) promotes export and inhibits import. Cell **67**:117–130.

14. **Pavlovic J**, **Haller O**, **Staeheli P**. 1992. Human and mouse Mx proteins inhibit different steps of the influenza virus multiplication cycle. J Virol **66**:2564–9.

15. **Xiao H**, **Killip MJ**, **Staeheli P**, **Randall RE**, **Jackson D**. 2013. The Human Interferon-Induced MxA Protein Inhibits Early Stages of Influenza A Virus Infection by Retaining the Incoming Viral Genome in the Cytoplasm. J Virol **87**:13053–13058.

16. **Ashour J**, **Schmidt FI**, **Hanke L**, **Cragnolini J**, **Cavallari M**, **Altenburg A**, **Brewer R**, **Ingram J**, **Shoemaker C**, **Ploegh HL**. 2015. Intracellular Expression of Camelid Single-Domain Antibodies Specific for Influenza Virus Nucleoprotein Uncovers Distinct Features of Its Nuclear Localization. J Virol **89**:2792–2800.

17. **Schmidt FI**, **Hanke L**, **Morin B**, **Brewer R**, **Brusic V**, **Whelan SPJ**, **Ploegh HL**. 2016. Phenotypic lentivirus screens to identify functional single domain antibodies. Nat Microbiol **1**:16080.

18. **Noah DL**, **Twu KY**, **Krug RM**. 2003. Cellular antiviral responses against influenza A virus are countered at the posttranscriptional level by the viral NS1A protein via its binding to a cellular protein required for the 3' end processing of cellular pre-mRNAS. Virology **307**:386–395.

19. **Tarus B**, **Bakowiez O**, **Chenavas S**, **Duchemin L**, **Estrozi LF**, **Bourdieu C**, **Lejal N**, **Bernard J**, **Moudjou M**, **Chevalier C**, **Delmas B**, **Ruigrok RWH**, **Di Primo C**, **Slama-Schwok A**. 2012. Oligomerization paths of the nucleoprotein of influenza A virus. Biochimie **94**:776–785.

20. **Shen Y-F**, **Chen Y-H**, **Chu S-Y**, **Lin M-I**, **Hsu H-T**, **Wu P-Y**, **Wu C-J**, **Liu H-W**, **Lin F-Y**, **Lin G**, **Hsu P-H**, **Yang A-S**, **Cheng Y-SE**, **Wu Y-T**, **Wong C-H**, **Tsai M-D**. 2011. E339…R416 salt bridge of nucleoprotein as a feasible target for influenza virus inhibitors. Proc Natl Acad Sci **108**:16515–16520.

21. **Schmitz KR**, **Bagchi A**, **Roovers RC**, **Van Bergen En Henegouwen PMP**, **Ferguson KM**. 2013. Structural evaluation of EGFR inhibition mechanisms for nanobodies/VHH domains. Structure **21**:1214–1224.

22. **Ng AK**, **Zhang H**, **Tan K**, **Li Z**, **Liu JH**, **Chan PK**, **Li SM**, **Chan WY**, **Au SW**, **Joachimiak A**, **Walz T**, **Wang JH**, **Shaw PC**. 2008. Structure of the influenza virus A H5N1 nucleoprotein: implications for RNA binding, oligomerization, and vaccine design. Faseb J **22**:3638–3647.

23. **Krissinel E**, **Henrick K**. 2007. Inference of Macromolecular Assemblies from Crystalline State. J Mol Biol **372**:774–797.

24. **Kukol A**, **Hughes DJ**. 2014. Large-scale analysis of influenza A virus nucleoprotein sequence conservation reveals potential drug-target sites. Virology **454**–**455**:40–47.

25. **Gabriel G**, **Herwig A**, **Klenk HD**. 2008. Interaction of polymerase subunit PB2 and NP with importin α1 is a determinant of host range of influenza A virus. PLoS Pathog **4**:e11.

26. **Tamuri AU**, **Dos Reis M**, **Hay AJ**, **Goldstein RA**. 2009. Identifying changes in selective constraints: Host shifts in influenza. PLoS Comput Biol **5**.

27. **Naffakh N**, **Massin P**, **Escriou N**, **Crescenzo-Chaigne B**, **Van Der Werf S**. 2000. Genetic analysis of the compatibility between polymerase proteins from human and avian strains of influenza A viruses. J Gen Virol **81**:1283–1291.

28. **Miotto O**, **Heiny AT**, **Albrecht R**, **García-Sastre A**, **Tan TW**, **August JT**, **Brusic V**. 2010. Complete-proteome mapping of human influenza A adaptive mutations: Implications for human transmissibility of zoonotic strains. PLoS One **5**.

29. **Allen JE**, **Gardner SN**, **Vitalis E a**, **Slezak TR**. 2009. Conserved amino acid markers from past influenza pandemic strains. BMC Microbiol **9**:77.

30. **Finkelstein DB**, **Mukatira S**, **Mehta PK**, **Obenauer JC**, **Su X**, **Webster RG**, **Naeve CW**. 2007. Persistent host markers in pandemic and H5N1 influenza viruses. J Virol **81**:10292–10299.

31. **Riegger D**, **Hai R**, **Dornfeld D**, **Mänz B**, **Leyva-Grado V**, **Sánchez-Aparicio MT**, **Albrecht R a**, **Palese P**, **Haller O**, **Schwemmle M**, **García-Sastre A**, **Kochs G**, **Schmolke M**. 2014. The nucleoprotein of newly emerged H7N9 influenza A virus harbors a unique motif conferring resistance to antiviral human MxA. J Virol **89**:2241–2252.

32. **Gotz V**, **Magar L**, **Dornfeld D**, **Giese S**, **Pohlmann a**, **Hoper D**, **Kong BW**, **Jans D a**, **Beer M**, **Haller O**, **Schwemmle M**. 2016. Influenza A viruses escape from MxA

restriction at the expense of efficient nuclear vRNP import. Sci Rep **6**:23138.

33. **Mänz B**, **Dornfeld D**, **Götz V**, **Zell R**, **Zimmermann P**, **Haller O**, **Kochs G**, **Schwemmle M**. 2013. Pandemic Influenza A Viruses Escape from Restriction by Human MxA through Adaptive Mutations in the Nucleoprotein. PLoS Pathog **9**:e1003279.

34. **Kao RY**, **Yang D**, **Lau L-S**, **Tsui WHW**, **Hu L**, **Dai J**, **Chan M-P**, **Chan C-M**, **Wang P**, **Zheng B-J**, **Sun J**, **Huang J-D**, **Madar J**, **Chen G**, **Chen H**, **Guan Y**, **Yuen K-Y**. 2010. Identification of influenza A nucleoprotein as an antiviral target. Nat Biotechnol **28**:600–5.

35. **Gerritz SW**, **Cianci C**, **Kim S**, **Pearce BC**, **Deminie C**, **Discotto L**, **McAuliffe B**, **Minassian BF**, **Shi S**, **Zhu S**, **Zhai W**, **Pendri A**, **Li G**, **Poss MA**, **Edavettal S**, **McDonnell PA**, **Lewis HA**, **Maskos K**, **Mörtl M**, **Kiefersauer R**, **Steinbacher S**, **Baldwin ET**, **Metzler W**, **Bryson J**, **Healy MD**, **Philip T**, **Zoeckler M**, **Schartman R**, **Sinz M**, **Leyva-Grado VH**, **Hoffmann H-H**, **Langley DR**, **Meanwell NA**, **Krystal M**. 2011. Inhibition of influenza virus replication via small molecules that induce the formation of higher-order nucleoprotein oligomers. Proc Natl Acad Sci U S A **108**:15366–71.

36. **Mujić-Delić A**, **De Wit RH**, **Verkaar F**, **Smit MJ**. 2014. GPCR-targeting nanobodies: Attractive research tools, diagnostics, and therapeutics. Trends Pharmacol Sci **35**:247–255.

37. **Arranz R**, **Coloma R**, **Chichon FJ**, **Conesa JJ**, **Carrascosa JL**, **Valpuesta JM**, **Ortin J**, **Martin-Benito J**. 2012. The structure of native influenza virion ribonucleoproteins. Science (80-) **338**:1634–1637.

38. **Moeller A**, **Kirchdoerfer RN**, **Potter CS**, **Carragher B**, **Wilson I a**. 2012. Organization of the influenza virus replication machinery. Science **338**:1631–4.

39. **Lindenmann J**, **Lane C a**, **Hobson D**. 1963. the Resistance of a2G Mice To Myxoviruses. J Immunol **90**:942–951.

40. **Verhelst J**, **Hulpiau P**, **Saelens X**. 2013. Mx proteins: antiviral gatekeepers that restrain the uninvited. Microbiol Mol Biol Rev **77**:551–66.

41. **Verhelst J**, **Parthoens E**, **Schepens B**, **Fiers W**, **Saelens X**. 2012. Interferon-inducible protein Mx1 inhibits influenza virus by interfering with functional viral ribonucleoprotein complex assembly. J Virol **86**:13445–55.

42. **Bruce VJ**, **Lopez-Islas M**, **McNaughton BR**. 2016. Resurfaced cell-penetrating nanobodies: A potentially general scaffold for intracellularly targeted protein discovery. Protein Sci **25**:1129–1137.

43. **Jittavisutthikul S**, **Thanongsaksrikul J**, **Thueng-In K**, **Chulanetra M**, **Srimanote P**, **Seesuay W**, **Malik AA**, **Chaicumpa W**. 2015. Humanized-VHH transbodies that inhibit HCV protease and replication. Viruses **7**:2030–2056.

44. **Guimaraes CP**, **Witte MD**, **Theile CS**, **Bozkurt G**, **Kundrat L**, **Blom AEM**, **Ploegh HL**. 2013. Site-specific C-terminal and internal loop labeling of proteins using sortase-mediated reactions. Nat Protoc **8**:1787–99.

45. **Kamentsky L**, **Jones TR**, **Fraser a**, **Bray M a**, **Logan DJ**, **Madden KL**, **Ljosa V**, **Rueden C**, **Eliceiri KW**, **Carpenter a E**. 2011. Improved structure, function and compatibility for Cell Profiler: modular high-throughput image analysis software. Bioinformatics **27**:1179–1180.

46. **Otwinowski Z**, **Minor W**. 1997. Processing of X-ray diffraction data collected in

oscillation mode. Methods Enzymol **276**:307–326.

47. **Adams PD**, **Afonine P V.**, **Bunkóczi G**, **Chen VB**, **Davis IW**, **Echols N**, **Headd JJ**, **Hung LW**, **Kapral GJ**, **Grosse-Kunstleve RW**, **McCoy AJ**, **Moriarty NW**, **Oeffner R**, **Read RJ**, **Richardson DC**, **Richardson JS**, **Terwilliger TC**, **Zwart PH**. 2010. PHENIX: A comprehensive Python-based system for macromolecular structure solution. Acta Crystallogr Sect D Biol Crystallogr **66**:213–221.

48. **Emsley P**, **Lohkamp B**, **Scott WG**, **Cowtan K**. 2010. Features and development of Coot. Acta Crystallogr Sect D Biol Crystallogr **66**:486–501.

49. **Wu WWH**, **Weaver LL**, **Panté N**. 2009. Purification and visualization of influenza a viral ribonucleoprotein complexes. J Vis Exp 5–7.

50. **Pang B**, **Cheung NN**, **Zhang W**, **Dai J**, **Kao RY**, **Zhang H**, **Hao Q**. 2016. Structural Characterization of H1N1 Nucleoprotein-Nucleozin Binding Sites. Sci Rep **6**:29684.

51. **Dougan SK**, **Ashour J**, **Karssemeijer R a**, **Popp MW**, **Avalos AM**, **Barisa M**, **Altenburg AF**, **Ingram JR**, **Cragnolini JJ**, **Guo C**, **Alt FW**, **Jaenisch R**, **Ploegh HL**. 2013. Antigen-specific B-cell receptor sensitizes B cells to infection by influenza virus. Nature **503**:406–9.

Chapter 4

Phenotypic Lentivirus Screens to Identify Functional Single-Domain Antibodies

Nature Microbiology, June 2016

Florian I. Schmidt[1], **Leo Hanke**[1], Benjamin Morin[2], Rebeccah Brewer[1], Vesna Brusic[2], Sean P.J. Whelan[2], and Hidde L. Ploegh[1,3]

[1]Whitehead Institute for Biomedical Research, Cambridge, Massachusetts

[2]Department of Microbiology and Immunobiology, Harvard Medical School, Boston, Massachusetts

[3]Department of Biology, Massachusetts Institute of Technology, Cambridge, Massachusetts

Abstract

Manipulation of proteins is key in assessing their *in vivo* function. While genetic ablation is straightforward, reversible and specific perturbation of protein function remains a challenge. Single domain antibody fragments, such as camelid-derived VHHs, can serve as inhibitors or activators of intracellular protein function, but functional testing of identified VHHs is laborious. To address this challenge, we developed a lentiviral screening approach to identify VHHs that elicit a phenotype when expressed intracellularly. We identified 19 antiviral VHHs that protect human A549 cells from lethal infection with influenza A virus (IAV) or vesicular stomatitis virus (VSV), respectively. Both negative-sense RNA viruses are vulnerable to VHHs uniquely specific for their respective nucleoproteins. Antiviral VHHs prevented nuclear import of viral ribonucleoproteins or mRNA transcription, respectively, and may provide clues for novel antiviral reagents. In principle, the screening approach described here should be applicable to identify inhibitors of any pathogen or biological pathway.

Introduction

To identify proteins essential to a biological pathway, small molecule inhibitors or activators may be used to manipulate protein function transiently. Alternatively, screens involving mutagenesis, a reduction in levels or complete elimination of gene products are common (1, 2). As applied to mammalian cells, these methods usually seek to achieve the removal of a protein from its normal biological context. Many proteins are multi-functional, or are components of multi-subunit complexes. Depletion of any single component may cause unexpected phenotypes due to the collapse of entire protein complexes. Small molecule inhibitors often lack specificity (3) and at best can target a fraction of all proteins of interest. The screening of chemically diverse libraries must be paired with sophisticated methods to identify the molecular targets of any hit identified. Antibodies have been used as intracellular perturbants of protein function after microinjection (4) or cytosolic expression of single chain variable antibody fragments (5), but technical challenges have limited their application to few selected cases.

In addition to conventional antibodies, the immune system of camelids generates heavy chain-only antibodies (6). Their antigen binding site only consists of the variable domain of the heavy chain. This domain can be expressed on its own and is referred to as a VHH or nanobody, an entity that can retain its function in the reducing environment of the cytosol and independent of glycosylation (7). Many VHHs bind to their targets with affinities comparable to conventional antibodies. VHHs expressed in the cytosol can therefore act as molecular perturbants by occluding interfaces involved in protein-protein interactions, by binding in the active sites of enzymes, or through recognition or stabilization of distinct conformations of their targets (8, 9). Both phage and yeast display, as well as mass spectrometry in combination with high throughput sequencing, allow the identification of VHHs based on their binding properties (10–12). Still, the identification of inhibitory VHHs remains a time-consuming process. VHHs obtained through biochemical screening methods must be expressed individually in the relevant cell type to test for the functional consequences of VHH expression. To address this challenge, we developed a phenotypic VHH screening method in living cells.

Results

A functional VHH screen identifies VHHs that block IAV or VSV infection

To identify VHHs that perturb or modulate protein function in living cells, we established a lentiviral screening strategy in which cells are selected based on the phenotype elicited by the VHHs expressed intracellularly. In two independent screens, we have identified VHHs that protect human A549 cells from lethal infection with influenza A virus (IAV) and vesicular

stomatitis virus (VSV), negative-sense RNA viruses that replicate in the nucleus and cytosol, respectively.

We immunized two alpacas with inactivated IAV and VSV, isolated peripheral blood lymphocytes, extracted RNA, and amplified VHH coding sequences by PCR using VHH-specific primers (Fig. 1). VHH coding sequences were cloned into a lentiviral vector that allows their expression under a doxycycline (Dox)-inducible promoter in transduced cells. VSV G-pseudotyped lentivirus was produced in 293T cells and used to transduce A549 cells with a multiplicity of infection (MOI) of 0.25 to ensure that, on average, cells were infected by a single lentivirus. Based on the expression of the selection marker neomycin phosphotransferase II, we determined the transduction rate to be 33% in the IAV screen and 55% in the VSV screen, indicating that 81 and 65% of the cells were expected to be transduced with a single lentivirus (assuming a Poisson distribution). Following the induction of VHH expression by Dox treatment, the pool of cells was challenged with a lethal dose of IAV (MOI 13) or VSV (MOI 4.5). To increase the stringency of the selection procedure, cells were trypsinized two days post infection because infected cells can stay adherent to tissue culture dishes but do not usually reattach once removed by trypsin treatment. To prevent continuous superinfection with VSV produced by non-VHH protected cells, ammonium chloride was added to the media for the first three days to prevent the endosomal acidification required for VSV G-mediated virus fusion. Survivors that adhered after trypsinization were grown under carboxymethyl cellulose overlays to prevent diffusion and further spread of VSV. Such precautions were not necessary for the IAV screen, since progeny IAV produced by A549 cells is not infectious unless HA is cleaved by trypsin or other proteases. Cells that survived the virus challenge were cultured for 3-4 weeks and cells were collected as individual colonies, expanded and analyzed.

Each clone of surviving cells was tested individually in a single-round, flow cytometry-based, infection assay in the absence or presence of Dox to see whether infection was blocked by VHH expression. Of 257 of the cell clones obtained from the IAV screen, 166 showed a Dox-dependent reduction of infection by at least 40% (Fig. 2a). In the majority of clones (132), VHH expression reduced infection by more than 80%. 143 of the 282 cell clones obtained from the VSV screen exhibited a Dox-dependent reduction of infection by more than 40%, most of them (127) by more than 80%. A substantial fraction of cell clones that did not meet the hit criteria could no longer be infected even in the absence of Dox, which we attribute to leaky expression of the VHH in the absence of induction, or due to the selection of cell clones that were resistant to infection by genetic abnormalities. We did not pursue these clones further. Anti-viral activity of identified VHHs

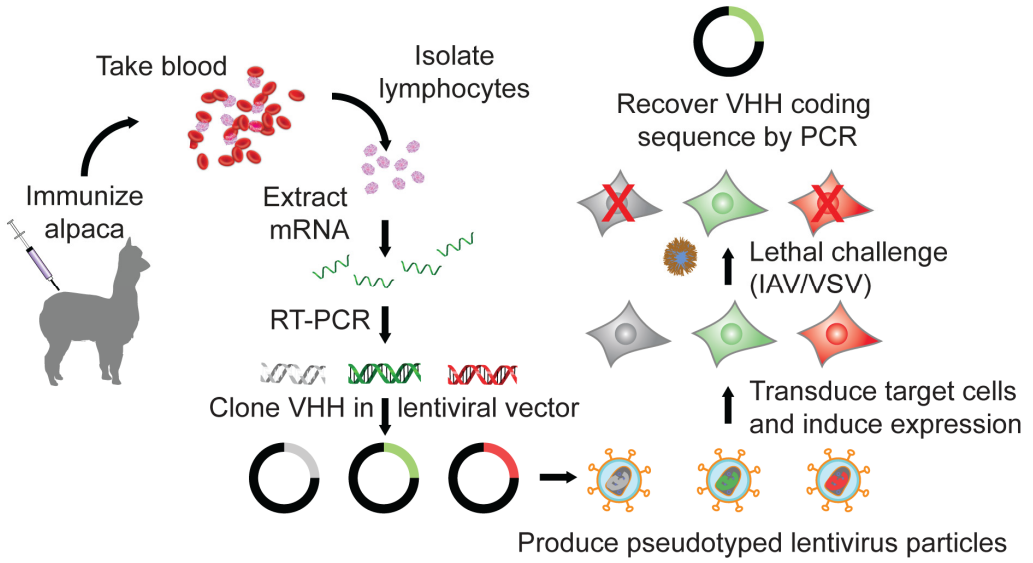

Figure 1 | Lentiviral screening approach. Alpacas are immunized with the desired antigen mix (here: inactivated influenza A virus, IAV, and vesicular stomatitis virus, VSV). After repeated immunizations, we draw a blood sample, purify lymphocytes, extract mRNA, reversely transcribe RNA to cDNA, amplify VHH coding sequences and clone them into a lentiviral vector. Alternatively, VHH coding sequences can be subcloned from an existing VHH library. 293T cells are transfected with the lentiviral library as well as packaging vectors, and lentivirus is harvested from the supernatant 2 days later. We transduce the cell line of interest (here: A549 cells) and induce VHH expression with doxycycline. Cells are then subjected to a selection assay that allows identification of cells expressing the desired VHHs (here: survival of a lethal infection with IAV or VSV). Finally, we prepared genomic DNA from selected (surviving) cells, amplified the VHH sequences by PCR and determined the VHH sequence encoded.

For each of the hits, representative monoclonal cell lines obtained in the screen were further characterized. Cells were infected with IAV and VSV in the absence and presence of Dox (Fig. 3). As a positive control, we used cell lines that inducibly express VHH NP1 (13), a VHH against IAV NP that blocks IAV infection, or VHH HA68 (14), a VHH specific for the extracellular portion of IAV HA that does not impair infection when expressed in the cytosol. To assess IAV infection by flow cytometry, we stained for NP with fluorescently labeled VHH NP2(13), another VHH specific for IAV NP (Fig. 3a). The VSV strain used expresses EGFP in addition to VSV structural proteins, and infection was therefore quantified by measuring EGFP-positive cells (Fig. 3b). VHH expression was quantified by staining the HA-tagged VHHs. With the exception of VHHs 135, 170, and 355, which reduced IAV infection by 42, 83, and 78%, all IAV hits blocked IAV infection by more than 90%, but did not impair infection with VSV. Vice versa, all VSV hits blocked VSV infection by at least 90%, but allowed IAV infection to proceed to normal levels. Remarkably, almost complete abrogation of infection was in some cases achieved with VHHs expressed at barely detectable levels. To verify that the Dox-dependent resistance to infection indeed depended on the expressed VHH, we transduced A549 cells with lentiviruses that allow inducible expression of the respective VHHs and confirmed

their antiviral activity. Specificity of inhibition was thus confirmed unambiguously for the respective virus-specific VHHs

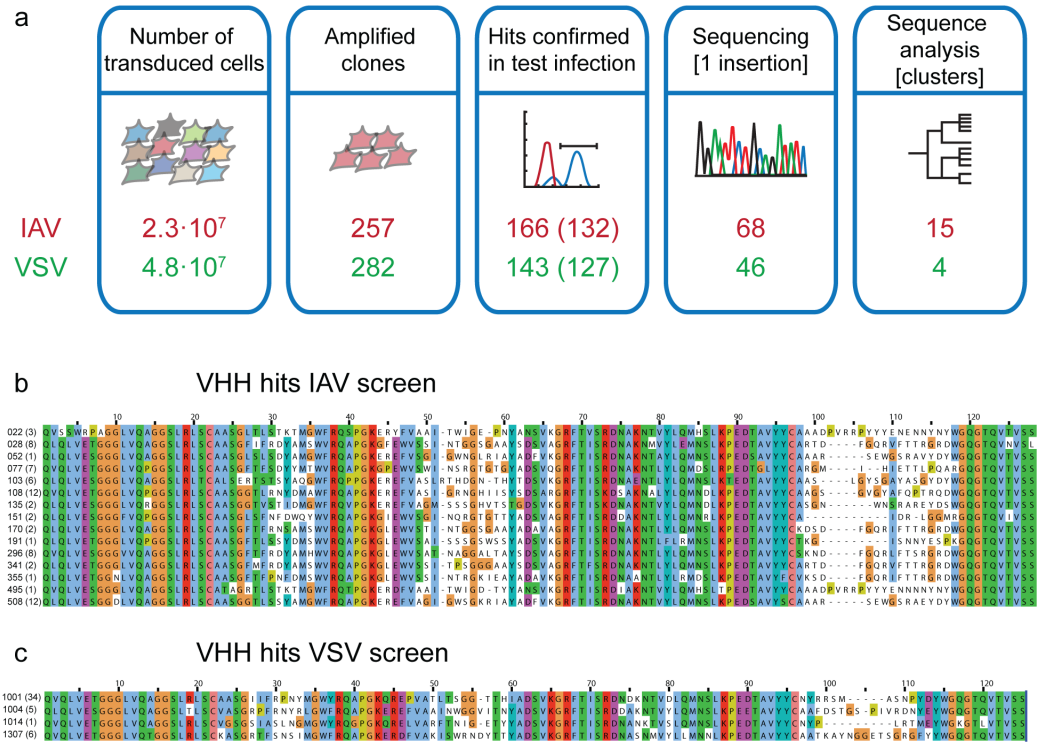

Figure 2 | Overview of the antiviral VHH screen hits. (a) Summary of the number of transduced cells, amplified cell clones, number of confirmed hits reducing infection by more than 40% (80%), number of hits containing a single insertion, and number of different VHH clusters in the IAV and VSV screens. Amino acid sequences of the obtained anti-IAV **(b)** and anti-VSV **(c)** VHHs are presented (number independent identifications in parentheses).

Anti-viral activity of identified VHHs

For each of the hits, representative monoclonal cell lines obtained in the screen were further characterized. Cells were infected with IAV and VSV in the absence and presence of Dox (Fig. 3). As a positive control, we used cell lines that inducibly express VHH NP1 (13), a VHH against IAV NP that blocks IAV infection, or VHH HA68 (14), a VHH specific for the extracellular portion of IAV HA that does not impair infection when expressed in the cytosol. To assess IAV infection by flow cytometry, we stained for NP with fluorescently labeled VHH NP2(13), another VHH specific for IAV NP (Fig. 3a). The VSV strain used expresses EGFP in addition to VSV structural proteins, and infection was therefore quantified by measuring EGFP-positive cells (Fig. 3b). VHH expression was quantified by staining the HA-tagged VHHs. With the exception of VHHs 135, 170, and 355, which reduced IAV infection by 42, 83, and 78%, all IAV hits blocked IAV infection by more than 90%, but did not impair infection with VSV. Vice versa, all VSV hits blocked VSV infection by at least 90%, but allowed IAV infection to

proceed to normal levels. Remarkably, almost complete abrogation of infection was in some cases achieved with VHHs expressed at barely detectable levels. To verify that the Dox-dependent resistance to infection indeed depended on the expressed VHH, we transduced A549 cells with lentiviruses that allow inducible expression of the respective VHHs and confirmed their antiviral activity. Specificity of inhibition was thus confirmed unambiguously for the respective virus-specific VHHs

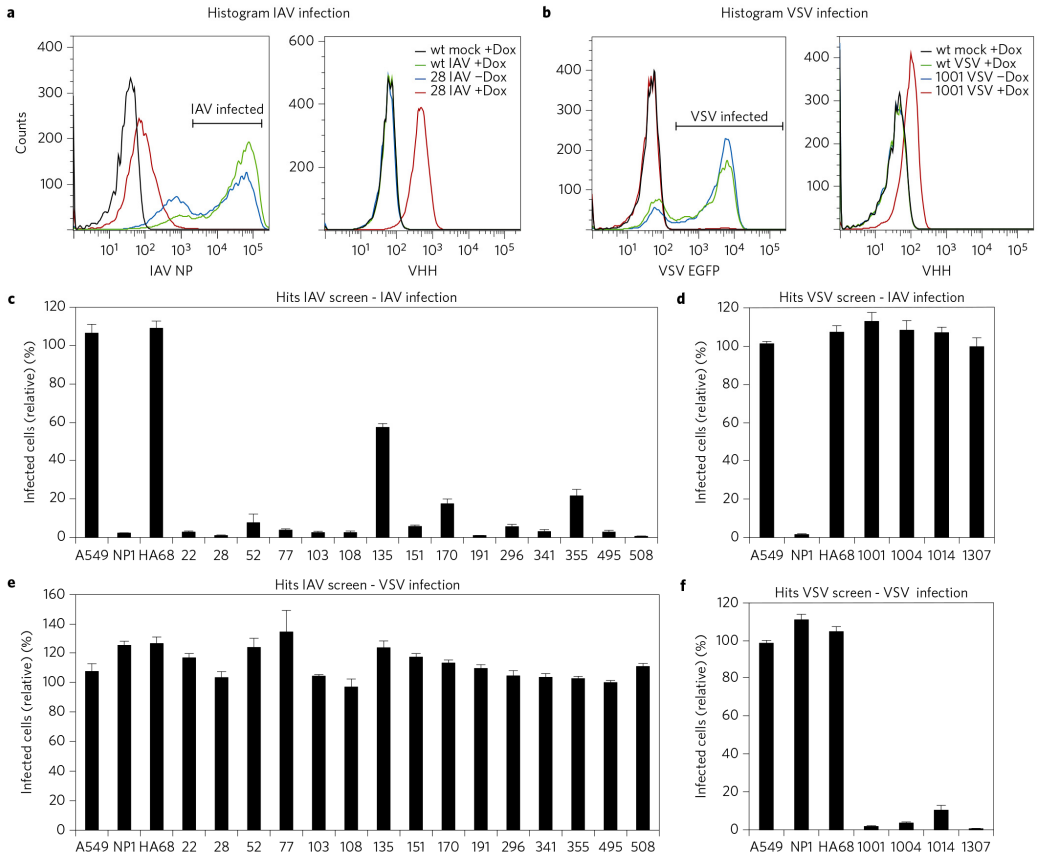

Figure 3 | Validation of antiviral VHHs. A549 cells or clones inducibly expressing the indicated VHHs were treated without or with 1 µg/mL doxycycline (Dox) for 24 h and subsequently infected with IAV WSN **(a, c, d)** or VSV Indiana EGFP (38) **(b, e, f)** for 6 or 4 h, respectively. IAV-infected cells were stained for NP and VHH-HA expression; VSV-infected cells were stained for VHH-HA expression. Cells were analyzed by flow cytometry (sample histograms in **(a)** and **(b)**); the fraction of infected cells in the presence of Dox was quantified and normalized to infection in the absence of Dox. Hits from IAV screen are displayed in **(c)** and **(d)**, hits from VSV screen in **(e)** and **(f)**. All data is from three independent experiments ± s.e.m.

Figure 4 | (next page) Identification of VHH targets. (a, c) 293T cells were transfected with expression vectors for the indicated HA-tagged VHHs and structural proteins of IAV **(a)** or VSV **(c)** fused to Renilla luciferase. Lysates of the respective cells were incubated with immobilized anti-HA antibodies in 96-well plates. Wells were washed and incubated with Renilla luciferase substrates to measure co-purified luciferase activity. Emitted light was normalized to luciferase activity in the lysate. Data from three independent experiments ± s.e.m. is displayed. **(b,d)** Purified IAV NP **(b)** or VSV N-RNA **(d)** was pre-incubated with the His_6-tagged VHHs indicated at the top and subsequently subjected to immunoprecipitation with the specified biotinylated VHH. Precipitation of NP/N and the respective VHH was analyzed by SDS-PAGE and colloidal Coomassie staining. Competition due to overlapping

binding epitopes of the VHHs is indicated with red squares, successful co-purification with green squares. Representative data from at least three experiments is displayed.

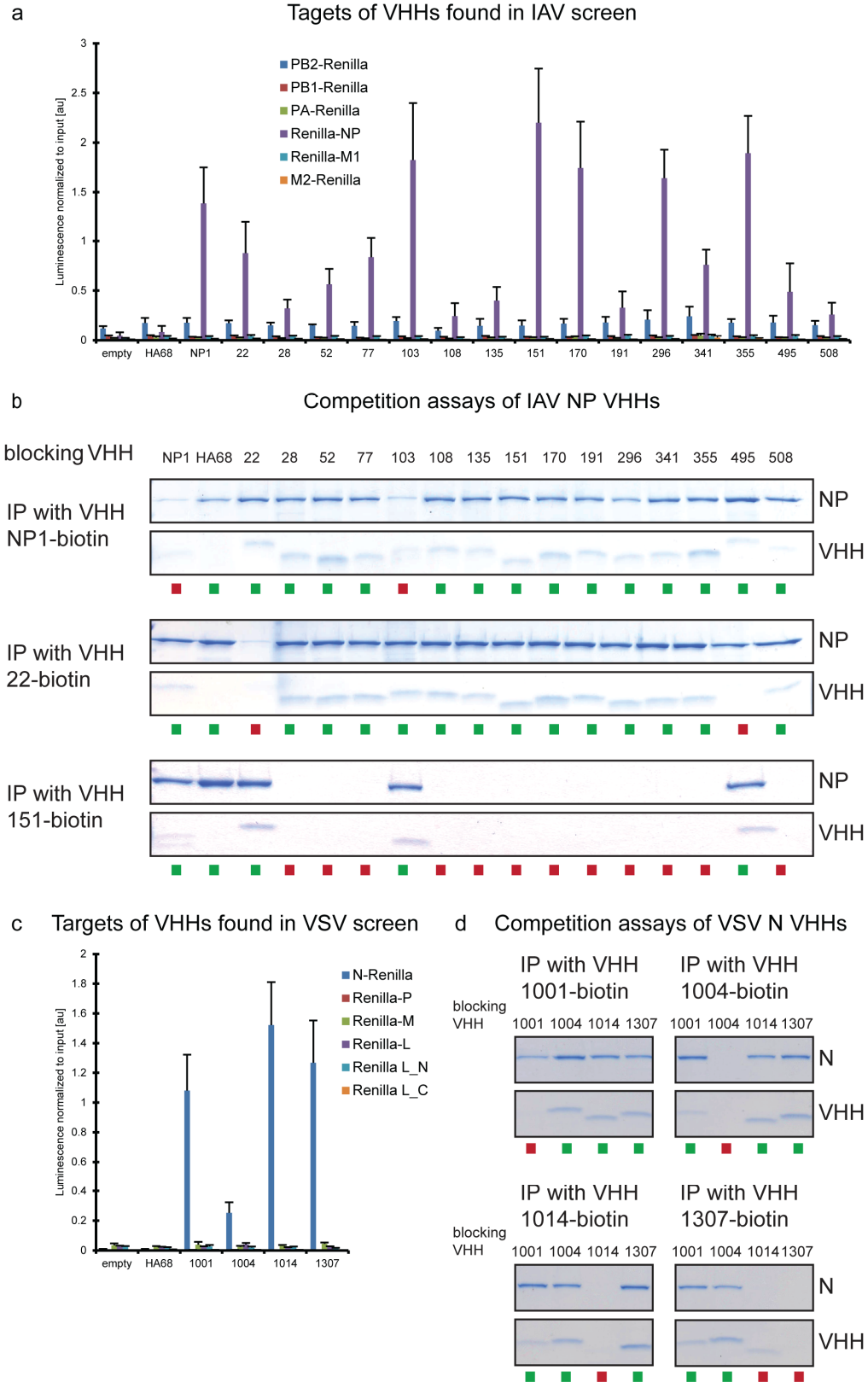

Identification of the targets recognized by antiviral VHHs

The VHH library used for both screens was constructed based on RNA obtained from animals immunized with inactivated virions. The identified antiviral VHHs therefore most likely targeted structural virus proteins. We applied LUMIER assays (15) to test the recognition of viral proteins fused to Renilla luciferase by transiently expressed HA-tagged VHHs. We limited this analysis to virus proteins exposed to the cytosol or nucleus: the polymerase subunits PB2, PB1 and PA, as well as nucleoprotein NP, matrix protein M1, and the ion channel M2 in the case of IAV; the polymerase L, nucleoprotein N, phosphoprotein P, and matrix protein M in the case of VSV. We found that all newly identified anti-IAV VHHs recognized the viral nucleoprotein NP (Fig. 4a), and that anti-VSV VHHs targeted the viral nucleocapsid N (Fig 4c). These findings suggest that viral RNA binding proteins represent an underappreciated vulnerability of negative-stranded RNA viruses. To efficiently block infection, antiviral VHHs may have to target incoming viruses at an early step of the life cycle, which may have biased the screening results towards VHHs that target components of incoming vRNPs. The exclusive identification of antiviral NP- and N-binders likely also reflects the abundance of the respective proteins in the virions used for immunization.

We expressed the virus-specific VHHs in bacteria and tested the extent to which the purified VHHs compete for epitopes on IAV NP and VSV N. For competition assays, purified NP or N was pre-incubated with an excess of His_6-tagged VHHs. VHHs site-specifically biotinylated by means of a sortase reaction (16) were then used for co-precipitation experiments with streptavidin-coupled beads. NP or N was recovered by the biotinylated VHH, unless pre-incubation with an unlabeled VHH masked the epitope recognized by the biotinylated VHHs.

We could thus categorize the IAV NP-binding VHHs into three groups (Fig. 4b): Group I included VHH 103, Group II included VHHs 22 and 495, and Group III was comprised of VHHs 28, 52, 77, 108, 135, 151, 170, 191, 296, 341, 355, and 508. VHH NP2, a VHH specific for IAV NP identified previously(13) and used to quantify IAV infection, did not compete with any of the VHHs identified in this screen.

Binding of the VSV N-specific VHHs 1001, 1004, and 1014 was not affected by any of the other VSV N VHHs, including VHH 1307 (Fig. 4d). Immunoprecipitation of N by VHH 1307, however, was impaired by preincubation with VHH 1014, although the reverse setup allowed successful co-immunoprecipitation of N and the His-tagged VHH. This suggests that 1001, 1004, and 1014 bind to separate epitopes of VSV N, while 1307 may bind to an epitope that is partially overlapping with VHH 1014 or altered by binding of VHH 1014.

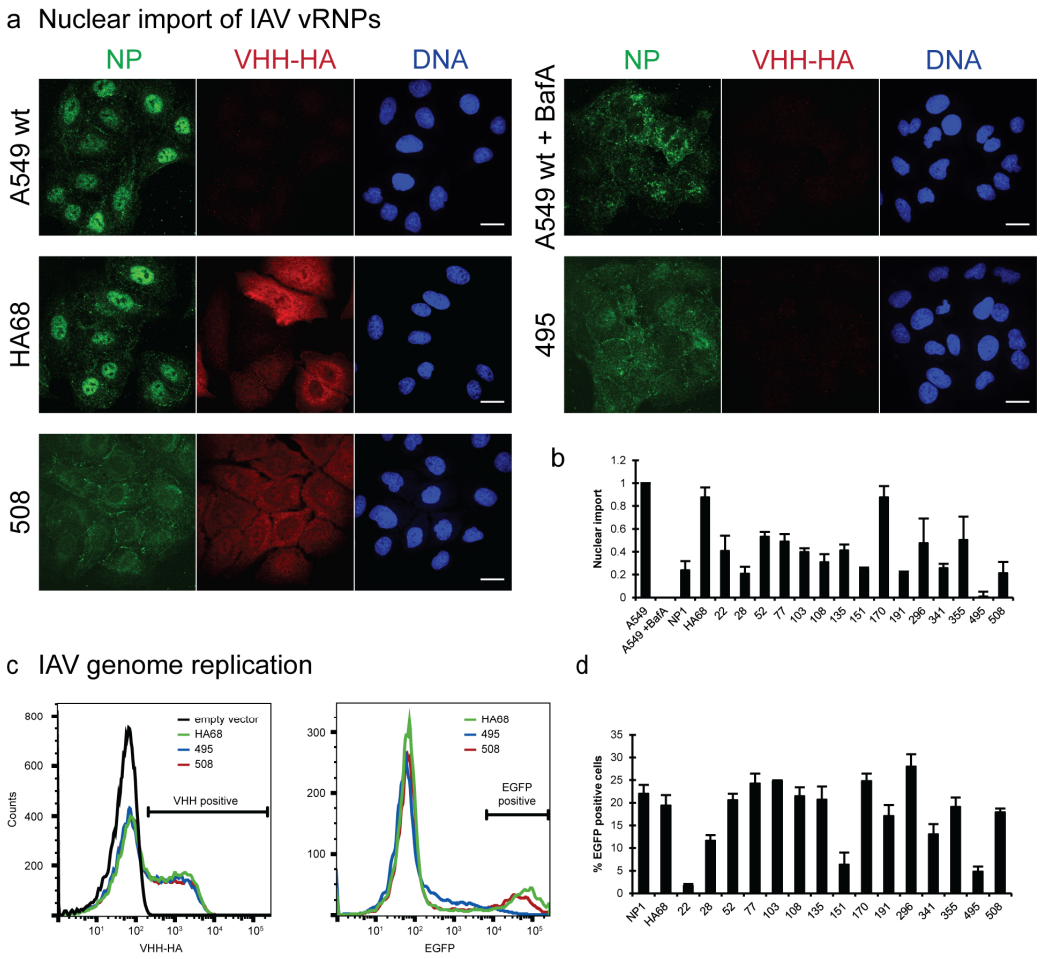

Figure 5 | Anti-IAV VHHs block nuclear import of vRNPs and mRNA transcription. (a, b) A549 cells or clones expressing the indicated VHHs were treated with 1 µg/mL Dox for 24 h and infected with IAV WSN (MOI 230) in the presence of 1 mM cycloheximide for 4 h. Controls were treated with 50 nM bafilomycin A1 (BafA). Cells were stained for NP, HA, DNA, and actin; Z-stacks were recorded by confocal microscopy and Z projections of representative examples are displayed in **(a)**. Scale bars represent 20 µm. NP staining in the nucleus and cytoplasm was quantified with CellProfiler and ratios of nuclear/cytoplasmic signal intensities were quantified and normalized to untreated cells (nuclear import = 1.0) and BafA-treated cells (nuclear import = 0). Values from three independent experiments ± s.e.m. are shown. **(c, d)** 293T cells were transfected with expression vectors for IAV WSN PA, PB1, PB2, NP, pPolI-EGFP, and the indicated HA-tagged VHHs. 24 h post transfection, cells were stained for HA and analyzed by flow cytometry. The fraction of VHH-HA-positive cells that expressed high levels of EGFP was quantified. Exemplary histograms are shown in **(c)**, and average data from three independent experiments ± s.e.m. are displayed in **(d)**.

Anti-IAV VHHs block nuclear import of vRNPs and viral mRNA transcription

We next sought to define the step of the viral replication cycle at which the anti-IAV VHHs block infection. After fusion of the viral membrane with that of late endosomes, viral ribonucleoproteins (vRNPs) are released into the cytosol, followed by import into the nucleus to allow replication and transcription of viral RNAs. To quantify nuclear import of vRNPs, we infected VHH-expressing cell lines with a high MOI of IAV in the presence of cycloheximide

to block translation of new viral proteins. We then determined the localization of incoming vRNPs by confocal fluorescence microscopy (Fig. 5). NP predominantly localized to the nucleus in untreated A549 cells and in cells expressing the control VHH HA68. Treatment of A549 cells with bafilomycin A1, an inhibitor of the endosomal vATPase, blocks endosomal acidification and virus fusion, and thus nuclear import of vRNPs – causing an absence of nuclear NP staining. To quantify nuclear import in VHH-expressing cells, we calculated the ratio of NP signal strength in the nucleus and in the cytoplasm, and determined relative nuclear import by comparison with untreated cells (relative nuclear import = 1) and cells treated with bafilomycin (relative nuclear import = 0). With the exception of VHH 170, all VHHs blocked nuclear import substantially, with relative nuclear import values ranging from 0 to 0.5. Binding of VHHs to NP must impair binding of importins to vRNPs, inhibit translocation of vRNPs through the nuclear pore complex, or interfere with an unknown step that precedes nuclear import *per se*. The VHH expressors were challenged with a very high dose of virus: the respective VHHs must therefore be capable of potently blocking nuclear import, for some VHHs even when expressed at a relatively low level. It is possible that the effects of VHH 170 on nuclear import were overcome in the experimental setup used.

Inhibition of vRNP nuclear import likely explains the antiviral properties of the identified anti-IAV VHHs, but it is possible that NP-specific VHHs perturb other functions of the viral nucleoprotein. Following nuclear import of vRNPs, the viral RNA polymerase transcribes the viral subgenomic segments and replicates the viral RNA genomes (vRNA). NP associates with vRNA and complementary RNA (cRNA), and is essential for complete replication and transcription of viral RNA by IAV polymerase (17). We therefore used a minigenome replication assay, in which polymerase activity is assessed in the absence of a natural infection: The viral RNA polymerase subunits PB2, PB1, and PA as well as NP and the respective VHHs were transiently expressed in the presence of a model IAV genome segment encoding EGFP (Fig. 5c and 5d). Viral mRNAs encoding EGFP were transcribed from the model genome and translated. EGFP expression required the presence of NP as well as each RNA polymerase subunit, but did not rely on the nuclear import of vRNPs, shown to be sensitive to antiviral VHHs. Most of the antiviral VHHs and the control VHH HA68 did not perturb viral gene expression. This suggests that the binding of a VHH to vRNP templates is in principle compatible with transcription, at least at the ratio of NP and VHHs achieved in the experimental setup. However, VHHs 22, 151, and 495 substantially reduced RNA polymerase activity. We thus identified three VHHs that bind to NP epitopes crucial for NP-dependent RNA polymerase activity. VHHs 22 and 495, while distinct in sequence, exhibit similar CDRs and bind to overlapping epitopes on NP, confirming the functional importance of this binding site. None of the expressed VHHs prevented nuclear import of free NP.

In summary, we found that 14 of the 15 newly identified IAV NP-specific VHHs block nuclear import of incoming vRNPs, and that at least three of these also block NP-dependent viral RNA polymerase activity. Our functional VHH screen therefore discloses vulnerabilities of IAV NP that may represent druggable targets.

Anti-VSV VHHs block viral mRNA transcription

In the course of VSV entry, viral membranes fuse with limiting membranes of early endosomes to release the viral genomes with associated proteins into the host cell cytosol. The genomes are coated by the nucleocapsid protein N (N-RNA) and are associated with the polymerase L, bound through its co-factor P. N-RNA serves as a template for polymerase-catalyzed mRNA transcription, which involves transcription of an uncapped leader sequence, followed by transcription of five capped and polyadenylated mRNA species, all catalyzed by the multifunctional RNA polymerase (18, 19).

To quantify mRNA transcription directly, we infected the VHH-expressing cell lines with VSV and metabolically labelled the produced RNA species with [^{3}H]-uridine (Fig. 6a,b). While all five mRNA species could be detected in the absence of VHH expression, mRNA was undetectable in VSV-infected cells expressing VHH 1001, 1004, and 1307, and substantially reduced in cells expressing VHH 1014. This confirms that anti-VSV VHHs prevent viral gene expression by directly or indirectly blocking mRNA transcription. The viral mRNAs detected in infected cells are the products of both primary transcription from incoming viral genomes and transcription from replicated genomes. To specifically analyze primary transcription, we performed *in vitro* polymerase assays in the absence and presence of VHHs using purified components, including N-RNA templates obtained from virions (20, 21) (Fig. 6c). At a ratio of 10 molecules of VHH per 63 molecules of N, the maximum concentration at which all VHHs remained soluble, VHH 1001 and 1307 abrogated RNA transcription almost completely, while VHH 1004 and 1014 did not substantially block RNA transcription. The lack of inhibition by VHH 1004 and 1014 could be attributed to 1) a binding site on N that allows replication in the presence of bound N when the VHH is present at substoichiometric levels, 2) lower affinity of the VHHs to N, or 3) the fact that the respective VHHs target a step that is not fully recapitulated in the in vitro assay, e.g. by exclusively binding to newly generated N during infection in cells, which would directly perturb genome replication and therefore reduce the amount of mRNA transcripts by preventing secondary transcription.

In sum, all anti-VSV VHHs block viral mRNA transcription by binding to the nucleoprotein N. At substoichiometric levels, VHH-binding to different epitopes of N impaired polymerase activity to variable degrees, suggesting that different mechanisms of action apply. The exact binding sites may hold clues to potential antiviral drugs targeting RNA transcription.

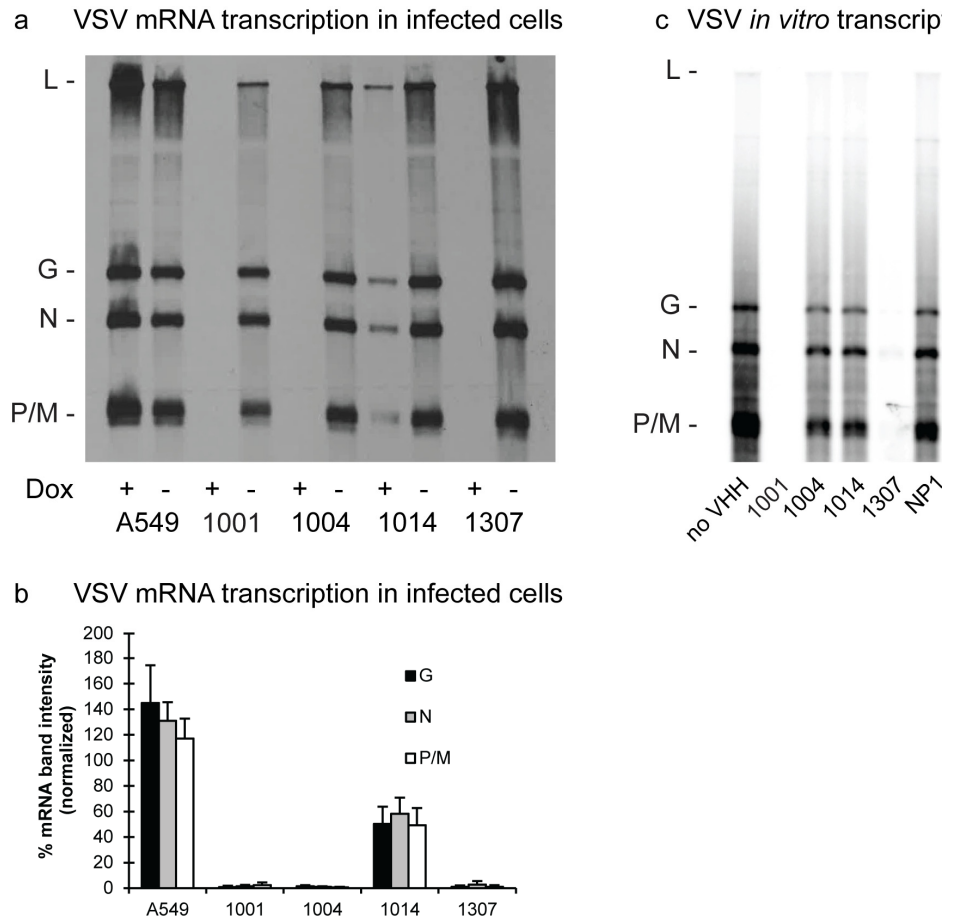

Figure 6 | Anti-VSV VHHs impair mRNA transcription. (**a,b**) A549 cells or clones expressing the indicated VHHs were treated with 1 µg/mL Dox for 24 h, infected with VSV Indiana, and viral RNAs metabolically labeled with [^{3}H]-uridine. We purified the RNA from cell lysates and separated RNA species by acid agarose-urea gel electrophoresis. An autoradiogram representative of three independent experiments is shown; the positions of the mRNAs of the respective viral genes are indicated. Band intensities of G, N, and P/M mRNAs were quantified and normalized to band intensities in the absence of Dox. Average values from three independent experiments ± s.e.m. are shown. (**c**) To test the effects of anti-VSV VHHs on polymerase activity *in vitro*, we incubated recombinantly expressed L and P with N-RNA templates purified form VSV virions. Reactions were performed in the absence or presence of the indicated VHHs as well as NTPs, including [α-^{32}P]-GTP. RNA species were separated by acid agarose-urea gel electrophoresis. An autoradiogram representative of three independent experiments is shown; the positions of the mRNAs of the respective viral genes are indicated.

Discussion

The perturbation of molecular processes in the cell has mostly relied on methods that involve genetic intervention (gene knockout, mutagenesis, or knock-down) or the application of small molecule compounds as inhibitors or activators. The available arsenal of well-defined pharmacological inhibitors to reversibly interfere with protein function level is small and mostly limited to 'druggable' proteins. Many such compounds were discovered serendipitously and their specificity is not always easy to establish. The approach described here allows the

functional screening of camelid single domain antibodies to identify highly specific gain and loss of function molecular perturbants. Provided a suitable assay is at hand, VHHs can be identified as inhibitors or modulators of any biological process by such phenotypic screens. VHHs can then be inducibly expressed to perturb protein function in a highly specific and reversible manner and thus present a valuable research tool orthogonal to genetic ablation.

The use of VHH libraries from animals immunized with a distinct set of desired protein targets substantially increases the likelihood of obtaining the desired antibody fragments. Large numbers of candidates can be tested in lentiviral screens, an approach that could perhaps be applied to synthetic libraries as well. To identify VHHs, the cytosolic expression of which blocks pathogen infection, it may even be sufficient to harvest the VHH repertoire from a naturally infected animal. Selection of VHHs is not limited to lethal screens, but can be extended to fluorescence-activated cell sorting (FACS) and other enrichment strategies following reporter gene expression or turnover of fluorogenic substrates. There is no reason why the selected phenotypes should be limited to functional perturbation in the cytosol, and similar screens may exploit expression of VHHs targeted to other organelles or rely on display of VHHs at the cell surface. Although we selected and amplified clonal cell lines from cells that survived the screens, high throughput sequencing methods could be used instead to identify enriched VHHs. This approach would be compatible with selection of VHHs in terminally differentiated cells or in cells that have to be fixed prior to cell sorting.

In the screen described here, we identified 19 VHHs that specifically block infection of cells with IAV or VSV. Previous attempts to identify virus specific VHHs using phage display with VHH libraries from the same animals yielded fewer hits that inhibited infection less potently (13). The screening approach described here thus complements other VHH screening techniques based on affinity, and is likely to be better at identifying VHH-based intracellular inhibitors or activators. The identification of epitopes, the occlusion of which blocks the infectious cycle, may inform the development of small molecule inhibitors, in particular if they are well conserved among different serotypes of a virus. In theory, antiviral application of VHHs fused to cell-penetrating peptides is conceivable as well (22). These anti-viral VHHs should further help elucidate the vulnerable steps of the viral life cycle. Ongoing structural analysis of the anti-IAV VHHs bound to NP may shed light on how incoming vRNPs are imported into the nucleus and how NP interacts with the necessary cellular factors. Structures of VHHs capable of inhibiting IAV RNA polymerase activity will help unravel how NP contributes to the formation of full length viral mRNA, vRNA, and cRNA transcripts. Similarly, VHHs that target VSV N will be helpful in the molecular analysis of VSV RNA polymerase activity. The finding here that VHHs have different inhibition properties on *in vitro* transcription and the synthesis of RNA in cells indicates that such tools may well aid in the

discrimination of N-related functions in transcription vs replication. Of note, homologues of the VSV polymerase and nucleocapsid are found in many human pathogens of the order mononegavirales, including rabies virus, Ebola virus, mumps virus, measles virus, and respiratory syncytial virus (RSV) (23).

Methods

Cell lines

Human epithelial A549 and HEK 293T cells, canine MDCK cells, and hamster BHK-21 cells were obtained from ATCC and grown in DMEM supplemented with 10% FBS. A549 cell lines inducibly expressing HA-tagged VHHs were cultivated in the presence of 500 μg/mL geneticin. All cell lines used for experiments were negative for *Mycoplasma* as judged by the absence of of cytosolic Hoechst 33342-positive foci in immunofluorescence microscopy samples.

Virus

A/WSN/33 strain of influenza virus was propagated in MDCK cells and concentrated by sedimentation (75,000 g, 4° C, 2h) through a 20% sucrose cushion (in 20 mM Tris pH 7.6, 150 mM NaCl), followed by resuspension in desorption buffer (0.245% BSA in 20 mM Tris pH 7.6, 150 mM NaCl). VSV Indiana and VSV Indiana GFP were propagated in BHK-1 cells. Clarified supernatants were used for flow cytometry-based infection assays.

Reagents

Doxycycline hyclate (Dox) was purchased from Sigma Aldrich. Hybridoma cells secreting mouse monoclonal anti-IAV NP (clone H16-L10-4R5, ATCC HB-65)(24) were obtained from ATCC and antibodies in the supernatant purified using a protein G column. Polyclonal rabbit anti-neomycin phosphotransferase II (NPTII) was purchased from Fitzgerald Industries International. Mouse anti-HA.11 (clone 16B12) was acquired from BioLegend, polyclonal rabbit anti-HA (Y-11) from Santa Cruz. Mouse anti-HA.11 (clone 16B12) coupled to Alexa Fluor (AF) 488 or AF594, as well as fluorescently-labeled secondary antibodies and AF647 Phalloidin were obtained from Life Technologies.

Generation of lentiviral plasmid VHH library

In order to raise heavy chain-only antibodies against structural components of IAV and VSV, two male alpacas were immunized five times with a mixture of ethanol-inactivated IAV PR8 and VSV Indiana (ca. 10^{12} plaque forming units of each virus per injection) according to a protocol authorized by the Tufts University Cummings Veterinary School Institutional Animal Care and Use Committee. RNA from peripheral blood lymphocytes was extracted and used as a template to generate cDNA using three sets of primers (random hexamers, oligo(dT), and primers specific for the constant region of the alpaca heavy chain gene) (10, 25). VHH coding

sequences were amplified by PCR using VHH-specific primers, cut with NotI and AscI, and ligated into the M13 phagemid vector pJSC to yield the VHH phagemid plasmid library described in our previous study (13). A derivative of pInducer20 (26), pInducer20-NA, was generated by removing all NotI restriction sites and by replacing the gateway cassette with a DNA fragment containing NotI and AscI restriction sites. VHHs were subcloned into pInducer20-NA and the library amplified in electroporation competent *Escherichia coli* (*E. coli*) ElectroTen-Blue while maintaining the diversity of the phagemid library ($2.4 \cdot 10^7$ ampicillin-resistant colonies obtained).

Generation of lentivirus library

Lentiviral particles were generated by transfecting HEK 293T cells in 15 cm dishes with psPax2, pMD2.G (both kind gifts from Didier Trono, École polytechnique fédérale de Lausanne, Switzerland), and the pInducer20-NA VHH library using Lipofectamine 2000 (Life Technologies). Supernatants were harvested 48 h post transfection and filtered through 0.4 µm filters. Virus stocks were titered on A549 cells by flow cytometry using anti-NPII, goat anti-rabbit AF647 and a BD Biosciences LSRFortessa flow cytometer.

Lentivirus VHH screen

A549 cells in 15 cm dishes were transduced with the lentivirus library at a multiplicity of infection (MOI) of 0.25 in the presence of 10 µg/mL polybrene. VHH expression was induced 8 h post transduction by the addition of Dox to a final concentration of 1 µg/mL. 48 h post transduction, cells were infected with IAV/WSN/33 in DMEM (0.2% BSA) at an MOI of 13 or VSV EGFP Indiana in DMEM at an MOI of 4.5. The inoculum was removed 1 h post infection and cells were covered with fresh DMEM containing 10% FCS, 1 µg/mL Dox, Penicillin/Streptomycin, and Fungizone Antimycotic (Life Technologies); medium of VSV-infected cells was supplemented with 100 mM NH_4Cl and 20 mM Hepes. 48 h post infection with IAV or VSV, cells were washed with PBS, trypsinized, split 1:2, and seeded in DMEM with 20% FCS, 1 µg/mL Dox, Penicillin/Streptomycin, and Fungizone Antimycotic (as well as 100 mM NH_4Cl and 20 mM Hepes in case of VSV-infected cells). The medium of the IAV plates was replaced every 2-3 days until most cells had detached. Adherent cells of the VSV plates were covered with DMEM containing 1.5% carboxymethyl cellulose, 20% FCS, 500 µg/mL G418, 1 µg/mL Dox, Penicillin/Streptomycin, and Fungizone Antimycotic and left unperturbed. 3-4 weeks later, cell colonies were harvested from the plates, individually amplified, tested in infection assays, and frozen. To prevent infection of cell clones with residual VSV, freshly picked clones of the VSV screen were grown in 1.5 µg/mL VSV-neutralizing antibody IE2 (27) and controlled for EGFP expression. To retrieve the VHH sequences encoded by surviving cell clones, we lysed cells in 1% SDS, 50 mM Tris,100 mM NaCl, 1 mM EDTA, 100 µg/mL proteinase K at 55°C for 2h. Genomic DNA was subsequently

precipitated by addition of one volume of isopropanol, dried in a fume hood, and resuspended in ddH_2O. VHH sequences were amplified with lentivirus-specific primers using the Platinum PCR Super Mix (Life Technologies) and directly sequenced from PCR products. VHH sequences were analyzed by ClustalW alignment, and neighbor-joining trees were constructed to group identical or highly similar sequences (<3 aa differences in CDRs). One representative sequence of each group was chosen for further analysis. The antiviral VHH sequences were deposited in the NCBI GenBank sequence data base with the accession numbers KX022606-KX022624.

Flow cytometry-based infection assays

To quantify infection by flow cytometry, A549 cell lines were seeded in 24-well plates 40 h before infection ($2 \cdot 10^4$ cells/well). Cells were treated with 1 µg/mL Dox 24 h before infection to induce VHH expression. Cells were infected with appropriate amounts of IAV WSN/33 (in 0.2% BSA/DMEM) or VSV Indiana GFP (in DMEM) to infect 50% of wild-type cells. 30 minutes post infection, inocula were removed and cells cultivated for 5:30 h (IAV) or 3:30 h (VSV) in full medium. Cells were trypsinized, fixed in 4% formaldehyde/PBS, and stained with 1 µg/mL AF647-coupled VHH NP2 and mouse anti-HA AF488 (IAV-infected cells), or mouse anti-HA AF594 (VSV-infected cells), all under permeabilizing conditions. Fluorescence was quantified using a BD Biosciences LSRFortessa flow cytometer and the FlowJo software package.

LUMIER Assay

Protein interactions in transfected HEK 293T cells were quantified using the LUMIER assay according to a protocol modified from Taipale *et al.* (28). HEK 293T cells in 24-wells were transfected with 0.25 µg bait expression vectors (pCAGGS VHH-HA) and 0.25 µg prey expression vectors (IAV: empty vector, pEXPR PB2-Renilla, pEXPR PB1-Renilla, pEXPR PA-Renilla, pEXPR Renilla-NP, pEXPR Renilla-M1, or pEXPR M2-Renilla; VSV: empty vecor, pEXPR N-Renilla, pEXPR Renilla-P, pEXPR Renilla-M, pEXPR Renilla-L, pEXPR Renilla-L_N, or pEXPR Renilla-L_C; all expression vectors are derived from pcDNA3-ccdB-Renilla, a kind gift of Mikko Taipale, Susan Lindquist laboratory, Whitehead Institute, Cambridge, MA, USA) using Lipofectamine 2000. 24 h post transfection, cells were lysed in 120 µL LUMIER IP buffer (50 mM Hepes pH 7.9, 150 mM NaCl, 2 mM EDTA pH 8.0, 0.5% Triton X-100, 5% glycerol, protease inhibitor cocktail (Roche)). 90 µL of the lysates were transferred to blocked LUMITRAC™ 600 plates (Greiner) coated with mouse anti-HA.11 and incubated at 4°C for 3 h. After extensive washing steps with IP buffer, incubated wells (or 10 µL lysate) were incubated with Coelenterazine-containing Renilla luciferase substrate mix (BioLux Gaussia Luciferase Assay Kit, New England BioLabs) and light emission quantified

using a SpectraMax M3 microplate reader (Molecular Devices). Renilla luciferase activity in the immunoprecipitation samples was normalized by Renilla luciferase activity in the lysates.

Protein Expression and Purification

For periplasmic bacterial expression, VHH coding sequences were cloned into a derivative of pHEN6(29) encoding a C-terminal sortase recognition site (LPETG) followed by a His_6-tag. VHH-LPETG-His_6 fusion proteins were expressed in *E. coli* WK6 cells and purified from periplasmic extracts using Ni-NTA affinity purification and size exclusion chromatography with a HiLoad 16/600 Superdex 75 pg column. To fluorescently label or biotinylate VHHs using sortase, proteins were incubated with sortase and GGG-Alexa Fluor 647 or GGG-biotin as described before (Guimaraes et al., 2013), followed by removal of His-tagged sortase with Ni-NTA beads and desalting.

The IAV/WSN/33 NP cds was cloned into pET30b+. NP-His_6 was expressed in *E. coli* LOBSTR(30) and purified by Ni-NTA purification, Mono S cation exchange chromatography, and size exclusion chromatography with a HiLoad 16/60 Superdex 200 column. VSV Indiana N was purified as described before (31). In brief, *E. coli* BL21(DE3) was transformed with pET N/P to co-express VSV N and P protein. The N/P complex associated with RNA was purified by Ni-NTA purification, P precipitated during dialysis against an acidic buffer (100 mM citrate, pH 4.0, 250 mM NaCl), and N-RNA further purified by gel filtration with a HiLoad 16/60 Superdex 200 column.

Competition assays

Immunoprecipitations for competition assays were performed with 2 µg C-terminally biotinylated VHH (16) bound to streptavidin magnetic beads (MyOne Dynabeads; Life Technologies) and 7.5 µg of recombinant IAV WSN NP. Before addition to the beads, NP was blocked with 50 µg of the individual His-tagged VHHs. Bound NP was eluted in 0.2 M glycine, pH 2.2, and analyzed by SDS-PAGE and colloidal Coomassie staining.

IAV nuclear import assay

To quantify nuclear import of vRNPs, A549 cell lines were seeded in 24-well plates 40 h before infection (10^4 cells/well). Cells were treated with 1 µg/mL Dox 24 h before infection to induce VHH expression. IAV WSN/33 (in 0.2% BSA/DMEM) at an MOI of 230 was bound to the cells on ice for 1h in the presence of 1 mM cycloheximide (CHX). Cells were subsequently covered with fresh BSA/DMEM with CHX and incubated at 37° C for 4 h. Cells were fixed with 4% formaldehyde and permeabilized in permeabilisation buffer (PS) (0.05% saponin, 1% BSA, 0.05% NaN_3 in PBS) for 20 min. Samples were incubated with mouse anti-NP (clone HB-65, 1 µg/mL in PS) and rabbit anti-HA (1:200 in PS) for 2 h, washed with PBS, and subsequently incubated with AF488-coupled goat anti-mouse IgG and AF594-coupled goat

anti-rabbit IgG (both 1:1,000 in PS), Hoechst 33342 (1:5,000), and AF647 Palloidin (1:100) for 1 h. Samples were washed with PBS and H_2O, and mounted with Fluoromount-G (Southern Biotech). Z stacks were acquired using a PerkinElmer Ultraview Spinning Disk Confocal microscope and Z projections from 3 fields of view with a 40x objective (typically containing ca. 50 cells) were analyzed using CellProfiler(32). Gaussian filters were applied to the DNA and actin channels, which were subsequently used to segment nuclei and cells, respectively. For each cell, the mean intensity of the NP signal in the nucleus was divided by the mean intensity of the NP signal in the cytoplasm. Average values for all cells in one experimental condition were calculated and normalized to the values for untreated A549 cells (nuclear import = 1.0) and BafA-treated cells (nuclear import = 0).

IAV minigenome replication assay

To quantify polymerase activity of transiently expressed IAV polymerase, 293T cells were transfected with 150 ng of each pCAGGS PB2, pCAGGS PB1, pCAGGS PA, pCAGGS NP(33), pPolI-EGFP-RT (a derivative of pPolI-NS-RT(34) in which the NS coding sequence was replaced with EGFP, and which allowed transcription of the model IAV genome segment by host cell RNA polymerase I), and the respective pCAGGS VHH-HA vector (or empty vector) using Lipofectamine 2000. 24 h post transfection, cells were fixed and stained with AF594 mouse anti-HA. VHH-HA expression was measured and EGFP fluorescence in HA-positive cells quantified using a BD Biosciences LSRFortessa flow cytometer and the FlowJo software package.

VSV mRNA transcription assay in infected cells

To analyze viral RNA species in infected cells, A549 cell lines were seeded in 60 mm dishes and, where indicated, VHH expression induced with 1 µg/mL Dox for 24 h hours. 85% confluent cells were infected with VSV at an MOI of 100 in 1 ml of DMEM with 1 µg/ml of Dox (where indicated). After 45 min at 34° C, 2 ml of DMEM complemented with 60 µl actinomycin D (0.5 mg/ml), 50 µl of [5,6-^{3}H]-Uridine (38 Ci/mmol, Moravek Biochemicals) and 1 µg/ml of Dox (where indicated) were added to the cells. After 5 h of incubation at 34° C, cytoplasmic extracts were prepared and RNA was purified by phenol/chloroform extraction as described previously(35). Purified RNA extracts were analyzed by acid/agarose gel electrophoresis and autoradiography (36).

VSV in vitro transcription assay

Genomic N-RNA templates were prepared from VSV virions as previously described (20). Polymerase assays were carried out as described(37) using 0.25 µg of N-RNA with 0.2 µM of VSV L and 0.3 µM of VSV P in a reaction mixture containing 20 mM Tris, pH 8.0, 50 mM NaCl, 6 mM MgCl2, 500 µM UTP, 250 µM GTP, 1 mM ATP, 1 mM CTP, 165 nM of [α^{32}P]-

GTP (3000 Ci/mmol) (Perkin-Elmer) and, where indicated, 80 μM of the respective VHHs. Reactions were incubated at 30° C for 2.5 h and stopped by addition of EDTA/formamide. Reactions products were resolved using acid/agarose gel electrophoresis and autoradiography (36).

References

1. **Mohr SE**, **Smith JA**, **Shamu CE**, **Neumüller RA**, **Perrimon N**. 2014. RNAi screening comes of age: improved techniques and complementary approaches. Nat Rev Mol Cell Biol **15**:591–600.

2. **Kim H**, **Kim JS**. 2014. A guide to genome engineering with programmable nucleases. Nat Rev Genet **15**:321–334.

3. **Cohen P**. 2010. Guidelines for the effective use of chemical inhibitors of protein function to understand their roles in cell regulation. Biochem J **425**:53–54.

4. **Doxsey SJ**, **Brodsky FM**, **Blank GS**, **Helenius A**. 1987. Inhibition of endocytosis by anti-clathrin antibodies. Cell **50**:453–463.

5. **Gargano N**, **Cattaneo A**. 1997. Rescue of a neutralizing anti-viral antibody fragment from an intracellular polyclonal repertoire expressed in mammalian cells. FEBS Lett **414**:537–540.

6. **Hamers-Casterman C**, **Atarhouch T**, **Muyldermans S**, **Robinson G**, **Hamers C**, **Songa EB**, **Bendahman N**, **Hamers R**. 1993. Naturally occurring antibodies devoid of light chains. Nature **363**:446–8.

7. **Muyldermans S**. 2013. Nanobodies: Natural Single-Domain Antibodies. Annu Rev Biochem **82**:775–797.

8. **Helma J**, **Cardoso MC**, **Muyldermans S**, **Leonhardt H**. 2015. Nanobodies and recombinant binders in cell biology. J Cell Biol **209**:633–644.

9. **Schmidt FI**, **Lu A**, **Chen JW**, **Ruan J**, **Tang C**, **Wu H**, **Ploegh HL**. 2016. A single domain antibody fragment that recognizes the adaptor ASC defines the role of ASC domains in inflammasome assembly. J Exp Med **213**:771–90.

10. **Maass DR**, **Sepulveda J**, **Pernthaner A**, **Shoemaker CB**. 2007. Alpaca (Lama pacos) as a convenient source of recombinant camelid heavy chain antibodies (VHHs). J Immunol Methods **324**:13–25.

11. **Ryckaert S**, **Pardon E**, **Steyaert J**, **Callewaert N**. 2010. Isolation of antigen-binding camelid heavy chain antibody fragments (nanobodies) from an immune library displayed on the surface of Pichia pastoris. J Biotechnol **145**:93–98.

12. **Fridy PC**, **Li Y**, **Keegan S**, **Thompson MK**, **Nudelman I**, **Scheid JF**, **Oeffinger M**, **Nussenzweig MC**, **Fenyo D**, **Chait BT**, **Rout MP**. 2014. A robust pipeline for rapid production of versatile nanobody repertoires. Nat Methods **11**:1253–1260.

13. **Ashour J**, **Schmidt FI**, **Hanke L**, **Cragnolini J**, **Cavallari M**, **Altenburg A**, **Brewer R**, **Ingram J**, **Shoemaker C**, **Ploegh HL**. 2015. Intracellular Expression of Camelid Single-Domain Antibodies Specific for Influenza Virus Nucleoprotein Uncovers Distinct Features of Its Nuclear Localization. J Virol **89**:2792–2800.

14. **Dougan SK**, **Ashour J**, **Karssemeijer R a**, **Popp MW**, **Avalos AM**, **Barisa M**, **Altenburg AF**, **Ingram JR**, **Cragnolini JJ**, **Guo C**, **Alt FW**, **Jaenisch R**, **Ploegh HL**. 2013. Antigen-specific B-cell receptor sensitizes B cells to infection by influenza virus. Nature **503**:406–9.

15. **Barrios-Rodiles M**, **Bose R**, **Liu Z**, **Donovan RS**, **Shinjo F**, **Liu Y**, **Dembowy J**, **Taylor IW**, **Luga V**, **Przulj N**, **Robinson M**, **Suzuki H**, **Hayashizaki Y**, **Jurisica I**, **Wrana JL**. 2005. High-Throughput Mapping of a Dynamic Signaling Network in Mammalian Cells. Science (80-) **307**:1621–1625.

16. **Guimaraes CP**, **Witte MD**, **Theile CS**, **Bozkurt G**, **Kundrat L**, **Blom AEM**, **Ploegh HL**. 2013. Site-specific C-terminal and internal loop labeling of proteins using sortase-mediated reactions. Nat Protoc **8**:1787–99.

17. **Fodor E**. 2013. The RNA polymerase of influenza a virus: mechanisms of viral transcription and replication. Acta Virol **57**:113–22.

18. **Emerson SU**, **Wagner RR**. 1972. Dissociation and reconstitution of the transcriptase and template activities of vesicular stomatitis B and T virions. J Virol **10**:297–309.

19. **Green TJ**, **Luo M**. 2009. Structure of the vesicular stomatitis virus nucleocapsid in complex with the nucleocapsid-binding domain of the small polymerase cofactor, P. Proc Natl Acad Sci U S A **106**:11713–11718.

20. **Rahmeh A a**, **Schenk AD**, **Danek EI**, **Kranzusch PJ**, **Liang B**, **Walz T**, **Whelan SPJ**. 2010. Molecular architecture of the vesicular stomatitis virus RNA polymerase. Proc Natl Acad Sci U S A **107**:20075–80.

21. **Baltimore D**, **Huang AS**, **Stampfer M**. 1970. Ribonucleic acid synthesis of vesicular stomatitis virus, II. An RNA polymerase in the virion. Proc Natl Acad Sci U S A **66**:572–6.

22. **Li T**, **Bourgeois JP**, **Celli S**, **Glacial F**, **Le Sourd AM**, **Mecheri S**, **Weksler B**, **Romero I**, **Couraud PO**, **Rougeon F**, **Lafaye P**. 2012. Cell-penetrating anti-GFAP VHH and corresponding fluorescent fusion protein VHH-GFP spontaneously cross the blood-brain barrier and specifically recognize astrocytes: Application to brain imaging. FASEB J **26**:3969–3979.

23. **Morin B**, **Kranzusch PJ**, **Rahmeh AA**, **Whelan SPJ**. 2013. The polymerase of negative-stranded RNA viruses. Curr Opin Virol **3**:103–10.

24. **Yewdell JW**, **Frank E**, **Gerhard W**. 1981. Expression of influenza A virus internal antigens on the surface of infected P815 cells. J Immunol **126**:1814–9.

25. **Sosa BA**, **Demircioglu FE**, **Chen JZ**, **Ingram J**, **Ploegh HL**, **Schwartz TU**. 2014. How lamina-associated polypeptide 1 (LAP1) activates Torsin. Elife **3**:e03239.

26. **Meerbrey KL**, **Hu G**, **Kessler JD**, **Roarty K**, **Li MZ**, **Fang JE**, **Herschkowitz JI**, **Burrows AE**, **Ciccia A**, **Sun T**, **Schmitt EM**, **Bernardi RJ**, **Fu X**, **Bland CS**, **Cooper TA**, **Schiff R**, **Rosen JM**, **Westbrook TF**, **Elledge SJ**. 2011. The pINDUCER lentiviral toolkit for inducible RNA interference in vitro and in vivo. Proc Natl Acad Sci U S A **108**:3665–70.

27. **Lefrancois L**, **Lyles DS**. 1982. The interaction of antibody with the major surface glycoprotein of vesicular stornatitis virus II. Monoclonal antibodies to nonneutralizing and cross-reactive epitopes of Indiana and New Jersey serotypes. Virology **121**:168–174.

28. **Taipale M**, **Krykbaeva I**, **Whitesell L**, **Santagata S**, **Zhang J**, **Liu Q**, **Gray NS**, **Lindquist S**. 2013. Chaperones as thermodynamic sensors of drug-target interactions reveal kinase inhibitor specificities in living cells. Nat Biotechnol **31**:630–637.

29. **Conrath KE**, **Lauwereys M**, **Galleni M**, **Matagne A**, **Frère JM**, **Kinne J**, **Wyns L**, **Muyldermans S**. 2001. Beta-lactamase inhibitors derived from single-domain antibody fragments elicited in the camelidae. Antimicrob Agents Chemother **45**:2807–12.

30. **Andersen KR**, **Leksa NC**, **Schwartz TU**. 2013. Optimized E. coli expression strain LOBSTR eliminates common contaminants from His-tag purification. Proteins Struct Funct Bioinforma **81**:1857–1861.

31. **Green TJ**, **Rowse M**, **Tsao J**, **Kang J**, **Ge P**, **Zhou ZH**, **Luo M**. 2011. Access to RNA Encapsidated in the Nucleocapsid of Vesicular Stomatitis Virus. J Virol **85**:2714–2722.

32. **Kamentsky L**, **Jones TR**, **Fraser a**, **Bray M a**, **Logan DJ**, **Madden KL**, **Ljosa V**, **Rueden C**, **Eliceiri KW**, **Carpenter a E**. 2011. Improved structure, function and compatibility for Cell Profiler: modular high-throughput image analysis software. Bioinformatics **27**:1179–1180.

33. **Schickli JH**, **Flandorfer A**, **Nakaya T**, **Martinez-Sobrido L**, **García-Sastre A**, **Palese P**. 2001. Plasmid-only rescue of influenza A virus vaccine candidates. Philos Trans R Soc B Biol Sci **356**:1965–1973.

34. **Fodor E**, **Devenish L**, **Engelhardt OG**, **Palese P**, **Brownlee GG**, **García-Sastre A**. 1999. Rescue of influenza A virus from recombinant DNA. J Virol **73**:9679–82.

35. **Pattnaik a K**, **Wertz GW**. 1990. Replication and amplification of defective interfering particle RNAs of vesicular stomatitis virus in cells expressing viral proteins from vectors containing cloned cDNAs. J Virol **64**:2948–2957.

36. **Lehrach H**, **Diamond D**, **Wozney JM**, **Boedtker H**. 1977. RNA molecular weight determinations by gel electrophoresis under denaturing conditions, a critical reexamination. Biochemistry **16**:4743–4751.

37. **Morin B**, **Rahmeh A a**, **Whelan SPJ**. 2012. Mechanism of RNA synthesis initiation by the vesicular stomatitis virus polymerase. EMBO J **31**:1320–9.

38. **Cherry S**, **Doukas T**, **Armknecht S**, **Whelan S**, **Wang H**, **Sarnow P**, **Perrimon N**. 2005. Genome-wide RNAi screen reveals a specific sensitivity of IRES-containing RNA viruses to host translation inhibition. Genes Dev **19**:445–452.

Chapter 5

Vesicular Stomatitis Virus N Protein-Specific Single-Domain Antibody Fragments Inhibit Replication

Accepted for publication in EMBO reports, March 2017

Leo Hanke[1], Florian I. Schmidt[1], Kevin E. Knockenhauer[2], Benjamin Morin[3], Sean P.J. Whelan[3], Thomas U. Schwartz[2] and Hidde L. Ploegh[1,2]

[1]Whitehead Institute for Biomedical Research, Cambridge, Massachusetts, USA, Massachusetts

[2]Department of Biology, Massachusetts Institute of Technology, Cambridge, Massachusetts, USA

[3]Department of Microbiology and Immunobiology, Harvard Medical School, Boston, Massachusetts

Abstract

The transcription and replication machinery of negative-stranded RNA viruses present possible targets for interference in the viral life cycle. We demonstrate the validity of this concept through the use of cytosolically expressed single domain antibody fragments (VHHs) that protect cells from a lytic infection with vesicular stomatitis virus (VSV) by targeting the viral nucleoprotein N. We define the binding sites for two such VHHs, 1004 and 1307, by X-ray crystallography to understand their inhibitory properties and the structural features that are targeted. We found that VHH 1307 competes with binding of the essential polymerase cofactor P to N and thus inhibits replication and mRNA transcription, while binding of 1004 likely only affects genome replication. The functional relevance of these epitopes is confirmed by the isolation of escape mutants able to replicate in the presence of the inhibitory VHHs. The determined structures pave the way for targeted antiviral intervention.

Introduction

Vesicular stomatitis virus (VSV) is a member of the *Rhabdoviridae* family, which includes the human pathogen rabies virus. The VSV single-stranded RNA genome is negative-sense, non-segmented, and encodes 5 viral proteins: the nucleoprotein N, the phosphoprotein P, matrix protein M, glycoprotein G and the RNA-dependent RNA polymerase L. Expression levels of the viral proteins correlate with their position within the single-stranded RNA genome, with N being the most abundant and L the least abundant. The VSV genome is tightly encapsidated by N to form a nucleocapsid (N-RNA), which serves as the template during RNA synthesis. In the absence of N, transcription can be initiated but no full length RNAs are produced (1). As it encapsidates the 11,161 nucleotide genome, the nucleocapsid adopts a bullet shape in the virion, whereas it shows an elongated, more flexible representation in the cytosol of infected cells (2). Recombinant expression of the N protein, together with the RNA polymerase cofactor P in *E. coli*, results in ring shaped, decameric nucleocapsid-like particles that encapsidate bacterial RNA non-specifically (3).

Crystallographic analysis has provided molecular details of RNA encapsidation and N oligomerization (3). The N protein consists of an N- and a C-terminal lobe in between which the RNA is packed. Each N protomer makes cross-molecular contacts with three neighboring N protomers, for which an extension of the N-terminal lobe (N-arm) and a large loop in the C-terminal lobe (C-loop) are critical. Removal of the N-arm reduces incorporation of RNA (4), while mutations in the C-loop affect VSV RNA replication and transcription differentially (5). In the nucleocapsid, the RNA is largely protected against digestion with RNAse; only harsh treatment with RNAse leads to RNA removal (6). How the polymerase L accesses the tightly encapsidated RNA in the course of transcription remains elusive. The L protein is unable to bind to the nucleocapsid directly. Instead, this interaction is mediated by P, a non-enzymatic polymerase cofactor that interacts with both L and N proteins. P can interact with N in two different ways. First, the extreme N terminus of P can chaperone the free N protein (N^0) to prevent it from premature oligomerization and association with random RNA. Instead, it directs N to encapsidate the viral RNA (7). The second interaction is mediated by the C-terminal domain of P, which binds to the C-lobes of two adjoining N protomers and thus is a nucleocapsid-specific interface (8). This interaction properly positions the L protein, which in turn could impose a conformational change on N that permits access to the RNA. As the complex moves along the template, N folds back and encapsidates the RNA while N^0 molecules encapsidate the newly synthesized strand of RNA.

The three proteins essential for VSV transcription and replication, N, P and L, provide attractive possible targets for intervention in the virus life cycle. We have explored the use of single

domain antibody fragments, derived from the variable region of the heavy chain of camelid heavy chain-only antibodies (VHHs), as antiviral agents that can be expressed intracellularly with retention of antigen-binding properties. We immunized an alpaca with inactivated VSV and selected VHHs using a lentiviral screening approach that relies on inducible expression of cytosolic VHHs and selection of cells that survive a lethal dose of VSV (9). All four identified VHHs specific for VSV (VHH 1001, 1004, 1014, and 1307) target the N protein and impede VSV replication when expressed cytosolically by blocking viral mRNA transcription. In an *in vitro* transcription assay with purified L, P and N-RNA template, only two VHHs (1001 and 1307) blocked mRNA transcription, indicating that the identified VHHs inhibit the virus in different ways. Competition analysis showed that all four N-specific VHHs recognize distinct epitopes (9).

To provide a molecular explanation for the inhibitory properties of N-specific VHHs, we defined the VHH binding sites on the N protein for three of the identified VHHs. We obtained crystal structures of N in complex with two VHHs and could map the binding site of a third VHH by generating VSV escape mutants grown in the presence of the inhibitory VHH. The defined binding sites provide a rationale for the inhibitory properties of the VHHs and explain relevance and function of the bound subdomains during viral replication.

Results

Inhibitory characteristics of VSV N specific VHHs

We reported the identification of several VSV N protein specific VHHs that, if expressed cytosolically, protect cells from VSV infection (9). To uncover the underlying vulnerabilities of the virus, we defined the inhibitory properties of three N-specific VHHs in more detail. First, we tested the effect of the VHHs on VSV infection in A549 cell derivatives in which cytosolic VHH expression is doxycycline-inducible. We induced VHH expression and infected cells 24 hours (h) later with VSV-GFP, a VSV Indiana strain that -in addition to the structural proteins of VSV- expresses GFP as a measure of a successful infection. We infected cells with different doses (multiplicities of infection, MOIs) of virus to test whether increasing amounts of virus could overcome the inhibitory potential of the VHHs (Fig 1A). Cells were harvested 4 h post infection and the percentage of GFP-positive cells was assessed by flow cytometry. All cell lines that expressed any of the N protein-specific VHHs blocked VSV when infected at an MOI of 10, while the cell line that expressed the control VHH was readily infected (control VHH: αNP-VHH1, influenza A nucleoprotein-specific (10)). An up to 32-fold increase in the amount of virus barely allowed infection of cells expressing VHH 1001. For cells that expressed VHH 1004, the fraction of GFP-positive cells increased with increasing MOI, reaching 37% GFP-positive cells when infected with the highest dose (MOI 320). Inhibition of infection in cells

that expressed VHH 1307 could be more easily overcome by increasing the virus dose, yielding more than 80% of GFP positive cells at a 4-fold increase of virus (MOI 40). Two VHH characteristics might contribute to the differential response to increasing doses of virus: (I) the expression level of the VHH, and (II) the mechanism by which the VHH inhibits the virus. To assess VHH expression levels, we stained for the HA-tagged VHHs with anti-HA-DL650 and quantified fluorescence intensity by flow cytometry (Fig 1B). Expression levels were highest for VHH 1001 and low for VHH 1307, explaining their robustness and vulnerably to increasing doses of virus, respectively. Despite only mild susceptibility to increasing amounts of virus, levels for VHH 1004 were barely detectable, suggesting a potent mechanism of inhibition for this VHH.

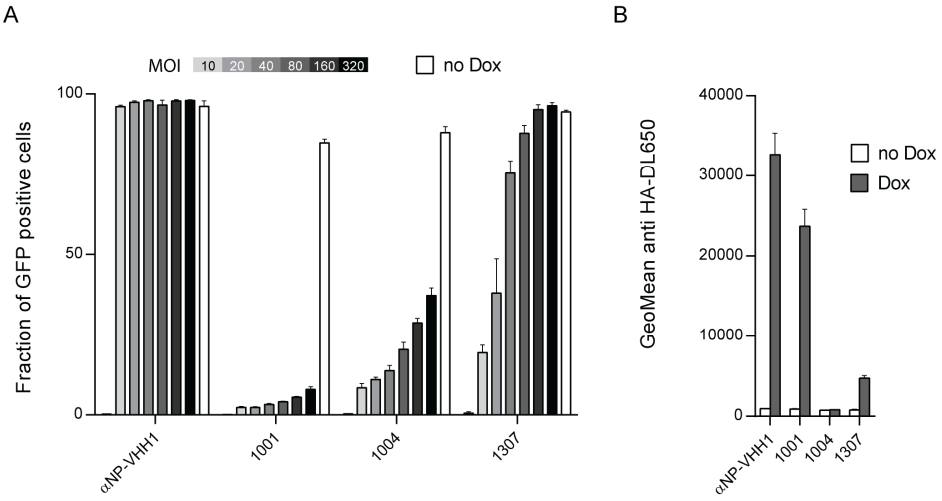

Figure 1 | Inhibitory properties of VSV N specific VHHs. (A) N protein specific VHHs differentially cope with increasing doses of VSV. A549 cells expressing VHHs in a doxycycline (Dox)-inducible manner were seeded 24 h before VSV infection. VHH expression was induced (grey - black bars) with Dox or cells left untreated (white bars). Each cell line was infected with increasing amounts of VSV-GFP (MOI = 0 – 320). Cells were harvested 4 h post infection and the percentage of infected cells (GFP positive) was quantified by flow cytometry. Average data from three independent experiments (± s.e.m.) is shown. **(B)** Quantification of VHH expression levels in A549 cells. Cells were seeded and HA-tagged VHH expression was induced with Dox. After 24 h, cells were harvested and stained for VHH-HA using anti-HA-DL650 antibodies. The geometric mean of anti-HA-DL650 fluorescence was quantified by flow cytometry and compared to uninduced cells lines. Data from three independent experiments (± s.e.m.) is shown.

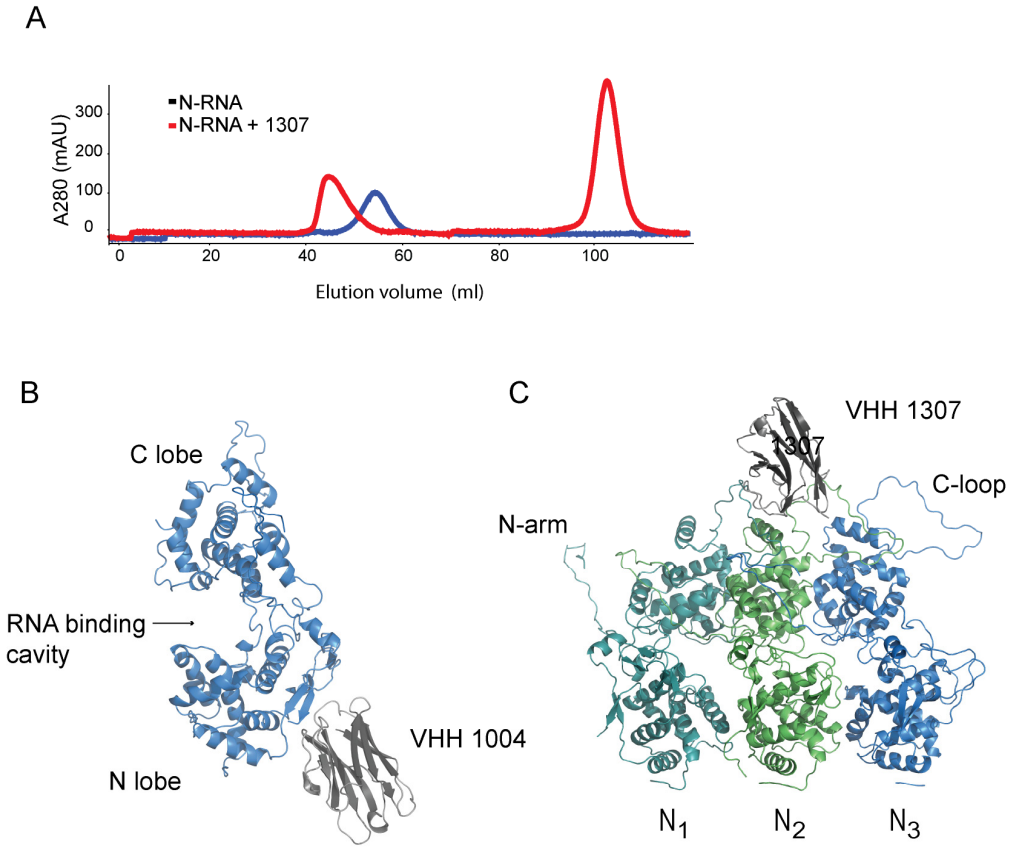

Figure 2 | Crystal structures of VHH 1004 and VHH 1307 in complex with VSV N-RNA (A) Purified N-RNA alone (blue), or preincubated with an excess of VHH (red), was subjected to size exclusion chromatography on a Superdex 200 column. Absorbance at 280 nm of the elution profile is displayed. Data exemplarily shown for N-RNA and N-RNA in complex with VHH 1307. **(B/C)** Ribbon representation of VHH 1004 and 1307 in complex with VSV N. **(B)** Side view of VHH 1004 (grey) bound to the N-lobe of a single N protomer (blue). **(C)** VHH 1307 (grey) and three N protomers are displayed (dark cyan, green and blue); view from the outside of the 10-mer ring. The VHH binds to the C-lobes of two adjacent N protomers. In the depicted structure, the VHH interacts with the left N-protomer (N_1, dark cyan) and the N protomer in the center (N_2, green).

VHH 1004 in complex with N-RNA

To uncover the inhibitory mechanism and epitope of the identified VHHs, we defined the binding site on the N protein by X-ray crystallography. We produced recombinant VHHs and N protein individually in E. coli and purified the proteins. We then combined VHH and N protein in a 3:1 molar ratio and purified the complex by size-exclusion chromatography. For all VHH:N-RNA complexes, we detected a clear shift in the elution profile, indicative of VHH binding to the N-RNA 10-mer ring (Fig 2A). The collected peak fractions were concentrated to 2.5 – 5 mg/ml and used to set up crystal screens of the VHH:N-RNA complexes. We were able

to obtain diffraction quality crystals for N-RNA in complex with VHH 1004 and VHH 1307 respectively.

Crystals of the N-RNA:1004 complex diffracted to 5.45 Å (Table 1). We solved the structure by molecular replacement (MR) (details in the Methods section) and refined to a final Rwork of 33.9% and Rfree of 34.0%. Besides the bound VHH, the structure resembles previously characterized N-RNA structures, in which N forms a 10-mer ring that encapsidates RNA (RMSD 0.89 – 0.99 Å). VHH 1004 binds the N-terminal lobe of the N protein, and decorates the circumference of the 10-mer N-RNA ring (Figs 2B and EV1). The VHH buries an area of ~500 Å2 on the N protein surface. The VHH contacts residues that are dispersed over three polypeptide segments of the same N protomer, which suggests that VHH 1004 should also be capable of binding to monomeric N0. VHH 1004, when expressed in the cytosol, strongly inhibits VSV replication, whereas in vitro transcription catalyzed by purified components (L, P and N-RNA) is barely affected by its presence (9). To replicate or transcribe the RNA, the VSV polymerase L must access the encapsidated RNA. Because VHH 1004 does not cover the known P binding site on the N protein (8), it either prevents L association with N and thus polymerase processivity, or manipulates N in such a way that prevents L from gaining access to the RNA, for example by perturbing the necessary flexibility for conformational changes. Since in vitro replication was not affected, it is likely that VHH 1004 only affects genome replication, but not mRNA transcription. This would substantially reduce the amount of genomes that serve as templates for mRNA transcription in infected cells.

VHH 1307 in complex with N-RNA

For the N-RNA:VHH 1307 complex, we obtained crystals that diffracted to 3.2 Å (Table 1). We solved the structure by MR and refined to a final R_{work} of 23.5% and R_{free} of 27.4%. The complex crystallizes as two 10-mer rings of N-RNA that are crowned at both ends with 10 VHHs each, yielding 40 protein subunits to the asymmetric unit (Fig EV1). The VHH binds to the C-terminal lobe of N-RNA, makes contact with two adjacent protomers, and thus binds to a nucleocapsid-specific interaction interface (Fig 2C). No drastic changes in N structure upon VHH binding can be detected (RMSD 0.81-0.96 Å). We identified the residues involved in the N:VHH 1307 binding interface using PDBePISA (11). VHH 1307 makes direct contact to residues from two adjacent protomers to a nucleocapsid-specific epitope that overlaps with the binding site of the polymerase cofactor P (8). This binding site suggests that the VHH may inhibit viral transcription by preventing P from binding to the nucleocapsid, which would block the P mediated access of the polymerase L to the RNA template. Accordingly, VHH 1307 inhibits transcription *in vitro,* and gene expression in infected cells, the latter of which likely relies on both genome replication and mRNA transcription (9). Experiments that interchanged the position of N and P proteins on the VSV genome, and thus switched expression levels

showed the importance of a balance between N and P proteins (12). VHH 1307 perturbs this balance, but because of this VHH's comparatively low expression levels, increasing amounts of virus may overcome antiviral restriction as shown in Figure 1.

Table 1 Data collection and refinement statistics

Protein	**VSV N:VHH 1004 native**	**VSV N:VHH 1307 native**
Organism	*Vesicular stomatitis virus, Vicugna pacos*	*Vesicular stomatitis virus, Vicugna pacos*
PDB ID	5UKB	5UK4
Data collection		
Space group	$P2_12_12$	P1
a, b, c (Å)	240.117, 335.497, 75.899	147.555, 156.008, 217.450
α, β, γ (°)	90.0, 90.0, 90.0	79.24, 75.66, 62.27
Wavelength (Å)	0.9791	0.9791
Resolution range (Å)	195.26 - 5.50 (5.70 - 5.50) [a]	128.45 – 3.20 (3.31 – 3.20)
Total reflections	227207	614436
Unique reflections	20655	250547
Completeness (%)	99.7 (98.3)	92.4 (92.5)
Redundancy	11.0 (5.5)	2.5 (2.4)
R_{sym} (%)	16.6 (100.0)	20.4 (67.5)
$R_{p.i.m.}$ (%)	5.2 (46.0)	15.2 (50.2)
I/σ	16.2 (0.86)	5.1 (1.4)
$CC_{1/2}$ (%)	99.7 (55.6)	99.3 (61.9)
Refinement		
Resolution range (Å)	195.26 - 5.50	128.45 – 3.20
R_{work} (%)	33.9	23.6
R_{free} (%)	34.0	28.7
Coordinate error (Å)	1.01	0.44
Number of Reflections		
Total	20603	250544
R_{free} reflections	2000	1990
Number of non-hydrogen atoms	21875	88846
Protein atoms	21875	88846
R.m.s. deviations		
Bond lengths (Å)	0.004	0.013
Bond angles (°)	0.85	0.94
Average B factors (Å²)		
Protein	305.1	58.33
Ramachandran (%)		
Favored (%)	94.4	93.9
Allowed (%)	5.1	5.9
Outlier (%)	0.5	0.2
Clashscore	37.39	13.4
Molprobity score	2.44	2.04
Molprobity percentile	97th	97th

[a]Values in parentheses are for highest-resolution shell.

VHH 1307 in complex with N-RNA

For the N-RNA:VHH 1307 complex, we obtained crystals that diffracted to 3.2 Å (Table 1). We solved the structure by MR and refined to a final R_{work} of 23.5% and R_{free} of 27.4%. The complex crystallizes as two 10-mer rings of N-RNA that are crowned at both ends with 10 VHHs each, yielding 40 protein subunits to the asymmetric unit (Fig EV1). The VHH binds to the C-terminal lobe of N-RNA, makes contact with two adjacent protomers, and thus binds to a nucleocapsid-specific interaction interface (Fig 2C). No drastic changes in N structure upon VHH binding can be detected (RMSD 0.81-0.96 Å). We identified the residues involved in the N:VHH 1307 binding interface using PDBePISA (11). VHH 1307 makes direct contact to residues from two adjacent protomers to a nucleocapsid-specific epitope that overlaps with the binding site of the polymerase cofactor P (8). This binding site suggests that the VHH may inhibit viral transcription by preventing P from binding to the nucleocapsid, which would block the P mediated access of the polymerase L to the RNA template. Accordingly, VHH 1307 inhibits transcription *in vitro,* and gene expression in infected cells, the latter of which likely relies on both genome replication and mRNA transcription (9). Experiments that interchanged the position of N and P proteins on the VSV genome, and thus switched expression levels showed the importance of a balance between N and P proteins (12). VHH 1307 perturbs this balance, but because of this VHH's comparatively low expression levels, increasing amounts of virus may overcome antiviral restriction as shown in Figure 1.

VHH 1307 and P bind to the same or overlapping epitopes on N

We found that VHH 1307 and P bind to overlapping epitopes of N (Fig 3A). To test biochemically whether VHH 1307 prevents binding of P to N or vice versa, we addressed the interaction of VHHs with N alone or N in complex with stoichiometric amounts of P (Fig 3B). We biotinylated VHH 1001, 1004, 1307 and a control VHH (αNP-VHH1, influenza A nucleoprotein specific (10)), and immobilized them on streptavidin beads. We incubated the beads with purified N, or the N/P complex, and analyzed the bound protein by SDS-PAGE and Coomassie staining. With the exception of the control VHH, all VHHs immunoprecipitated the N protein alone. VHH 1001 and 1004 also immunoprecipitated intact N/P complexes. In contrast, VHH 1307 only retrieved N from the complexes, indicating that the VHH displaced P from the complex. These data confirm that 1307 and P bind to overlapping epitopes on the N protein, and suggests that VHH 1307 can also displace P from viral nucleocapsids.

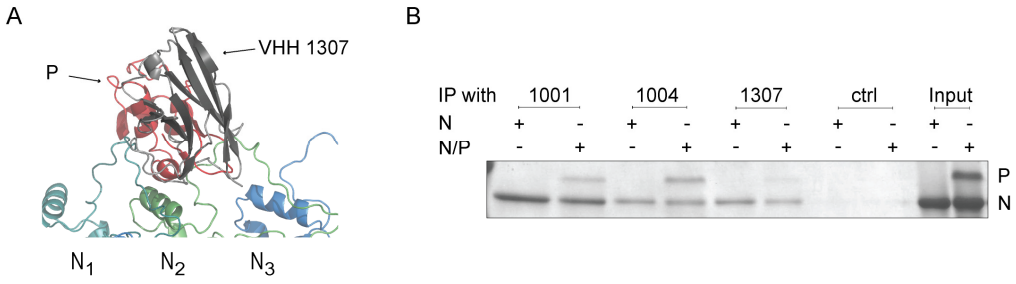

Figure 3 | VHH 1307 competes with P for binding to N. (A) Magnified view and superposition of the C-terminal domain of P (red) and 1307 (grey) at their binding site at the N-RNA C-loop region. **(B)** VHH binding to N and the N/P complex. Biotinylated, N specific VHHs and a control VHH (αNP-VHH1, influenza A nucleoprotein specific) were immobilized on streptavidin beads and N alone, or N in complex with P was added to the beads. Bound protein was eluted and subjected to 10% SDS-PAGE (75:1 acrylamide/bis-acrylamide) and Commassie staining. A representative gel from three independent experiments is shown.

Functional determination of binding site by escape mutants.

To independently identify VHH binding sites on N based on function, we generated VSV escape mutants by serial passage of infectious supernatants in cells that expressed the different VHHs. We diluted cell supernatants after passaging, infected a new monolayer of cells and analyzed the resulting plaques by RT-PCR and sequencing. For VHH 1001 all four analyzed plaques carried different mutations in N. All plaques analyzed from escape mutants of VHH 1004 carry the mutation G75R in N, while all escape mutants of VHH 1307 contain the mutation D374N in N (Table 2). All identified escape mutation residues are surface-exposed and are not in close proximity to each other (Figs 4 and 5), confirming that the identified anti-VSV N VHHs have unique binding sites (9).

Table 2 List of observed escape mutations in N

VHH	**clone**	**Mutations**	**Sequence change**
1001	1	A771C	E257D
	2	C778A	Q260K
	3	A779G	Q260R
	4	A728G	E243G
1004	1,2,3	G223A	G75R
1307	1,2,3	G1120A	D374N

The glycine residue 75 mutated in VHH 1004 escape mutants is positioned in the center of the binding site as determined crystallographically (Fig 5A). The D374N substitution found in all VHH 1307 escape mutants is likewise located in the established binding site of VHH 1307 (Fig 5B). Because this subdomain of N is also bound by the essential polymerase cofactor P, this mutant must retain the ability to engage P. While many of the interaction/interface residues of VSV P and VHH 1307 overlap, residue D374 is exclusively engaged by VHH 1307 but not by

P (Fig 4) (8). The escape mutant therefore affects the interaction of the nucleocapsid and VHH 1307 without altering the binding to P.

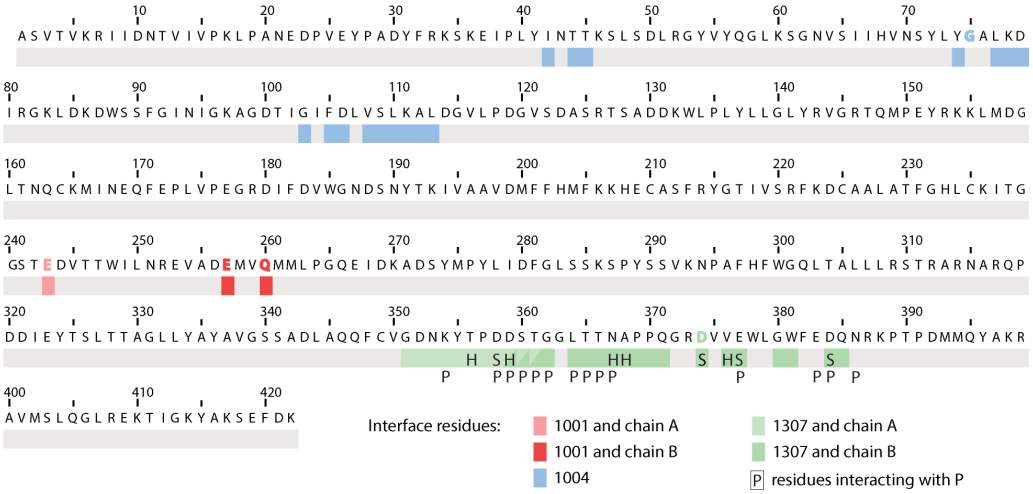

Figure 4 | Amino acid sequence overview of VSV N protein. Protein sequence of VSV Indiana N protein. Binding interface residues for VHH 1004 are shown in blue. Interface residues for VHH 1307 are shown in light green (N_1) or dark green (N_2). Residues engaged from two VHH 1307 molecules are colored in both green tones. The better resolution of the N-RNA:1307 crystal allowed to specify the interaction types. 'H' labels residues involved in hydrogen bonds and 'S' labels residues engaged in salt bridge. A 'P' labels residues interacting with the phosphoprotein P (8). Amino acids changed in escape mutants (Table 2) are highlighted with the VHHs color. Escape mutations for VHH 1001 colored in light red (N_1) or darker red (N_2).

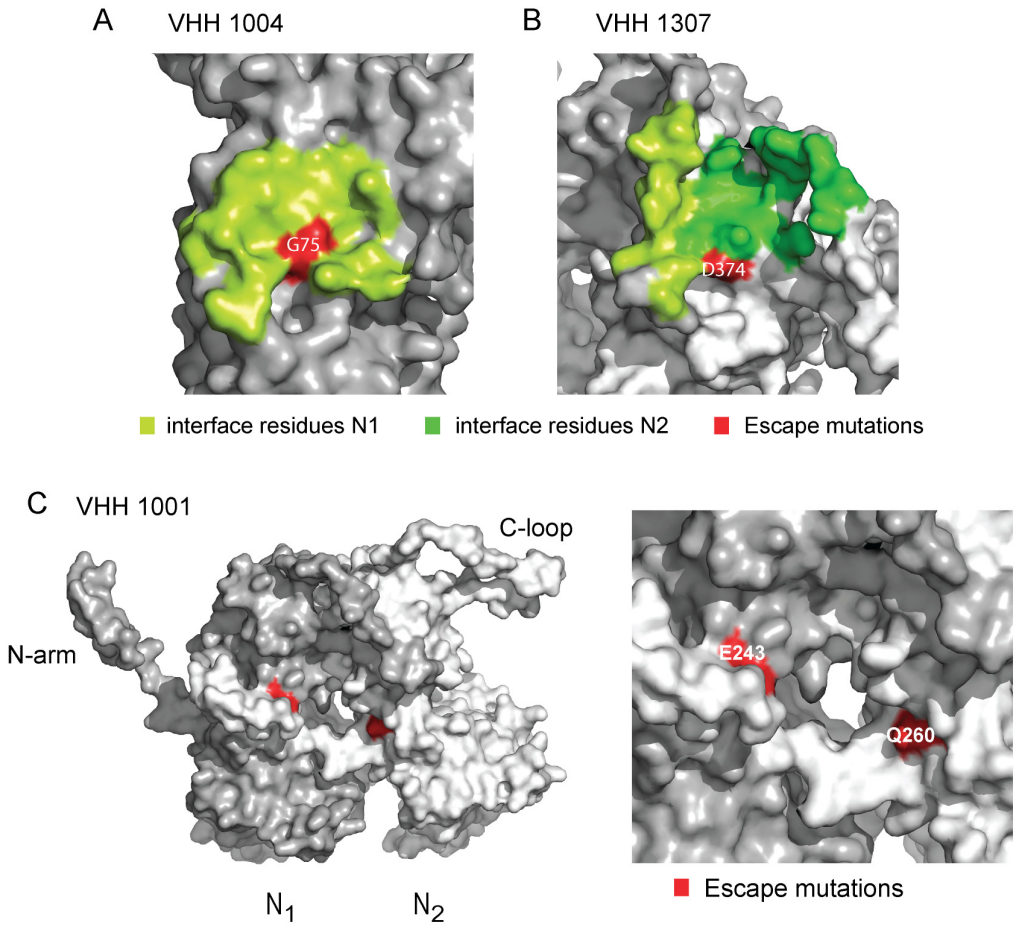

Figure 5 | VSV escape mutations for VHH 1001, 1004 and 1307. Surface representation of the N protein. **(A)** VHH 1004 binding interface residues on a single N protomer are shown in green, the escape mutant residue G75R is shown in red. **(B)** The two adjoining N protomers that are bound by VHH 1307 are shown in grey and silver. Interface residues of the left protomer (N_1) are colored in light green, interface residues of the right protomer (N_2) are shown in dark green. Location of escape mutation D374N is shown in red. **(C)** Two adjoining N protomers with magnified view of the VHH 1001 binding site. Locations of the escape mutations E243G on the left protomer (N_1) and Q260K/R on the right protomer (N_2) are shown in red. Escape mutation E257D is also surface exposed but located behind Q260K/R and cannot be seen from this angle. All illustrations were generated in PyMOL.

We were unable to obtain diffraction quality crystals for VHH 1001 in complex with N, but successfully generated VSV escape mutants instead. Because the escape mutants for VHH 1004 and 1307 were located precisely in the binding site as determined by crystallography, and the residues mutated under pressure from VHH 1001 are similarly solvent exposed, we presume that the identified escape mutations correspond to the VHH 1001 binding site. VHH 1001 inhibits VSV mRNA transcription if expressed in the cytosol and blocks in vitro transcription as well. In the lentiviral screening approach that led to the identification of VHH 1001, this particular VHH was found in 34 of 41 independently identified clones, which we attribute to its comparatively higher expression levels and potent mechanism of inhibition (9). For VHH 1001 we analyzed 4 plaques (Table 2). Each carried a different mutation that resulted in 4 independent changes in the N protein sequence (E243G, E257D, Q260R, Q260K). Mutated

residue E243G and residues E257D, Q260K are located on opposite sides of the C-terminal lobe of an N protomer. The location of the escape mutations suggests that the VHH engages an interface of N-RNA that is composed of two adjacent N protomers, rather than a single N protomer (Fig 5C). The distance of the identified residues in two adjacent protomers is ~2 nm and therefore equivalent to the diameter of a typical VHH (~2x3.5 nm). At this interface, the VSV nucleocapsid exhibits a small notch between two N molecules that would perfectly accommodate a VHH. It is possible that VHH 1001 binding stabilizes the nucleocapsid by forming a bridge between two adjacent N protomers. The resulting reduced flexibility might prevent the LP complex to gain access to the RNA for transcription and replication.

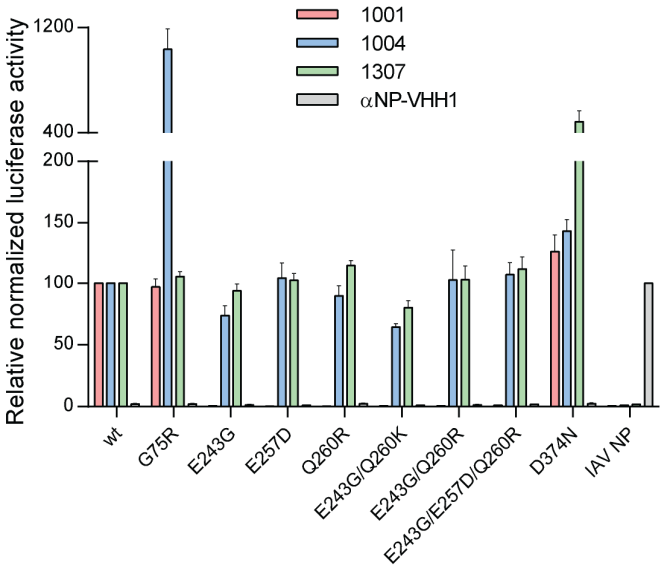

Figure 6 | VHH binding to VSV N escape variants. **(A)** Indicated, HA-tagged VHHs and mutated versions of N fused to Renilla luciferase or influenza A NP fused to Renilla luciferase were transiently co-expressed in 293T cells. 96-well plates coated with anti-HA anti-body to capture the VHHs were incubated with cell lysates. Activity of the co-purified luciferase was measured. Emitted light was normalized to luciferase activity in the lysate. Data are from three independent experiments (±s.e.m.).

Binding of VHHs to the escape mutants.

Not all escape mutations resulted in drastic changes of amino acid characteristics at the mutated site. While mutations G75R, E243G or D374N are major changes in size, polarity or charge of the surface exposed amino acids, the mutation E257D represents a single methylene group difference. To test how these mutations in N affect recognition by the VHHs, we applied LUMIER assays with mutated versions of the N protein (Fig 6) (9, 13). In this assay, an HA-tagged VHH and a Renilla luciferase fusion of N are transiently co-expressed in 293T cells. After 24 h, cells are lysed and the HA-tagged VHH is immobilized in 96-well plates coated with anti-HA antibody. Renilla luciferase activity is quantified as a measure of how much N-protein is bound to the VHH. All Renilla-N mutants were expressed to comparable levels (data not shown, but used for normalization), and all N protein specific VHHs were able to retrieve wild type (WT) N protein. Escape mutations observed for VHH 1001, as single mutations or as combinations, abolished binding of VHH 1001, indicating that these surface exposed residues are indeed critical for VHH 1001 binding. N protein carrying these escape mutations were still

readily retrieved by VHH 1004 and 1307, indicating that these mutations did not alter overall N structure. A loss of VHH binding as observed for VHH 1001 is the expected escape strategy from inhibitory VHHs. Surprisingly, the VHH 1004 escape mutation G75R resulted in a strong increase of retrieved N by VHH 1004, while VHH 1001 and 1307 recovered this N variant at levels comparable to WT N. Similarly, VHH 1307 retrieved higher levels of its escape mutant D374N mutant compared to its WT counterpart.

To better understand the escape mutations that failed to eliminate binding, we performed bio-layer interferometry to analyze binding kinetics. When binding of N-RNA to immobilized VHHs was analyzed, we could confirm all binding activities observed in LUMIER assays, but could not deduce any binding constants due to the lack of dissociation. We thus immobilized WT and mutant version of N and measured VHH association and dissociation. For VHH 1001 and 1004, we observed poor association, likely because of their lateral VHH binding sites, steric hindrance and unfavorable orientations of the N-RNA ring in this assay geometry. VHH 1307 associated slightly faster to the D374N mutant compared to WT N, but, importantly, dissociated more than 1000-fold faster (Table 3 and Fig EV2). In the LUMIER assay, fast dissociation is likely prevented by avidity affects and the larger amount of retrieved mutant protein is a result of faster association. During infection however, the more dynamic binding allows VHH 1307 to be more easily replaced by P, undermining the VHHs inhibitory properties. In conclusion, abolished or altered binding dynamics allowed VSV N to escape from VHH-mediated restriction.

Table 3 Binding affinities of VHH 1307 to WT or mutant N.

VHH 1307 binding to	KD (M)	Kon (1/Ms)	Koff (1/s)
WT N	5.53×10^{-11}	1.18×10^{6}	6.51×10^{-5}
D374N N	6.47×10^{-8}	1.28×10^{6}	8.25×10^{-2}

Discussion

Virus infections continue to fuel the threat of future epidemics. While vaccine strategies directed against viral glycoproteins have been remarkably successful, the selective pressure exerted by the immune system can generate escape variants against which the vaccine-elicited response is no longer effective, as so well documented for influenza A (14). Targeting enzymatic functions unique to particular viruses offers a viable alternative, exemplified by drugs that exploit influenza virus neuraminidase activity or herpesvirus kinases (15, 16). VSV is a prototypic non-segmented RNA virus. To better understand the transcription/replication process, and to identify new vulnerabilities of this class of viruses, we used cytosolically expressed VHHs, also called nanobodies, that target the VSV nucleoprotein N and block infection. To relate the inhibitory properties of the N specific VHHs to the structural features

they recognize, we determined the binding sites of three VHHs by means of X-ray crystallography and the analysis of escape mutants. One identified VHH binds to the N-terminal lobe of N, and two VHHs bind to different epitopes on the C-terminal lobe of N. Escape mutants showed single mutations at the established binding sites and thus confirm them by functional biological criteria.

Because the N protein encapsidates the RNA in a tight manner, a close coordination of the LP complex with the N-RNA template is necessary to allow RNA access and polymerase processivity. Our VHHs are likely to perturb this coordination and there are at least two possible ways to do so: First, by competing with, or sterically excluding the binding of other viral or host proteins to the N-RNA template or, by preventing a conformational change and dislocation of N from the RNA during the process of transcription. Both scenarios could, in combination or alone, hamper polymerase processivity, transcription and replication.

The structural data presented here readily explain the inhibitory mechanism of VHH 1307, which is further supported by immunoprecipitation experiments. The binding site of VHH 1307 overlaps with the binding site of the polymerase cofactor P. Although VHH 1307 effectively blocks transcription and likely replication, the inhibitory properties can be overcome by infecting with an increased virus dose. This could be due either to a complete absorption of the inhibitory VHH and a surplus of N-RNA genomes that thus remain unbound by a VHH, or, that an increased concentration of P suffices to outcompete the VHH. The latter explanation would be in line with the model of a highly dynamic interaction of the N protein and C-terminal domain of P during transcription and replication.

In contrast, the (presumptive) binding sites for VHH 1001 and 1004 do not readily explain their antiviral mechanism. Both VHHs can bind to the N/P complex, thus likely inhibit transcription in a manner different from that of VHH 1307. Further, both VHHs show inhibitory potential against high doses of virus. While the high expression levels of VHH 1001 are a likely contributing factor, the comparatively low levels of VHH 1004 that suffice for inhibition illustrate the potency of its mechanism of inhibition. Nevertheless, we did not find VHH 1004 to be a potent inhibitor in *in vitro* transcription assays with purified components, suggesting that VHH 1004 only indirectly affects mRNA transcription in infected cells, e.g. by interfering with genome replication, which ultimately substantially reduces the number of available templates for transcription (9). The detectable levels of GFP expression in VHH-producing cells infected at high MOIs might thus result from primary transcription of the incoming genomes. The strong VHH 1004-mediated inhibition despite low expression levels might indicate that the VHH does not have to bind to each protomer to block replication. However, we also cannot exclude that *in vitro* transcription does not accurately recapitulate the events

that occur in the cytosol of cells during infection. Differences that potentially have an impact include the non-natural ratios of N and L proteins, a structural difference of the isolated N-RNA template compared to its more flexible representation in the cytosol, or the lack of an additional factor. However, from the results obtained for VHH 1004 we conclude that not only the N-arm but the entire N-lobe of VSV N is of relevance for efficient replication.

Based on the nucleocapsid structure, binding of VHH 1001 would function similarly to the N-arm and stabilize the association of the two adjacent monomers bound. Removal of the N-arm reduces incorporation of RNA (4). VHH 1001 supports the N-arm and may stabilize the interaction between two protomers and thus reduces the flexibility of the N-RNA template. This flexibility might be of crucial importance when L and P engage the N-RNA template in order to access the viral RNA. Based on the binding site, we presume that VHH 1001 directly hinders N-RNA to function as a template for transcription and replication by preventing access to the encapsidated RNA.

While we see the expected loss of binding of VHH 1001 to its escape variants of N, VHH 1004 and 1307 retrieve increased amounts of their respective escape mutants. The binding kinetics revealed that VHH 1307 dissociates much faster from its N escape mutant compared to WT N and thus that the VHH may be replaced more readily by P, explaining how this mutant avoids VHH-mediated restriction. The observed increase in recovered protein in the LUMIER assay might primarily be the result of avidity effects that prevent fast dissociation from immobilized VHHs. The escape mechanism for VHH 1004 might work in similar fashion, based on more dynamic binding kinetics that allow polymerase processivity. Nevertheless, for the very low-expressing VHH 1004, an opposed escape mechanism is also conceivable, and increased binding affinity might be advantageous. If transcription of viral genes is unaffected by this VHH as it is *in vitro* (9), its inhibitory properties could be neutralized by newly produced N, and high affinity and limited dissociation would prevent interference with replication later during infection. Lastly, mutations in N, in the precise binding sites of the VHHs, altered binding kinetics to restore virus propagation.

In conclusion, we have shown that it is possible to use VHHs for a robust cycle of experiments that reveal insights into the molecular biology of their targets: first, we produced and selected VHHs that impede viral growth; second, accurately defined the epitope recognized at the structural level; third we used cytosolically expressed VHHs to select virus variants that escape VHH-imposed inhibition, and finally, -in at least one case- provide a rational explanation for the inhibitory mechanism of the VHH in question using the structure of the VHH in complex with its target. The defined binding sites leverage the use of these newly identified VHHs as tools to further investigate this non segmented RNA virus.

Expanded view figures

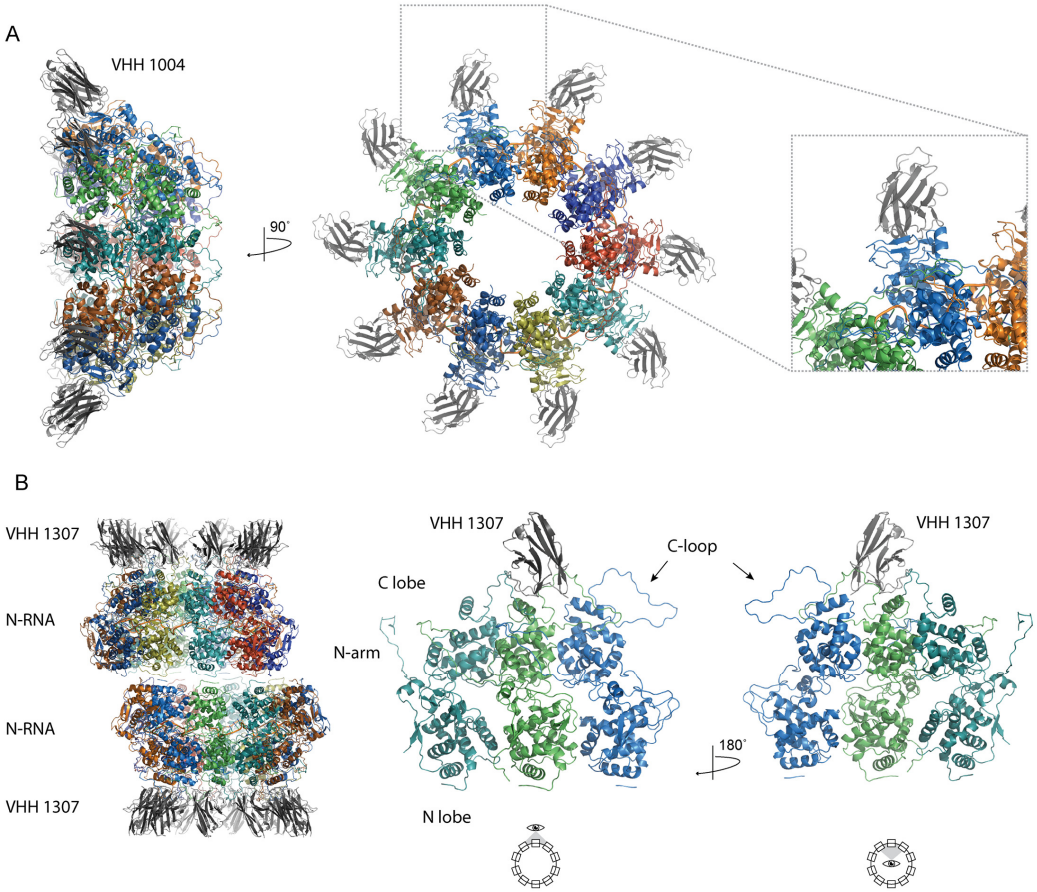

Figure EV1 | Overview of the N-RNA ring in complex with VHH 1004 (A) and in complex with VHH 1307 (B). VHHs are depicted in grey/black and N protomers are displayed in color. (**A)** VHH 1004 binds to the circumference of the 10-mer N-RNA ring and the N-terminal lobe of N. (B) VHH 1307 binds to the C lobe of the N-RNA ring.

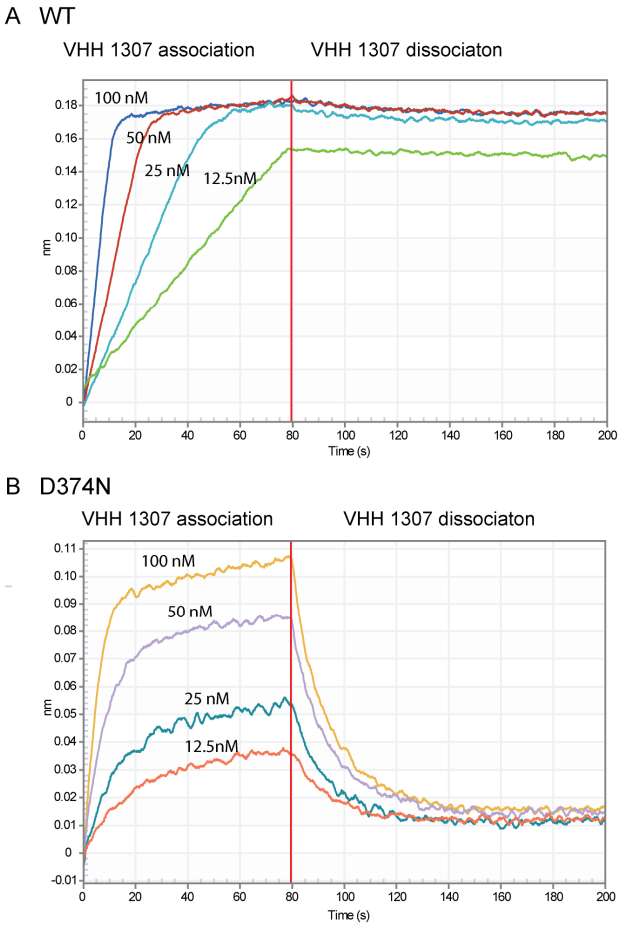

Figure EV2 | Binding affinity determination for VHH 1307. Octet RED96 sensorgrams with immobilized VSV N WT (A) or D374N (B). VHH 1307 association and dissociation is shown for VHH concentrations of 12.5 – 100 nM.

Materials and Methods

Virus, Cell lines and Reagents

VSV Indiana GFP was propagated in BHK-21 cells, which were obtained from ATCC. Clarified, infectious supernatants were used for flow cytometry-based infection assays. The A549 cell line inducible expressing VHH-HA, derived from A549 cells purchased from ATCC, and were generated using lentivirus produced with derivatives of pInducer20 (17), and selected in the presence of 500 µg/ml G418. HEK 293T cells were obtained from ATCC. Cells were cultivated in DME with 10% FBS and 500 µg/ml G418. Doxycycline hyclate (Dox) was purchased from Sigma Aldrich. Nickel-nitrilotriacetic acid (NTA) beads were purchased from Qiagen. Mouse anti-HA.11 (clone 16B12) was acquired from BioLegend. Mouse anti-HA.11 (clone 16B12) coupled to Dylight (DL) 650 was purchased from Abcam. VHHs were site-specifically biotinylated using sortase A and GGG-biotin as described earlier (18).

Infection Assay

To analyze the effect of the N protein specific VHHs on different doses (MOI) of virus, A549 cells inducibly expressing the VHHs were seeded and VHH expression was induced with 1 µg/ml doxycycline (final concentration). After 24 h, cells were infected with VSV Indiana GFP at an MOI between 0 and 320. 4 h post infection, cells were trypsinized, fixed in 4% PFA and analyzed by flow cytometry using a BD accuri and the FlowJo software package.

Protein expression and purification

The identification and production of VSV N specifc VHHs was described earlier (9). VSV N-RNA and its escape mutant variants were expressed and purified as described elsewhere (19). Sequences encoding the different VHHs with a C-terminal sortase recognition site (LPETG) followed by a His_6-tag were cloned into a pHEN6 expression vector for periplasmic expression. *E.coli* WK6 bacteria were transformed with the vector and expression was induced with 1 mM IPTG at OD600=0.6; cells were grown overnight at 30° C. VHHs were retrieved from the periplasm by osmotic shock and purified by Ni-NTA affinity purification and size-exclusion chromatography on a Superdex 75 column.

Crystallization

For co-crystallization, VHHs 1004 and 1307 were individually mixed in a 3:1 molar ratio with recombinant VSV N-RNA and purified by size-exclusion on a Superdex 200 column. A single peak of the 20-mer N-RNA:VHH complex was collected and VHH binding was confirmed by SDS-PAGE and Coomassie staining. We concentrated the complex to a concentration of 2 mg/ml in 50 mM Tris/HCl pH 7.5 and 150 mM NaCl buffer. Initial crystal growth was observed in 0.1 M sodium acetate pH 5.0, 1.5 M ammonium sulfate for VHH 1004 and 0.2 M sodium acetate, 0.1 M tri-sodium citrate pH 5.5, 5% (w/v) polyethylene glycol 4.000 for VHH 1307, in a vapor diffusion experiment in a 96-well sitting drop setup (Index HT, Hampton Research; Procomplex, Qiagen). Diffraction quality crystals were grown from crystal seeds in a 24-well vapor diffusion hanging drop set up in the same buffers where initial crystal growth was observed. Crystals were cryoprotected in 20% glycerol and flash frozen in liquid nitrogen.

Data processing and structure determination.

Datasets were collected at the Advanced Photon Source user end station 24-IDC. Data reduction was performed in HKL2000 (20). Molecular replacement was performed in the PHENIX suite using *PhaserMR* (21). We first analyzed N:RNA:1307 and used PDB ID 2GIC (3) (N-RNA) for molecular replacement and PDB ID 3HHZ (8) for P-VHH superposition. For the N-RNA:1004 structure we used the significantly improved N-RNA model from our first structure for molecular replacement. For MR of the VHH, we used PDB ID 4KRL, which had the highest degree of sequence similarity. We could place 4KRL to one N molecule, replaced amino acids

in the loop regions, applied non-crystallographic symmetry (NCS) and refined with target weight optimization.

LUMIER assays

To analyze binding of VHHs to mutated version of N, we applied LUMIER assay as described in detail before (9). 293T cells were co-transfected with pCAGGS VHH-HA and pEXPR N-Renilla as WT or escape mutant variants using Lipofectamine 2000. 24 h post transfection, cells were lysed and incubated in 96-well LUMITRAC 600 plates (Greiner) coated with anti-HA.11 antibody to capture the VHHs. Activity of the co-purified luciferase was quantified by addition of coelenterazine-containing Renilla luciferase substrate mix (BioLux Gaussia Luciferase Assay Kit, New England BioLabs) and light emission measured using a SpectraMax M3 microplate reader (Molecular Devices).

Bio-layer interferometry

The Octed RED96 (Fortebio, Pall) was used to measure affinity and kinetic parameters. Strepavidin biosensors were purchased from Pall, all measurements were performed in PBS, 1% BSA, 0.005 % Tween-20. N-RNA and its escape mutant variants were biotinylated via coupling to primary amines with the Chromalink NHS biotin reagent (Solulink, San Diego, CA) for 90 min in 100 mM phosphate buffer pH 7.4, 150 mM NaCl. Streptavidin biosensors were loaded with the biotinylated N-RNA variants at a concentration of 4 μg/ml. Association and dissociation of VHHs was recorded with dilutions at concentrations between 12.5 and 100 nM. Data was analyzed using the 2:1 heterogeneous ligand binding global fit model.

References

1. **Morin B**, **Rahmeh A a**, **Whelan SPJ**. 2012. Mechanism of RNA synthesis initiation by the vesicular stomatitis virus polymerase. EMBO J **31**:1320–9.
2. **Ge P**, **Tsao J**, **Schein S**, **Green TJ**, **Luo M**, **Zhou ZH**. 2010. Cryo-EM model of the bullet-shaped vesicular stomatitis virus. Science **327**:689–693.
3. **Green TJ**, **Zhang X**, **Wertz GW**, **Luo M**. 2006. Structure of the vesicular stomatitis virus nucleoprotein-RNA complex. Science (80-) **313**:357–360.
4. **Zhang X**, **Green TJ**, **Tsao J**, **Qiu S**, **Luo M**. 2008. Role of intermolecular interactions of vesicular stomatitis virus nucleoprotein in RNA encapsidation. J Virol **82**:674–682.
5. **Harouaka D**, **Wertz GW**. 2009. Mutations in the C-terminal loop of the nucleocapsid protein affect vesicular stomatitis virus RNA replication and transcription differentially. J Virol **83**:11429–11439.
6. **Green TJ**, **Rowse M**, **Tsao J**, **Kang J**, **Ge P**, **Zhou ZH**, **Luo M**. 2011. Access to RNA Encapsidated in the Nucleocapsid of Vesicular Stomatitis Virus. J Virol **85**:2714–2722.
7. **Leyrat C**, **Yabukarski F**, **Tarbouriech N**, **Ribeiro EA**, **Jensen MR**, **Blackledge M**, **Ruigrok RWH**, **Jamin M**. 2011. Structure of the Vesicular Stomatitis Virus N0-P Complex. PLoS Pathog **7**:e1002248.
8. **Green TJ**, **Luo M**. 2009. Structure of the vesicular stomatitis virus nucleocapsid in

complex with the nucleocapsid-binding domain of the small polymerase cofactor, P. Proc Natl Acad Sci U S A **106**:11713–11718.

9. **Schmidt FI**, **Hanke L**, **Morin B**, **Brewer R**, **Brusic V**, **Whelan SPJ**, **Ploegh HL**. 2016. Phenotypic lentivirus screens to identify functional single domain antibodies. Nat Microbiol **1**:16080.

10. **Ashour J**, **Schmidt FI**, **Hanke L**, **Cragnolini J**, **Cavallari M**, **Altenburg A**, **Brewer R**, **Ingram J**, **Shoemaker C**, **Ploegh HL**. 2015. Intracellular Expression of Camelid Single-Domain Antibodies Specific for Influenza Virus Nucleoprotein Uncovers Distinct Features of Its Nuclear Localization. J Virol **89**:2792–2800.

11. **Krissinel E**, **Henrick K**. 2007. Inference of Macromolecular Assemblies from Crystalline State. J Mol Biol **372**:774–797.

12. **Wertz GW**, **Moudy R**, **Ball LA**. 2002. Adding genes to the RNA genome of vesicular stomatitis virus: positional effects on stability of expression. J Virol **76**:7642–50.

13. **Barrios-Rodiles M**, **Bose R**, **Liu Z**, **Donovan RS**, **Shinjo F**, **Liu Y**, **Dembowy J**, **Taylor IW**, **Luga V**, **Przulj N**, **Robinson M**, **Suzuki H**, **Hayashizaki Y**, **Jurisica I**, **Wrana JL**. 2005. High-Throughput Mapping of a Dynamic Signaling Network in Mammalian Cells. Science (80-) **307**:1621–1625.

14. **van de Sandt CE**, **Kreijtz JHCM**, **Rimmelzwaan GF**. 2012. Evasion of Influenza A Viruses from Innate and Adaptive Immune Responses. Viruses **4**:1438–1476.

15. **McKimm-Breschkin JL**. 2013. Influenza neuraminidase inhibitors: antiviral action and mechanisms of resistance. Influenza Other Respi Viruses **7 Suppl 1**:25–36.

16. **Li R**, **Hayward SD**. 2013. Potential of protein kinase inhibitors for treating herpesvirus-associated disease. Trends Microbiol **21**:286–295.

17. **Meerbrey KL**, **Hu G**, **Kessler JD**, **Roarty K**, **Li MZ**, **Fang JE**, **Herschkowitz JI**, **Burrows AE**, **Ciccia A**, **Sun T**, **Schmitt EM**, **Bernardi RJ**, **Fu X**, **Bland CS**, **Cooper TA**, **Schiff R**, **Rosen JM**, **Westbrook TF**, **Elledge SJ**. 2011. The pINDUCER lentiviral toolkit for inducible RNA interference in vitro and in vivo. Proc Natl Acad Sci U S A **108**:3665–70.

18. **Guimaraes CP**, **Witte MD**, **Theile CS**, **Bozkurt G**, **Kundrat L**, **Blom AEM**, **Ploegh HL**. 2013. Site-specific C-terminal and internal loop labeling of proteins using sortase-mediated reactions. Nat Protoc **8**:1787–99.

19. **Green TJ**, **Macpherson S**, **Qiu S**, **Lebowitz J**, **Wertz GW**, **Luo M**. 2000. Study of the assembly of vesicular stomatitis virus N protein: role of the P protein. J Virol **74**:9515–9524.

20. **Otwinowski Z**, **Minor W**. 1997. Processing of X-ray diffraction data collected in oscillation mode. Methods Enzymol **276**:307–326.

21. **Adams PD**, **Afonine P V.**, **Bunkóczi G**, **Chen VB**, **Davis IW**, **Echols N**, **Headd JJ**, **Hung LW**, **Kapral GJ**, **Grosse-Kunstleve RW**, **McCoy AJ**, **Moriarty NW**, **Oeffner R**, **Read RJ**, **Richardson DC**, **Richardson JS**, **Terwilliger TC**, **Zwart PH**. 2010. PHENIX: A comprehensive Python-based system for macromolecular structure solution. Acta Crystallogr Sect D Biol Crystallogr **66**:213–221.

Chapter 6

Discussion

In the ongoing evolutionary arms race between pathogens and the immune system, most viruses have developed mechanisms to evade antiviral responses. One effective way for a virus to escape host immune responses is to mutate those proteins targeted by the immune system. The majority of such mutations occur in surface-exposed viral proteins that are targets of the host's antibody response. This is exemplified by the vast diversity of IAV HA sequences. In contrast, the diversity of intracellularly disposed viral proteins is far less pronounced, likely because of a less complex, but not necessarily less efficient, antiviral immune repertoire inside the cell, which is mostly innate and less specific. A tailored immune response to intracellular viral proteins is often limited to the presentation of viral peptides on MHC class I molecules to $CD8^+$ T cells, and not to fully-folded viral proteins. The complex enzymatic functions and interactions of viral proteins with host proteins inside the cell are often accompanied by functional or selective constraints which may limit the possibility of generating escape mutants. Furthermore, viruses are often highly adapted to interact with the intracellular proteins of a specific host leading to viral tropism. Thus, minor changes in the amino acid sequence of certain viral proteins can sometimes discriminate between virulent and non-virulent strains. Residue 627 in the avian IAV polymerase basic protein 2 (PB2) is a well-studied example of this. Avian IAV, which typically has a glutamic acid in position 627 of PB2, can overcome restriction to avian cells to infect and replicate in human cells with a mutation to lysine.

It is the functional constraints of intracellularly disposed viral proteins, which have led their surfaces to evolve for specific host interactions, that make them prone to antiviral interference. Therefore, using the diversity of the mammalian antibody repertoire that binds to those surfaces can aid in identifying viral vulnerabilities. The use of intracellularly-expressed, camelid-derived, single-domain antibody fragments (VHHs) has allowed us to implement this concept.

The goal of the work presented herein was to establish a continuous cycle of antiviral VHH development and characterization in order to identify new viral vulnerabilities. I demonstrated this process independently with two different, negative-strand RNA viruses: IAV and VSV, a segmented and non-segmented RNA virus, respectively. Alpacas were immunized with inactivated IAV and VSV to generate VHH libraries. We then used a phage display to select anti-IAV and anti-VSV VHH candidates (Chapter 2), and also employed a phenotypic screening approach based on cell survival of viral infection to identify VHHs with antiviral activity (Chapter 4). All identified and described VHHs were found to bind to the nuclear proteins of either IAV or VSV (NP or N protein, respectively), and protected cells from infection when expressed in the cytosol. Most IAV NP-specific VHHs prevented incoming vRNP complexes from reaching the nucleus, and thus inhibited viral transcription and replication, which take place in the nucleus. Several of these NP-specific VHHs also specifically inhibited viral transcription and replication in the nucleus in reconstitution assays,

which bypass vRNP nuclear import that was the primary inhibited process of most of the anti-NP VHHs. We then solved the crystal structure of one of these VHHs (αNP-VHH1) in complex with IAV NP. The crystal structure revealed that the VHH binding site overlapped with the putative binding site of antiviral Mx proteins. Superimposed on vRNP structural models, the VHH blocked the NLS of the adjacent NP molecule, which likely prevents Importin-α isotypes to associate with vRNPs and facilitate nuclear import. Thus, our findings provide a mechanism of action for the major antiviral activity of this VHH and possibly the antiviral mechanism of cytosolically localized Mx proteins. Once the vRNPs are in the nucleus, only transcription of longer transcripts is inhibited by αNP-VHH1. Again, this antiviral mechanism is surprisingly similar to that of Mx proteins localized in the nucleus, though why an occlusion of NP at this VHH binding site results in this phenotype remains unknown. However, an elegant analysis with mutated NP variants clearly showed the importance of intact NP, especially for longer transcripts (1). Specifically, mutated NP was sufficient to promote transcription of shorter transcripts but intact NP was necessary for RNA longer than 500 nucleotides. The results therefore suggest that αNP-VHH1 inhibits the function of NP for transcript elongation, likely by preventing specific conformations of the vRNP complex during transcription. High-resolution microscopy with one of the anti-NP VHHs presented herein may help to shed new light on the structure of vRNP during transcription and replication.

To show that our approach of identifying and screening for antiviral VHHs was not limited to IAV, we next demonstrated its suitability for VSV, an unrelated virus. As described in Chapters 4 and 5, we were able to generate four VSV N protein-specific VHHs that blocked viral transcription inside cells. We mapped the molecular binding sites for three of these VHHs by means of X-ray crystallography or the generation of escape mutants. For the first of these VHHs (VHH 1307), the binding site directly overlapped with the binding site of the essential non-enzymatic polymerase cofactor P, and thus readily provided an explanation for the antiviral mechanism of this VHH. The second VHH (VHH 1004), likely inhibited VSV replication, but not transcription, and was found to bind to a poorly characterized part of the N protein, the N terminal lobe. For the third VHH, (VHH 1001), we mapped the VHH binding site by the generation of escape mutants to a nucleocapsid specific interface at the C terminal lobe. This VHH presumably inhibited viral transcription and replication by stabilizing the capsid, thus locking the RNA into the N protein.

All screening for antiviral VHHs described in this thesis was performed with the VHH library generated from two alpacas immunized with inactivated IAV and VSV. Extensive screening of this library resulted in one VHH that targeted IAV HA (2). All other identified VHHs were specific for either IAV NP or VSV N protein, likely the most immunogenic and abundant

proteins of the immunization mixtures. All four VSV N protein-specific VHHs that bound to four unique epitopes interfered with the life cycle of the virus. All VHHs specific for IAV NP, which bound to at least 4 different epitopes on the protein's surface, inhibited replication. Since most IAV NP-specific VHHs primarily inhibited the nuclear import of incoming vRNPs, it suggested that this process is especially suitable for interference and inspired us to impede this process in a different way. Nuclear import of vRNPs is dependent on the cytosolic heat shock protein (Hsp)70. We could show that huntingtin interacting protein E (HYPE) mediated AMPylation disrupts influenza transcription and replication through inhibition of cytosolic HSP70 (Addendum 1, (3)). We thus provide an example of how VHH directed antiviral target identification and validation can stimulate the investigation of new ways to interfere with the life cycle of a virus.

Overall, our findings illustrate the excellent suitability of viral nuclear proteins as targets for interference.

Conclusions

Antibodies have a long history as tools to identify and validate drug targets. Due to their small size, excellent stability, and ease of expression, intracellular VHHs are ideal to transfer this concept to the interior of living cells. In this thesis, I present work that exemplifies and validates the suitability of such an approach: first, by screening an alpaca-derived single-domain VHH library to identify candidates specific for IAV and VSV proteins; second, by characterizing the inhibitory properties of the VHH candidates and determining the precise step in the viral life cycle that was inhibited; third, by defining the precise binding sites of one IAV NP-specific VHH and two VSV N protein-specific VHHs by X-ray crystallography. Lastly, I found that the antiviral activity of the IAV NP-specific VHHs was similar to that of endogenous Mx proteins, a finding supported by the results of structural analysis. Moreover, the structural data from the two VSV N protein-specific VHHs readily revealed the antiviral mechanism of action for one VHH while another structure shed light on the importance of the N-terminal lobe of the VSV N-protein.

Fortunately, viral propagation *in vitro* is often sufficient so that their use in cell-based or animal models is not the limiting factor to study them. However, to advance our understanding of viruses, additional methods that allow us to image and monitor intracellular localization and expression, determine function, identify interactions, and solve structures of viral proteins and viral-host protein complexes are still needed. The versatility of VHHs allows researchers to streamline such processes, as a single VHH can be used to monitor, perturb, and aid in the

crystallization of a target antigen or virus. Therefore -and as shown in this thesis- VHHs are a useful addition to the virologist's toolbox.

Future Directions

In this thesis I demonstrated the suitability of VHHs to screen for those that inhibit IAV and VSV. Based on these results, it is promising to extend the approach described herein to other viral proteins and other viruses. Together, such efforts may allow virologists to build more precise functional maps of viral proteins, which may in turn serve as a platform to develop novel antiviral strategies. To expand the spectrum of possible antiviral targets, one could explore the use the lentiviral-based VHH screens (as described in Chapter 4) to go beyond those that are expressed cytosolically. In such screens, VHHs could be directed to the ER, the nucleus, or displayed on the surface of cells. This latter approach, for example, would allow for the direct screening of IAV HA-specific, neutralizing VHHs, either displayed on the surface, or alternatively directed to the ER to prevent successful maturation of HA precursors.

Besides the aforementioned applications as crystallization chaperones, VHHs may also be helpful for cryo-EM. Because VHHs can trap their target molecules in specific conformations, they may improve cryo-EM sample quality by yielding more homogenous samples. Viral proteins often form larger oligomeric complexes that exhibit inherent structural flexibility, and are thus difficult to study structurally. An example of this is the vRNP complex of IAV. Although the structure has been solved independently by two different groups, the exact orientation of the NP, its major component, remains mostly unknown. For such cases, a VHH with a structurally defined binding site to a protomer of a complex, such as that of αNP-VHH1 to IAV NP (Chapter 2 and 3), may serve as a point of reference or help determine the stoichiometry of a complex.

It is important to note the importance of the source of immunogen used for the initial immunization of the alpaca. Quality and composition will have tremendous impact on the success of the screening results. To screen for VHHs against viral proteins that are present only in small numbers in the virions, the production and subsequent immunization with recombinant protein or protein domains should be considered. The same principle also applies to non-structural viral proteins that are not found in infectious virions, but may be interesting targets for intervention.

Finally, recent developments in the Ploegh lab in positron emission tomography (PET) imaging using VHHs have allowed us to visualize particular cells and their distribution *in vivo* (4, 5). Considering that the surface proteins of enveloped viruses are typically expressed on the surface of infected cells before budding occurs and before virions are released, this approach may allow

one to monitor a viral infection in a living animal. Additionally, this approach could be used to monitor immune cells, such as $CD8^+$ T cells in the context of a viral infection. Together, results from these types of studies could provide new information regarding tissue tropism of viral pathogens and how this tropism is influenced by, for example, an induced $CD8^+$ T cell response.

1. **Turrell L**, **Lyall JW**, **Tiley LS**, **Fodor E**, **Vreede FT**. 2013. The role and assembly mechanism of nucleoprotein in influenza A virus ribonucleoprotein complexes. Nat Commun **4**:1591.

2. **Dougan SK**, **Ashour J**, **Karssemeijer R a**, **Popp MW**, **Avalos AM**, **Barisa M**, **Altenburg AF**, **Ingram JR**, **Cragnolini JJ**, **Guo C**, **Alt FW**, **Jaenisch R**, **Ploegh HL**. 2013. Antigen-specific B-cell receptor sensitizes B cells to infection by influenza virus. Nature **503**:406–9.

3. **Truttmann MC**, **Zheng X**, **Hanke L**, **Damon JR**, **Grootveld M**, **Krakowiak J**, **Pincus D**, **Ploegh HL**. 2016. Unrestrained AMPylation targets cytosolic chaperones and activates the heat shock response. Proc Natl Acad Sci U S A **114**:201619234.

4. **Rashidian M**, **Keliher EJ**, **Bilate AM**, **Duarte JN**, **Wojtkiewicz GR**, **Jacobsen JT**, **Cragnolini J**, **Swee LK**, **Victora GD**, **Weissleder R**, **Ploegh HL**. 2015. Noninvasive imaging of immune responses. Proc Natl Acad Sci U S A **112**:6146–51.

5. **Rashidian M**, **Keliher EJ**, **Dougan M**, **Juras PK**, **Cavallari M**, **Wojtkiewicz GR**, **Jacobsen JT**, **Edens JG**, **Tas JMJ**, **Victora G**, **Weissleder R**, **Ploegh HL**. 2015. Use of 18 F-2-Fluorodeoxyglucose to Label Antibody Fragments for Immuno-Positron Emission Tomography of Pancreatic Cancer. ACS Cent Sci 150603073029009.

Addendum 1

Unrestrained AMPylation Targets Cytosolic Chaperones and Activates the Heat Shock Response

Proceedings of the National Academy of Sciences of the United States of America (PNAS), December 2016

Matthias C. Truttmann[1], Xu Zheng[1], **Leo Hanke**[1], Jadyn R. Damon[1], Monique Grootveld[1], Joanna Krakowiak[1], David Pincus[1] and Hidde L. Ploegh[1,2]

[1]Whitehead Institute for Biomedical Research, Cambridge, Massachusetts, USA, Massachusetts

[2]Department of Biology, Massachusetts Institute of Technology, Cambridge, Massachusetts, USA

Abstract

Protein AMPylation is a conserved post-translational modification with emerging roles in endoplasmic reticulum (ER) homeostasis. However, the range of substrates and cell biological consequences of AMPylation remain poorly defined. We expressed human and *Caenorhabditis elegans* AMPylation enzymes – HYPE and FIC-1, respectively – in *Saccharomyces cerevisiae*, a eukaryote that lacks endogenous protein AMPylation. Expression of HYPE and FIC-1 in yeast induced a strong cytoplasmic Hsf1-mediated heat shock response, accompanied by attenuation of protein translation, massive protein aggregation, growth arrest and lethality. Over-expression of Ssa2, a cytosolic Hsp70, was sufficient to partially rescue growth. In human cell lines, over-expression of active HYPE likewise induced protein aggregation and the HSF1-dependent heat shock response. Excessive AMPylation also abolished HSP70-dependent influenza virus replication. Our findings suggest a novel mode of Hsp70 inactivation by AMPylation and point towards a role for protein AMPylation in the regulation of cellular protein homeostasis beyond the ER.

Significance

The stability of the proteome is essential to cellular and organismic health- and lifespan. To maintain proteostasis, cells are equipped with a network of chaperones that support folding of nascent as well as refolding of unfolded or misfolded proteins. Aging and age-associated diseases progressively increase the accumulation of misfolded, damaged and aggregated proteins, thus taxing the chaperoning machinery to its limits. Here, we describe how AMPylation of cytosolic heat shock proteins leads to a collapse of proteostasis, the induction of a strong heat shock response, inhibition of translation as well as the formation of protein aggregates. AMPylation-mediated inhibition of HSP70 may represent a novel strategy for targeted ablation of this chaperone.

Introduction

How complex organisms maintain homeostasis in the midst of internal and environmental stress is a fundamental question in biology. The stability of the proteome is essential to maintain cellular processes and contributes to organismic health and lifespan. Cellular protein homeostasis (proteostasis) is continuously challenged by a variety of stressors that trigger protein misfolding and aggregation (1). Aging and age-associated diseases progressively increase the accumulation of misfolded, damaged and aggregated proteins, thus interfering with numerous biological processes (2).

To overcome proteotoxicity, cells are equipped with compartment-specific stress responses that provide protection through transcriptional, translational as well as post-translational regulation of protein degradation and protein folding (3). The mitochondrial unfolded protein response (UPR^{mt}) as well as the endoplasmic reticulum (ER) unfolded protein response (UPR^{ER}) regulate chaperone function and protein degradation pathways within these organelles (4). The heat shock response (HSR) controls extensive heat shock protein (Hsp) chaperone networks throughout the cell and is essential to survive acute stress (5). Together, these responses provide the cell with the capacity to react to and endure various stresses, while maintaining proteostasis.

Hsps are involved in all branches of cellular stress responses that support protein folding (6). The mitochondrion-resident mtHsp40 and mtHsp70 proteins ensure protein homeostasis within this critical organelle, while the ER-resident Hsp70-family chaperone BiP/Grp78 refolds unfolded and misfolded proteins within the ER and helps remove and degrade terminally damaged proteins from the ER. In addition to their direct involvement in protein folding, individual or complexed Hsps inhibit or inactivate stress response regulators, including the UPR^{ER} stress sensors IRE1 and PERK and the transcriptional regulator of the HSR, HSF1, in negative feedback loops (7, 8).

Recent work on BiP's function in ER homeostasis identified a major role for a particular post-translational modification, AMPylation, in the regulation of BiP's ATPase and chaperone activity (9-11). Protein AMPylation involves the transfer of AMP from ATP to a Ser or Thr side chain and is carried out by enzymes that contain a fic domain (Fic proteins), an evolutionarily conserved protein family present in both bacteria and metazoans, but lacking in fungi and plants (12, 13). In prokaryotes, Fic proteins are often associated with toxin-antitoxin systems, such as the VbhT-VbhA pair encoded by *Bartonella schoenbuchensis,* leading to modification of Gyrase and Topoisomerase IV (14, 15). Several human pathogens are equipped with fic-domain effector proteins that covalently AMPylate and inactivate small GTPases of the Rho and Rab family in their respective host cells (16, 17). Eukaryotic Fic proteins AMPylate a variety of molecular targets, including BiP, core histones as well as translation elongation

factors that contribute to the regulation of the UPR^{ER}, innate immunity and perception of light (10, 11, 18, 19). Nevertheless, our knowledge of the range of substrates and consequences of AMPylation remains incomplete.

Here we examine heterologous expression of Fic proteins in *S. cerevisiae*, which lacks endogenous protein AMPylation. In addition to activating the UPR, we find that expression of active *H. sapiens* HYPE or *C. elegans* FIC-1 in yeast results in the functional ablation of cytosolic chaperone pools with concomitant induction of a strong Hsf1-mediated heat shock response. Further, we observed massive protein aggregation and inhibition of translation, eventually causing growth arrest and lethality. *In vitro*, both FIC-1 and HYPE covalently AMPylated cytosolic Hsp40, Hsp70 and Hsp90. Over-expression of Ydj1 and Ssa2, a cytosolic Hsp40/Hsp70 pair, rescued growth of *S. cerevisiae*. Expression of active HYPE in human cells confirmed AMPylation-dependent interference with the chaperoning network involved in protein aggregation and the induction of the Hsf1-dependent heat shock response. Our findings identify a novel trigger that can cause collapse of the cellular chaperoning machinery and activate Hsf1, mediated by AMPylation of cytosolic chaperones. Protein AMPylation may thus regulate proteostasis beyond the ER and present a target for intervention.

Results

Protein AMPylation in *S. cerevisiae* results in growth arrest and cell death.

To explore the consequences of protein AMPylation in an unbiased manner, we introduced enzymes that carry out this modification into the budding yeast *S. cerevisiae*, a eukaryote that lacks endogenous AMPylation machinery. We expressed a set of Fic domain-containing proteins in yeast under the control of a galactose-inducible promoter. This set included *Vibrio parahaemolyticus* VopS, *C. elegans* FIC-1 and human HYPE, as well as mutant versions with increased or impaired AMPylation activity (14, 16). Upon galactose induction, cells that express active FIC-1 (E274G) and, to a lesser extent, active HYPE (E234G), showed attenuated cell growth (Fig. S1A – S1C). In contrast, expression of wild type or activity-impaired mutants (FIC-1 H404A, HYPE H363A) did not diminish growth. Moreover, expression of a mutant of FIC-1 that retains the ability to auto-AMPylate but cannot AMPylate other substrates (FIC-1 E274G/H404A) was also benign (Figure S1B). Overexpression of VopS, a potent bacterial Fic protein known to modify small GTPases (16), did not affect cell viability (Fig S1D). To exclude copy number variation as responsible for these findings, we engineered yeast strains that carry galactose-inducible FIC-1 or mutants thereof as single copy genomic integrations. While growth rates were indistinguishable when grown on dextrose, induction of FIC-1 (E274G) resulted in impaired growth and eventual growth arrest in liquid culture (Fig. 1A). Expression of FIC-1 (E274G) upon galactose induction was verified by immunoblotting (Fig. S1E). To test

whether the growth impairment was reversible or lethal, we transferred cells grown for three hours in galactose into repressive dextrose-containing media and monitored cell growth. Cells that express active FIC-1 (E274G) failed to recover from growth arrest upon promoter shut-off, indicating that in *S. cerevisiae* expression of FIC-1 (E274G) and the level of AMPylation associated with it is lethal (Fig. 1B and S1F).

AMPylation triggers the heat shock response in *S. cerevisiae.*

Given that AMPylation has been reported to target BiP and modulate ER homeostasis in mammalian cells (9-11), we wondered whether the toxicity of FIC-1 (E274G) seen in yeast could be attributed to ER stress. We introduced a fluorescent reporter of the unfolded protein response (UPRE-GFP) into strains bearing estradiol-inducible FIC-1 and HYPE genes. Upon ER stress, the transcription factor Hac1 activates the UPRE-GFP reporter, a signal that can be quantified by flow cytometry. For comparison, we also introduced reporters of cytosolic stress responses, including the heat shock response (HSE-YFP), activated by the transcription factor Hsf1, and the general stress response (STRE-GFP), activated by the transcription factors Msn2/4. FIC-1, FIC-1 (E274G) and HYPE (E234G) did induce the UPRE-GFP reporter in the presence of estradiol, but did so very weakly, and not significantly more than they induced the STRE-GFP reporter (Fig. S2A, B). In marked contrast, expression of both FIC-1 (E274G) and HYPE (E234G) robustly induced the HSE-YFP reporter (Fig. 2A).

To test whether AMPylation not only promoted HSE-YFP reporter activation but also induced a genome-wide heat shock response, we performed RNA deep sequencing (RNA-seq) to compare cells induced to express FIC-1 (E274G) for two hours to cells heat shocked at 39ºC for 30 minutes. We found that the two transcriptomes were highly correlated ($r = 0.81$). Gene ontology (GO) analysis of the set of 91 genes that were induced ≥ 4-fold by both heat shock and FIC-1 (E274G) showed a strong enrichment for the GO term "protein folding" ($p < 10^{-10}$). In contrast, there was no enrichment for biological processes or molecular functions in the set of 41 genes that were induced by FIC-1 (E274G) but not by heat shock. Expression of FIC-1 (E274G) thus mimics the response to elevated temperature (Fig. 2B, S2C). Among the most strongly up-regulated genes were canonical heat shock protein genes (HSPs) (e.g., *SSA4*, *SSE2*, *HSP10*, *HSP42*, *HSP82*); the most down-regulated set included ribosomal protein genes (RPGs) (e.g., *RPL31B*, *RPL21A*, *RPS22A*, *RPS12*, *RPS31*) (Fig. S2D, E). A comparison by RNA-seq of induction of FIC-1 (E274G) over time with a heat shock time course showed stable up-regulation of HSPs and down-regulation of RPGs in both conditions (Fig. 2C). Global gene expression remained correlated as well (Fig. S2C). However, AMPylation induced even larger maximal -fold changes in transcript levels than did heat shock: AMPylation is thus an even stronger inducer of the heat shock response than elevated temperature (Fig. 2C).

To determine whether the down-regulation of RPGs attenuated translation, we performed a ^{35}S-methionine/cysteine labeling experiment. Expression of FIC-1 (E274G) decreased global translation (Fig. 2D) and modified the overall translation profile, the most pronounced change being the appearance of a strong band running at approximately 70 kDa, likely representing Hsp70 family proteins, (Fig. S2F). In summary, FIC-1 (E274G) expression induces a strong heat shock response, accompanied by up-regulation of heat-shock proteins and attenuation of protein translation.

HYPE (E234G) triggers a heat-shock response in human cells and promotes the formation of HSF1 foci in the nucleus.

Since AMPylation is an artificial stressor for yeast, we turned our attention to human cells – which encode the endogenous AMPylation enzyme HYPE – to determine the wider validity of the yeast results. To this end, we performed RNA-seq on HeLa cells that ectopically express active HYPE (E234G) and compared its transcriptome to that of untransfected controls. Expression of HYPE (E234G) induced both UPR^{ER} target genes as well as HSF1 target genes. The set of genes upregulated ≥ 4-fold was enriched for the GO terms "stress response", "chaperone" and "response to unfolded protein" (Fig. 3A-C, S3A). We then focused on the apparent activation of the HSF1-mediated cytosolic stress response and employed an HSF1 reporter cell line that contains a GFP cassette driven by consensus heat-shock elements (HSE-GFP) (20), analogous to the HSE-YFP reporter used in yeast. Transfection of this reporter line with HYPE (E234G) triggered induction of GFP, while transfection with wild type HYPE, AMPylation-deficient HYPE (H363A) or a vector containing only mCherry failed to do so (Fig. S3B). Next, as an independent readout, we monitored HSF1 clustering into nuclear stress granules, the sub-nuclear foci that are a hallmark of HSF1 activation in human cells (21). Indeed, expression of HYPE (E234G) induced HSF1 to form sub-nuclear clusters that were similar to those formed in heat-shocked cells (Fig. 3D, representative images shown in S3C). By contrast, expression of wild type HYPE, HYPE (H363A) or mCherry did not trigger HSF1 clustering (Fig. 3D, S3C). Thus, RNA-seq, the HSE-GFP reporter and HSF1 immuno-fluorescence all indicate that HYPE (E234G) activated HSF1 and the heat shock response in human cells.

To assess protein translation in the presence of HYPE (E234G), we co-transfected HeLa cells with mCherry and various HYPE constructs and measured mCherry intensity after 24 hours. HYPE (E234G) led to a marked decrease in mCherry expression, as compared to wild type HYPE or AMPylation-deficient HYPE (H363A) (Fig. S3D). Metabolic (^{35}S-methionine/cysteine) labeling of *de novo* synthesized proteins in transfected HeLa cells

confirmed HYPE (E234G)-mediated attenuation of mCherry expression and showed additional changes in the protein translation profile (Fig. S3E). Notably, just as in yeast cells expressing FIC-1 (E274G), cells that express HYPE (E234G) produced an additional 70 kDa protein, presumably representing Hsp70 family members (Fig. S3E).

FIC-1 (E274G) and HYPE (E234G) disrupt cytosolic proteostasis.

HSF1 and the heat shock response are activated when the cytosolic chaperoning machinery fails and unfolded or misfolded proteins accumulate and aggregate. To determine whether AMPylation impairs proteostasis, we imaged yeast and human cells that express aggregation reporters. In yeast, we imaged Hsp104-YFP – a disaggregase that forms discrete foci marking aggregated proteins in stressed cells – upon induction of FIC-1 (E274G). Indeed, FIC-1 (E274G) – but not wild type FIC-1 or AMPylation-deficient FIC-1 (H404A) – triggered Hsp104-YFP to form foci, indicating that the function of cytosolic chaperones had been compromised (Fig. 4A). Next, we tagged FIC-1 (E274G) at its C-terminus with YFP, induced its expression with estradiol and imaged live cells. We observed localization to the perinuclear and cortical ER as demonstrated by the partial signal overlap with Ire1-mCherry, but also to juxtamembranous and cytosolic puncta that were distinct from the ER (Fig. 4B, upper panel). Indeed, cells co-expressing FIC-1 (E274)-YFP and mKate2-Ssa2 (a strictly cytosolic Hsp70 chaperone) showed co-localization of the two proteins (Fig. 4B, lower panel), suggesting that a fraction of FIC-1 (E274G) is present in the cytosol of *S. cerevisiae*. Subcellular fractionation of FIC-1 (E274G)-expressing animals confirmed that a small amount of FIC-1 (E274G) is present in the cytosol (Fig. S4A). To further support our hypothesis that FIC-1 (E274G) is also active in the cytoplasm, we generated nanobodies (VHHs) specific for FIC-1. Two unrelated FIC-1 specific nanobodies (VHH), $VHH_{FIC\text{-}1\_4}$ and $VHH_{FIC\text{-}1\_19}$,were isolated and shown to bind to FIC-1 but not its human ortholog HYPE (Fig. S4B). Variation of the VHH:FIC-1 (E274G) ratios inhibited target AMPylation *in vitro* in a dose-dependent manner, while the presence of inhibitory HYPE-specific VHH_1 did not affect FIC-1 (E274G) activity (Fig. S4C). Cytosolic expression of these FIC-1-specific VHHs in yeast showed that both $VHH_{FIC\text{-}1\_4}$ and $VHH_{FIC\text{-}1\_19}$ markedly improved growth when synthesis of FIC-1 (E274G) was induced (Fig. S4D). Co-expression of an irrelevant VHH (VHH_7, a Class II MHC-specific VHH) failed to rescue growth (Fig. S4D) This supports our hypothesis that FIC-1 (E274G)-promoted modification of cytosolic targets is the cause for the observed phenotypes in yeast.

In human cells, we used a destabilized mutant firefly luciferase (FlucDM-GFP) that clusters in stressed cells and loses its luciferase activity (22). We co-transfected HeLa cells with HYPE constructs and FlucDM-GFP and monitored reporter clustering as well as luciferase activity. We observed that the presence of HYPE (E234G) induced aggregation of the FlucDM-GFP and showed a significant reduction in luciferase activity – similar to cells co-expressing an

aggregation-prone poly-glutamine construct – while wild type HYPE or HYPE (H363A) did not (Fig. 4C). Together, these results demonstrate that AMPylation compromises proteostasis and triggers the formation of cytosolic protein aggregates in both yeast and human cells.

FIC-1 (E274G) and HYPE (E234G) modify Hsp40, Hsp70 and Hsp90 *in vitro*.

The cytosolic chaperones Hsp40, Hsp70 and Hsp90 support protein folding and are thought to repress HSF1. Since AMPylation activates HSF1, we wondered whether Hsp40, Hsp70 and Hsp90 might be substrates of FIC-1 (E274G) and HYPE (E234G). To test this, we expressed and purified recombinant *C. elegans* HSP-1 (cytosolic Hsp70 ortholog), HSP-3 (BiP ortholog) and DAF-21 (cytosolic Hsp90), as well as human Hsp40 and Hsp70 and performed *in vitro* AMPylation assays. Since recombinant wild-type AMPylases (FIC-1, HYPE) function only poorly *in vitro (9, 11, 14, 17, 23)*, we performed all experiments using only the constitutively active versions (FIC-1 E274G, HYPE E234G). FIC-1 (E274G) efficiently AMPylated HSP-1, HSP-3 and DAF-21 (Fig. S5A), while no detectable binding of □^{33}P-ATP to HSP-1, HSP-3 or DAF-21 was observed. Likewise, HYPE (E234G) AMPylated Hsp40, Hsp70 and Hsp90 (Fig. 5A-B). We also tested whether the two enzymes could modify non-endogenous substrates. While HYPE (E234G) AMPylated C. *elegans* proteins HSP-1, HSP-3 and DAF-21, FIC-1 (E274G) was unable to AMPylate human Hsp70 or Hsp90, but efficiently AMPylated human Hsp40 (Fig. S5B-D). Further, both enzymes catalyzed AMPylation of recombinant yeast Ssa2, the major cytosolic Hsp70 protein found in yeast (Fig. 5C). Similar reactions using a TPR-domain containing version of FIC-1$_{aa134\text{-}508}$ (E274G) as AMPylase confirmed that Hsp40, HSP-1, HSP-3 and Ssa2 but not Hsp70 were modified by FIC-1 $_{aa134\text{-}508}$ (E274G) (Fig. S5E). To map the sites of AMPylation on the newly identified HYPE targets (Hsp40, Hsp70), we subjected the modified proteins to mass spectrometry. We identified multiple sites of modification on both Hsp40 and Hsp70 (Fig. S5E – G). The modified residues clustered into well-defined subdomains of the chaperones: Hsp70 was modified on 5 threonine residues in the nucleotide binding (ATPase) domain, while Hsp40 was predominantly AMPylated on 6 residues in its C-terminal portion, with an additional single site N-terminal to the J domain (Fig S5H). In summary, these results show that HYPE and FIC-1 can efficiently modify a number of cytosolic chaperones, potentially altering their function.

FIC-1 (E274G) AMPylates cytosolic Hsp70 *in vivo*.

By analogy to the established finding that ER-localized Fic proteins AMPylate the Hsp70 chaperone BiP, we next tested whether cytosolic Hsp70 could also be AMPylated *in vivo*. To this end, we analyzed the *S. cerevisiae* model and examined time-resolved samples from cells that over-express FIC-1 (E274G) by immunoblot. Consistent with the increase in translation of a 70 kDa protein observed by ^{35}S-methionine/cysteine incorporation (Figure S2F), probing the

membrane with an Hsp70-specific antibody showed that intracellular Hsp70 levels increased over time (Fig. 6A, upper panel). To determine whether Hsp70 is AMPylated, we reprobed the membrane with a Thr-AMP-specific polyclonal antibody. Indeed, the Thr-AMP antibody demonstrated that Hsp70 is AMPylated in *S. cerevisiae* (Fig. 6A, lower panel). In contrast, similar experiments performed for yeast cells that express either FIC-1 or FIC-1 H404A failed to show upregluation of cytoplasmic HSP70s or their AMPylated equivalents (Fig. S6A). These results confirm that only expression of FIC-1 (E274G) triggers a heat-shock response accompanied by elevated levels of cytosolic HSP70 proteins. Cytosolic Hsp70 may thus be a major target of FIC-1 (E274G) in yeast.

Cytosolic Hsp70 detoxifies FIC-1 (E274G) overexpression in yeast.

Our data fit a model in which AMPylation of cytosolic chaperones causes a failure of cytosolic proteostasis, thus activating HSF1 and inducing the heat shock response. A prediction of this model is that additional chaperones should attenuate these effects. To test this prediction, we integrated additional copies of Ssa2 (Hsp70) and Hsc82 (Hsp90) into the genome of the *S. cerevisiae* strain that expresses FIC-1 (E274G) under the control of the estradiol-inducible promoter (Fig. 6B, S6B). Ssa2 partially suppressed the consequences of overexpression of FIC-1 (E274G) by improving growth in the presence of estradiol, yet without reducing intracellular FIC-1 (E274G) levels (Fig. S6C). Moreover, additional Hsc82 had no effect on cell viability (Fig. S6B) while co-expression of Ydj1 (a yeast Hsp40 ortholog that improves the efficiency of Ssa2's chaperone activity (24)) and Ssa2 further improved growth in the presence of FIC-1 (E274G) (Fig. 6B). Co-expression of Hsc82 with Ssa2 or with Ssa2 and Ydj1 antagonized the growth rescue afforded by these chaperones and reduced fitness in the presence of FIC-1 (E274G) (Fig. 6B). Hsp90 may therefore stabilize or potentiate the AMPylation activity of FIC-1 (E274G). In addition to suppressing the growth phenotype, Ssa2 also abrogated the breakdown in the cytosolic chaperoning machinery triggered by expression of FIC-1 (E274G), as evidenced by the decrease in Hsp104-YFP foci (Fig. 6C, S6D). Over-expression of FIC-1 (E274) in *S. cerevisiae* thus results in inactivation of cytosolic chaperones, especially Hsp70, thus disrupting proteostasis.

AMPylation of Hsp70 alters its cellular localization dynamics.

Heat shock triggers Hsp70 to partially relocalize to the nucleus (25). While wild-type Hsp70 shows a dynamic influx-efflux pattern, the chaperoning-impaired mutant Hsp70 K71E is almost completely immobilized and absent from the nucleus following heat shock (25). To directly monitor Hsp70 function in mammalian cells, we tested whether AMPylation would change the subcellular redistribution of Hsp70 during heat shock. We used GFP-Hsp70 and GFP-Hsp70 K71E constructs to monitor their localization in the presence of HYPE (E234G). HeLa cells

expressing HYPE, HYPE (E234G) or HYPE (H363A) together with GFP-Hsp70 or GFP-Hsp70 K71E were analyzed by fluorescence microscopy. In the absence of heat stress, fewer than 5% of cells contained a substantial fraction of GFP-Hsp70 in the nucleus (Fig 7A, S7A-B). Upon heat shock, approximately 30% of cells co-transfected with wild type HYPE or HYPE (H363A) showed GFP-Hsp70, but not GFP-Hsp70 K71E, relocalization to the nucleus. In contrast, cells co-expressing HYPE (E234G) and GFP-Hsp70 showed no relocalization, mimicking GFP-Hsp70 K71E (Fig. 7A, S7A-B). We conclude that AMPylation interferes with Hsp70 localization dynamics during stress.

AMPylation disrupts influenza virus replication and infectivity.

To examine the consequences of AMPylation-induced interference with Hsp70 function, we investigated the effects of AMPylation on influenza virus infection in 293T cells, an HSP70-dependent process. Influenza virus RNA polymerase activity requires nuclear localization of the viral ribonucleoproteins (vRNPs), a process that relies on active Hsp70 shuttling from the cytoplasm into the nucleus (26). We therefore hypothesized that AMPylation of Hsp70 would result in a reduction of vRNP nuclear localization and activity. We tested RNA polymerase activity in a mini-genome transcription/replication assay where transient expression and nuclear localization of the viral ribonucleoprotein complex (vRNP) components (NP, PB2, PB1 and PA) results in EGFP expression (27). As controls, we used VHHs previously demonstrated to inhibit (anti-NP) or not affect (anti-Class II MHC) assembly of vRNPs and virus replication, respectively (28). Indeed, while co-expression of HYPE or HYPE (H363A) together with the vRNP components had no effect on GFP synthesis, HYPE (E234G) reduced GFP expression, indicating impaired polymerase activity (Fig. 7B). HYPE (E234G) also efficiently attenuated viral infection as assessed by nucleoprotein levels 5 hours post infection (Fig. 7C). In summary, these results show that AMPylation can disrupt influenza transcription and replication through inhibition of cytosolic HSP70.

Discussion

Cells inevitably suffer exposure to various stressful cues that challenge protein homeostasis. Evolutionarily conserved stress responses help overcome and limit the damage imposed by stress. In this work, we uncovered a novel mode of induction of one such critical stress response pathway, the HSF1-driven heat shock response. We found that Fic protein-mediated AMPylation leads to disrupted proteostasis and activation of HSF1 in yeast and human cells. In yeast, this response is associated with irreversible damage that culminates in cell death. Importantly, the toxicity associated with AMPylation in yeast can be suppressed by overexpression of cytosolic Hsp70, further implicating disrupted proteostasis as the root of the growth defect in general and supporting the notion that AMPylation impairs cytosolic Hsp70

function. However, Hsp70 could suppress toxicity by generally promoting protein folding without being the consequential AMPylation target.

Introduction of heterologous AMPylation enzymes into *S. cerevisiae* produced catastrophic consequences. The irreversible toxicity imposed by AMPylation on yeast host underscores the potency of this modification and its potential to wreak havoc on cellular homeostasis. In our model for the consequences of AMPylation (Fig. 7D), we propose that AMPylation inhibits Hsp70 activity, leading to protein misfolding and aggregation. Increased protein aggregation not only sequesters diverse chaperones, removing them from the general pool required to support folding of nascent proteins, but may also limit the availability of diverse essential factors that fall victim to growing aggregates. HSF1 senses the dearth of available chaperones and induces expression of the heat shock response, only to have one of its major targets, Hsp70, continue to be inhibited. Moreover, a breakdown of the cytosolic chaperoning machinery is coupled to inhibition of *de novo* protein synthesis, another process essential for growth. Thus, unrestrained AMPylation generates a perfect storm that disrupts both protein synthesis and folding, and undermines the effectiveness of the heat shock feedback loop by continuing to inhibit Hsp70.

The concept of modulating the HSF1-mediated heat shock response has been explored as a potential route for the treatment of neurodegenerative diseases, viral infections and diverse cancers (29, 30). Although the detailed mechanisms of how protein aggregation-associated neurodegenerative diseases develop remain unclear, there is a large body of evidence suggesting a strong tie to the Hsp40/Hsp70/Hsp90 protein folding machinery as well as the HSR and UPR^{ER} (31). Since hyper-AMPylation disrupts proteostasis in both the ER and cytosol, modulation of HYPE activity may boost the homeostatic capacity of these compartments and counteract protein aggregation, potentially offering a novel avenue toward ameliorating these conditions. In the realm of viral infections, we show that active HYPE can prevent transcription and replication functions essential for propagation of influenza by inhibition of Hsp70 nuclear localization and activity. As such, induction of AMPylation may be an effective antiviral strategy. Finally, most cancer cells have elevated Hsp70 and Hsp90 levels that enable them to resist dysregulation of protein homeostasis during tumorigenesis or anti-cancer therapies, thus enhancing cancer cell survival and tumor growth (32). Harnessing AMPylation to inhibit Hsp70 activity could be a powerful and broad-spectrum anti-cancer therapy that may synergize profoundly with Hsp90 inhibitors to cripple cancer's proteostatic support system.

While the role of AMPylation in regulating stress responses via modification of Hsp70-class chaperones has been reported in several studies, it mostly confined the function of AMPylation

to tuning the activity of the UPR^{ER} by altering the activity of the ER-resident Hsp70 chaperone BiP (9-11). However, subcellular localization of metazoan Fic proteins remains a matter of debate. While several studies suggested that HYPE localizes to the ER and the adjacent nuclear envelope, we recently provided evidence for the presence of endogenous *C. elegans* FIC-1 in the cytoplasm (19). Further, global AMPylation studies in mammalian cells showed that the plurality of modified targets are cytosolic (33). When expressed in yeast, FIC-1 colocalized both with ER and cytosolic markers. Cytosolic expression of inhibitory VHHs partially prevented FIC-1 (E274G)-associated cell death, suggesting that the enzyme is active in the cytosol, too. These data support a broader localization of FIC-1 and HYPE that includes both the ER and the cytosol, allowing AMPylation to modulate proteostasis in both of these compartments. Further efforts are required to work out the details of whether or not endogenous HYPE AMPylates cytosolic targets under certain stress conditions.

Although overexpression of FIC-1 (E274G)- and HYPE (E234G) in yeast results in comparable outcomes, there are differences as well. FIC-1 (E274G) promotes far more pronounced phenotypes than does HYPE (E234G). In contrast, HYPE (E234G) *in vitro* AMPylates Ssa2 more efficiently than FIC-1 (E274G). However, while both enzymes modify similar targets in yeast, the residues involved and the extent to which the individual HSPs are AMPylated may vary. We also cannot exclude the possibility of targets uniquely AMPylated by either FIC-1 (E274G) or HYPE (E234G). Indeed, although target pools for FIC-1 (E274G) and HYPE (E234G) show substantial overlap, some targets are modified only by one of these AMPylases (19). Whether the functions of FIC-1 and HYPE are completely identical or show slight differences in the processes, they regulate in worm and man, respectively, is an open question.

Overall, our work describes a new mechanism for the simultaneous inactivation of Hsp70 and the activation of a robust HSR in the absence of heat stress. This mechanism depends on post-translational protein AMPylation by Fic proteins. We are struck by the observation that Fic proteins can directly modify the major cellular chaperones, Hsp40, Hsp70 and Hsp90, suggesting a critical role for AMPylation enzymes in modulating the proteostasis network. By deploying Fic proteins to different compartments, cells – and genetic engineers – can modulate proteostasis and stress response pathways beyond the ER.

Material and Methods

Yeast growth experiments

5 ml SR-CSM, SD-CSM or YPD was inoculated with respective strains and grown over night at 30 °C. The next day, cultures were diluted in intended growth medium to OD_{600} = 0.1-0.3 and continuously cultured at room temperature or 30 °C. For growth curve experiments,

samples were taken in duplicate or triplicate for each measured timepoint. For agar-plate experiments, cells were plated as a dilution series on respective plates.

Yeast stress reporter assays

Reporter constructs to assay for activation of the heat shock response (HSE), the general stress response (STRE) and the unfolded protein response (UPRE) consisted of GFP (STRE, UPRE constructs) or YFP (HSE constructs) with a series of 4xHSE, 4xSTRE, or 4xUPRE sequences in a crippled *CYC1* promoter combined in a single integrating vector backbone (34). Constructs were integrated into a wild type (W303a) yeast strain background at the *leu2* locus. To enable estradiol-mediated induction of FIC-1 and HYPE constructs, a chimeric, hormone-responsive transcriptional activator (GEM), consisting of the Gal4 DNA binding domain, the human estrogen receptor ligand binding domain and the activation domain from the yeast transcription factor Msn2 (35), was transformed into the reporter strains and integrated into the *his3* locus. Subsequently, the three reporter/GEM strains were transformed with 2 µ plasmids encoding the FIC-1 and HYPE constructs under the control of the *GAL1* promoter and transformants were selected on SD-URA plates. For assays, cells were grown from single colonies in SD-URA overnight, diluted into fresh media, and then left untreated or treated with 500 nM estradiol to induce the constructs for 4 h at 30 °C. Fluorescent reporters were measured by flow cytometry in a BD LSRFortessa equipped with a high-throughput sampler. Data were analyzed using FlowJo.

VHH generation, purification and evaluation

VHH generation, purification and evaluation was performed as described in (18). To test VHH-FIC-1 interaction in solution, approximately 100 □g of recombinant $HYPE_{aa187-437,}$ or FIC-$1_{aa258-508}$ was incubated with 100 □g VHH-TAMRA at 4 °C for 1 hour and analyzed on a Superdex S75 10/300 GL size exclusion column. Absorbance at 280 nm (proteins) as well as at 545 nm (TAMRA) was recorded to assess the occurrence of specific interactions as evidenced by co-elution of FIC-$1_{aa258-508}$ and a candidate VHH that results in overlapping peak maxima at both 280 nm and 545 nm.

Subcellular fraction of yeast cells

Cells were lysed with a coffee grinder (36), resuspended in 1 ml PBS and centrifuged at 300 g for 5 min to remove unlysed cells. Cleared total cell lysate was transferred into a fresh tube and centrifuged at 13.000 xg for 15 min to pellet the insoluble fraction (ER, nuclei, protein aggregates, etc). The soluble (cytosolic) fraction was transferred into a fresh tube and samples were analyzed by immunoblotting.

Cell culture

HeLa and HEK cells were cultured in Dulbecco's modified Eagle's medium (DMEM) supplemented with 10% fetal bovine serum (FBS).

Immunoblotting & Immunofluorescence staining, in vitro AMPylation assays

Samples were treated, visualized and analyzed exactly as described in (18). For analysis of nuclear Hsf-1 speaks formation and Hsp70-GFP localization, at least 10 randomly chosen frames from 3 independent samples were chosen and assessed by eye. Supplementary table 2 lists all antibodies used in this study. In vitro AMPylation assays were performed and analyzed as described (18).

Plasmid construction

Primers used for plasmid constructions are listed in supplementary table 1. Plasmids were routinely cloned using Gibson cloning (37).

Yeast ^{35}S-pulse labeling experiment

Yeast cells were grown in SR-CSM overnight at 25 °C. The next morning, cells were diluted to OD_{600} = 0.2 in SR-CSM without Cys/Met and incubated at 25 °C for 3 hours. All cultures were then supplemented with EasyTag Express ^{35}S Protein Labeling Mix (Perkin Elmer) and 2% Galactose to allow and induce transgene expression. Samples were collected at indicated time points post induction. For CPM analysis (to quantify total ^{35}S-Cys/Lys incorporation as shown in Fig. 2D), 200 µl OD-normalized culture was mixed with 200 µl 10% trichloroacetic acid (TCA) on ice and boiled for 15 minutes. 20 µl of each sample were transferred to a 1 cm^2 filter paper, air-dried, washed twice in individual containments with 10 ml 5% TCA, rinsed once with Acetone and air-dried over night. The next morning, filters were transferred into scintillation counter vials containing 5 ml Opti-Flour (Perkin Elmer) and analyzed. Samples were collected at indicated timepoints at least in duplicate. For autoradiographical visualization (to qualitatively assess changes in protein expression profiles as shown in Fig. S2E), 1 ml from the same culture was centrifuged and resulting pellets were resuspended in 30 µl PBS, boiled for 15 minutes, supplemented with 6x SDS-Sample buffer and boiled again for 20 minutes. Samples were then CPM-count-normalized prior to loading as described above.

Hela ^{35}S-pulse labeling experiment

Cells were grown in 6 well plates, transfected with Lipofectamine2000 (Life Technologies) according to manufacturer's instructions and incubated for 24 hours. Cells were starved in cysteine/methionine-free medium for 3 hours, supplemented with EasyTag Express ^{35}S Protein

Labeling Mix (Perkin Elmer) for 15 min and collected on ice. Total count normalization was done by scintillation counting as described above.

HSE-reporter assays, cell viability assays and FACS analysis

HSE-reporter cells were kindly provided by Susan Lindquist and assay was performed as described (20). For cell viability analysis, treated cells grown in 6 well plates were trypsinized and stained with LIVE/DEAD Fixable Violet Dead Cell Stain according to manufacturer's instructions (Life technologies).

Data acquisition was performed on a BD LSR II (BD Biosciences) using CellQuest Pro (BD Biosciences) software. Data were analyzed with FlowJo (Tree Star Inc.).

RNAseq

For yeast RNA-seq, 5 ml of cells were grown to OD_{600}=0.5 at 30 ºC and either left untreated, heat shocked at 39 ºC for 30 minutes or FIC-1(E274G) was induced with 500 nM estradiol for 2 hours. Cells were spun and pellets were snap frozen in liquid N_2 and stored at -80 ˚C. Pellets were thawed on ice, and total RNA was purified via phenol/chloroform separation using phase lock tubes (5 prime) followed by ethanol precipitation as described (35). For HeLa cells over-expressing mutants of HYPE, 10^7 cells were pelleted and stored at -80 ºC. Total RNA was extracted using a RNeasy kit (Qiagen). Total RNA samples were submitted to the Whitehead Genome Technology Core where polyA + RNA was purified, fragmented and sequencing libraries were prepared with barcoding. Samples were multiplexed in a single lane of an Illumina Hi-Seq 2500 and deep sequencing was performed. Reads were assigned by the barcode to the appropriate sample.

Data was processed using a local version of the Galaxy suite of next-generation sequencing tools. Reads were groomed and aligned to the SacCer3 *S. cerevisiae* reference genome or the Hg19 reference human genome using Tophat, transcripts were assembled and quantified using Cufflinks and fold changes were computed using Cuffdiff (38).

Gene ontology analysis was performed using Gorilla (39) and redundant GO terms were removed with REVIGO using a similarity threshold of 0.5 (40).

Protein purification

Purification of $HYPE_{aa187\text{-}437}$, $HYPE_{aa187\text{-}437}$ (E234G), $HYPE_{aa187\text{-}437}$ (H363A), FIC-$1_{aa258\text{-}508}$, FIC-$1_{aa258\text{-}508}$ (E274G), FIC-$1_{aa258\text{-}508}$ (H404A), FIC-$1_{aa134\text{-}508}$ (E274G), Hsp-1 and Hsp-3 has been described previously (19); Hsp40, Hsp70 and DAF-21 were purified accordingly. Human Hsp90 was purchased from Sigma.

VHH-HYPE interaction tests

Approximately 100 µg of recombinant $HYPE_{aa187-437,}$ or $FIC\text{-}1_{aa258-508}$ was incubated with 100 µg VHH-TAMRA at 4 °C for 1 hours and analyzed on a Superdex S75 10/300 GL size exclusion column. Absorbance at 280 nm (proteins) as well as at 545 nm (TAMRA) was recorded.

Mini-genome assay and influenza infection

293T cell were transfected with pCAGGS plasmids encoding for the viral NP, PB2, PB1 and PA proteins and pPolI-EGFP to provide an influenza model genome encoding for EGFP. HYPE variants or single domain antibodies (VHHs) as positive and negative control were co-expressed from pCDNA and pCAGGS plasmids, respectively. EGFP levels were measured 24 hours post transfection by flow cytometry.

For influenza A infection assays we transfected 293T cells with plasmids encoding for Hype variants or VHHs. 24 hours post transfection we infected the cells with influenza A/WSN/33 at an MOI of 5 for 5 hours. Cells were then trypsinized, fixed in 4 % PFA, permeabilized with 0.1 % saponin and stained with an influenza nucleoprotein specific VHH (αNPVHH1) (41) covalently coupled

Acknowledgments

We are grateful to the members of the Ploegh and Pincus labs for helpful comments and discussions. The Whitehead genome core facility is acknowledged for processing RNAseq and genomic DNA samples. We thank Justin Reemer for technical assistance and the Whitehead FACS facility for support with the reporter assays. George Bell and the Whitehead bioinformatics group are acknowledged for their help with GO analysis and Eric Spooner and the Whitehead Mass Spec facility for their help with MS-based target site mapping. M.C.T. is a recipient of an Advanced Postdoc. Mobility fellowship from the Swiss National Science Foundation (SNSF). This work was supported by an NIH Early Independence Award (DP5 OD017941-01 to D.P.), and a Cancer Research Fellowship from the Alexander and Margaret Stewart Trust (D.P.).

References

1. **Balch WE, Morimoto RI, Dillin A, & Kelly JW (2008) Adapting proteostasis for disease intervention.** *Science* 319(5865):916-919.

2. **Aguzzi A & O'Connor T (2010) Protein aggregation diseases: pathogenicity and therapeutic perspectives.** *Nat Rev Drug Discov* 9(3):237-248.

3. **Taylor RC, Berendzen KM, & Dillin A (2014) Systemic stress signalling: understanding the cell non-autonomous control of proteostasis.** *Nat Rev Mol Cell Biol* 15(3):211-217.

4. **Ron D & Walter P (2007) Signal integration in the endoplasmic reticulum unfolded protein response.** *Nat Rev Mol Cell Biol* 8(7):519-529.

5. **Akerfelt M, Morimoto RI, & Sistonen L (2010) Heat shock factors: integrators of cell stress, development and lifespan.** *Nat Rev Mol Cell Biol* 11(8):545-555.

6. **Kim YE, Hipp MS, Bracher A, Hayer-Hartl M, & Hartl FU (2013) Molecular chaperone functions in protein folding and proteostasis.** *Annu Rev Biochem* 82:323-355.

7. **Voellmy R & Boellmann F (2007) Chaperone regulation of the heat shock protein response.** *Adv Exp Med Biol* 594:89-99.

8. **Gardner BM, Pincus D, Gotthardt K, Gallagher CM, & Walter P (2013) Endoplasmic reticulum stress sensing in the unfolded protein response.** *Cold Spring Harb Perspect Biol* 5(3):a013169.

9. **Preissler S*, et al.* (2015) AMPylation matches BiP activity to client protein load in the endoplasmic reticulum.** *Elife* 4.

10. **Sanyal A*, et al.* (2015) A Novel Link Between Fic (Filamentation induced by cAMP)-mediated Adenylylation/AMPylation and the Unfolded Protein Response.** *J Biol Chem*.

11. **Ham H*, et al.* (2014) Unfolded protein response-regulated dFic reversibly AMPylates BiP during endoplasmic reticulum homeostasis.** *J Biol Chem*.

12. **Woolery AR, Luong P, Broberg CA, & Orth K (2010) AMPylation: Something Old is New Again.** *Front Microbiol* 1:113.

13. **Itzen A, Blankenfeldt W, & Goody RS (2011) Adenylylation: renaissance of a forgotten post-translational modification.** *Trends Biochem Sci* 36(4):221-228.

14. **Engel P*, et al.* (2012) Adenylylation control by intra- or intermolecular active-site obstruction in Fic proteins.** *Nature* 482(7383):107-110.

15. **Harms A*, et al.* (2015) Adenylylation of Gyrase and Topo IV by FicT Toxins Disrupts Bacterial DNA Topology.** *Cell Rep*.

16. **Yarbrough ML*, et al.* (2009) AMPylation of Rho GTPases by Vibrio VopS disrupts effector binding and downstream signaling.** *Science* 323(5911):269-272.

17. **Mattoo S*, et al.* (2011) Comparative analysis of Histophilus somni immunoglobulin-binding protein A (IbpA) with other fic domain-containing enzymes reveals differences in substrate and nucleotide specificities.** *J Biol Chem* 286(37):32834-32842.

18. **Truttmann MC*, et al.* (2015) HypE-specific Nanobodies as Tools to modulate HypE-mediated Target AMPylation.** *J Biol Chem*.

19. **Truttmann M.C. (2016) The Caenorhabditis elegans protein FIC-1 is an AMPylase that affects susceptibility to Pseudomonas aeruginosa infections** *PLoS Genet*.

20. **Santagata S, *et al.* (2013) Tight coordination of protein translation and HSF1 activation supports the anabolic malignant state.** *Science* 341(6143):1238303.

21. **Biamonti G & Vourc'h C (2010) Nuclear stress bodies.** *Cold Spring Harb Perspect Biol* 2(6):a000695.

22. **Gupta R, *et al.* (2011) Firefly luciferase mutants as sensors of proteome stress.** *Nat Methods* 8(10):879-884.

23. **Truttmann MC, *et al.* (2016) The Caenorhabditis elegans Protein FIC-1 Is an AMPylase That Covalently Modifies Heat-Shock 70 Family Proteins, Translation Elongation Factors and Histones.** *PLoS Genet* 12(5):e1006023.

24. **Cyr DM (1995) Cooperation of the molecular chaperone Ydj1 with specific Hsp70 homologs to suppress protein aggregation.** *FEBS Lett* 359(2-3):129-132.

25. **Zeng XC, *et al.* (2004) Hsp70 dynamics in vivo: effect of heat shock and protein aggregation.** *J Cell Sci* 117(Pt 21):4991-5000.

26. **Manzoor R, *et al.* (2014) Heat shock protein 70 modulates influenza A virus polymerase activity.** *J Biol Chem* 289(11):7599-7614.

27. **Ozawa M, *et al.* (2013) A cell-based screening system for influenza A viral RNA transcription/replication inhibitors.** *Sci Rep* 3:1106.

28. **Schmidt FI, *et al.* (2016) Phenotypic lentivirus screens to identify functional single domain antibodies.** *Nat Microbiol* 1(8):16080.

29. **Goloudina AR, Demidov ON, & Garrido C (2012) Inhibition of HSP70: a challenging anti-cancer strategy.** *Cancer Lett* 325(2):117-124.

30. **Taguwa S, *et al.* (2015) Defining Hsp70 Subnetworks in Dengue Virus Replication Reveals Key Vulnerability in Flavivirus Infection.** *Cell* 163(5):1108-1123.

31. **Jinwal UK, *et al.* (2010) Hsp70 ATPase Modulators as Therapeutics for Alzheimer's and other Neurodegenerative Diseases.** *Mol Cell Pharmacol* 2(2):43-46.

32. **Afanasyeva EA, *et al.* (2007) Drug-induced Myc-mediated apoptosis of cancer cells is inhibited by stress protein Hsp70.** *Int J Cancer* 121(12):2615-2621.

33. **Broncel M, Serwa RA, Bunney TD, Katan M, & Tate EW (2015) Global profiling of HYPE mediated AMPylation through a chemical proteomic approach.** *Mol Cell Proteomics*.

34. **Damon JR, Pincus D, & Ploegh HL (2015) tRNA thiolation links translation to stress responses in Saccharomyces cerevisiae.** *Mol Biol Cell* 26(2):270-282.

35. **Pincus D, Aranda-Díaz A, Zuleta IA, Walter P, & El-Samad H (2014) Delayed Ras/PKA signaling augments the unfolded protein response.** *Proc Natl Acad Sci U S A* 111(41):14800-14805.

36. **Solís EJ, *et al.* (2016) Defining the Essential Function of Yeast Hsf1 Reveals a Compact Transcriptional Program for Maintaining Eukaryotic Proteostasis.** *Mol Cell* 63(1):60-71.

37. **Gibson DG, *et al.* (2009) Enzymatic assembly of DNA molecules up to several hundred kilobases.** *Nat Methods* 6(5):343-345.

38. **Trapnell C, *et al.* (2013) Differential analysis of gene regulation at transcript resolution with RNA-seq.** *Nat Biotechnol* 31(1):46-53.

39. **Eden E, Navon R, Steinfeld I, Lipson D, & Yakhini Z (2009) GOrilla: a tool for discovery and visualization of enriched GO terms in ranked gene lists.** *BMC Bioinformatics* 10:48.

40. **Supek F, Bošnjak M, Škunca N, & Šmuc T (2011) REVIGO summarizes and visualizes long lists of gene ontology terms.** *PLoS One* 6(7):e21800.

41. **Ashour J, *et al.* (2015) Intracellular expression of camelid single-domain antibodies specific for influenza virus nucleoprotein uncovers distinct features of its nuclear localization.** *J Virol* 89(5):2792-2800.

Figure legends

Figure 1: Over-expression of *C. elegans* FIC-1 (E274G) in *S. cerevisiae* is lethal.

(A) Time courses of *S. cerevisiae* inducibly expressing genomically integrated FIC-1 genes grown in repressive (glu) or inductive (GAL) conditions. (B) growth of *S. cerevisiae* inducibly expressing genomically integrated FIC-1 genes in repressive (glu) condition following induction for 3 hours in (GAL) medium. P-values calculated using repeated measure ANOVA tests; ns = not significant ($p > 0.05$). Data shown represents average of 6 independent experiments.

Figure 2: Protein AMPylation induces a strong heat shock response in *S. cerevisiae*

(A) Induction of P_{4xHSE}YFP heat shock reporter in the presence of distinct Fic proteins. Results are normalized to empty vector controls. (B) Comparison of global changes in transcript levels induced by over-expression of FIC-1 (E274G) or heat shock. Heat shock protein genes (HSPs) are highlighted in blue, ribosomal protein genes (RPGs) are colored in red. (C) time-resolved analysis of gene transcription during heat shock (solid lines) or in the presence of FIC-1 (E274G) (dashed lines). Heat shock genes (HSGs) are highlighted in blue, ribosomal genes are colored in red. (D) protein translation in the presence of FIC-1 proteins as monitored by ^{35}S-Cys / ^{35}S-Met incorporation. Counts are OD-normalized to account for different growth behaviors of individual strains. FIC-1 (E274G) expression was induced at timepoint -2 hours when starting cell starvation. P-values calculated using repeated measure ANOVA tests (D) or student's t-test (A); ns = not significant ($p > 0.05$).

Figure 3: HYPE (E234G) triggers a heat shock response in human cells.

(A) Genome wide mRNA expression levels (FPKM) as measured by RNA seq in untransfected HeLa cells and in the presence of HYPE (E234G). Red dots are example HSF1 target genes; blue dots are example UPR target genes. (B) Gene ontology (GO) analysis of mRNA enrichments upon expression of HYPE (E234G). (C) HSF1 target gene mRNA expression levels in untransfected HeLa cells and in the presence of HYPE (E234G). (D) Quantification of HYPE (E234G)-induced nuclear spec formation. Bars represent means of at least 3 independent experiments. P-values calculated using student's t-test (A); ns = not significant ($p > 0.05$).

Figure 4: AMPylation induces cytosolic protein aggregation in *S. cerevisiae* and human cells and AMPylation enzymes partially localize to the cytosol

(A) Fluorescence microscopy of yeast cells expressing Hsp104-YFP to mark protein aggregates in the presence and absence of expression of FIC-1, FIC-1 (E274G) or FIC-1 (H404A) in *S. cerevisiae.* Quantification of the number of Hsp104-YFP aggregates/cell in the absence or presence of FIC-1 (E274G) is shown below. At least 50 cells were imaged in each condition.

(B) Fluorescence microscopy images of subcellular localization of FIC-1 (E274G)-YFP, SSa2-mKate2 and Ire-1-mCherry. Upper panel shows cells co-expressing FIC-1 (E274G)-YFP and Ire-1-mCherry, lower panel displays cells co-expressing FIC-1 (E274G)-YFP and SSa2-mKate2. (C) HYPE (E234G) induces protein aggregation in HeLa cells via quantification of luciferase activity of FlucDMGFP reporter. Q74-GFP is a polyglutamine protein that causes protein aggregation. P-values calculated using student's t-test (A); ns = not significant ($p > 0.05$).

Figure 5: FIC-1 (E274G) and HYPE (E234G) AMPylate Hsp40, Hsp70, Hsp90 and Hsf-1 *in vitro*.

(A-C) *in vitro* AMPylation reaction using □^{33}P-ATP as nucleotide substrate to monitor AMPylation of Hsp70, Hsp40 (A) and HSP90 (B) by HYPE (E234G) as well as *S. cerevisiae* Hsp70 (SSA2) by FIC-1 E274G and HYPE E234G (C). Solid black arrows depict auto-AMPylated enzymes (Hype (E234G), Fic-1 (E274G)); cyan arrows depict AMPylated target proteins.

Figure 6: FIC-1 (E274G) AMPylates cytosolic Hsp70 *in vivo* and Hsp70 suppresses FIC-1 (E274G)-mediated toxicity.

(A) Increase in *in vivo* Hsp70 AMPylation following expression of FIC-1 (E274G) in S. *cerevisiae*. Samples were collected at indicated time intervals, OD-normalized and probed with indicated antibodies. (B) Yeast growth test upon co-expression of FIC-1 (E274G) and Ydj2, Ssa2 and Hsc82. (C) Quantification of protein aggregation in the presence of FIC-1 (E274G) or FIC-1 (E274G) together with Ssa2.

Figure 7: AMPylation of Hsp70 alters its ATPase activity and cellular dynamics.

(A) Quantification of GFP-Hsp70 nuclear localization. Averages from at least three replicas with more than 100 cells/sample analyzed in each experiments are shown. (B-C) Hyper-AMPylation inhibits influenza virus polymerase activity and replication. Influenza Mini-genome assay to monitor vRNP polymerase activity in host cell nucleus (B) and influenza infection assay (C). Data normalized to non-relevant VHH-7-expressing cells. Average of three independent replicas including standard deviation shown here. (D) Schematic model depicting how AMPylation might trigger the activation of a heat shock response in eukaryotic cells. P-values calculated using student's t-test (A); ns = not significant ($p > 0.05$).

Figure 3

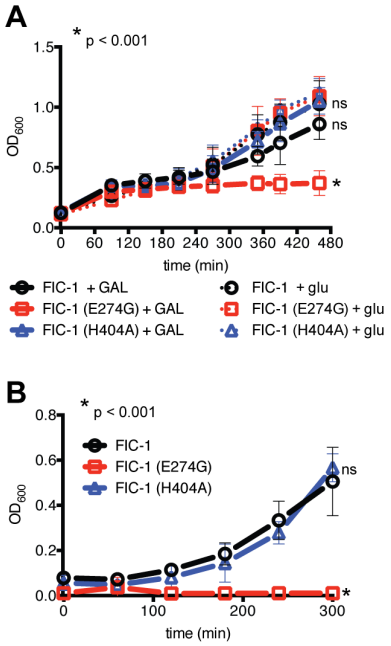

Figure 4

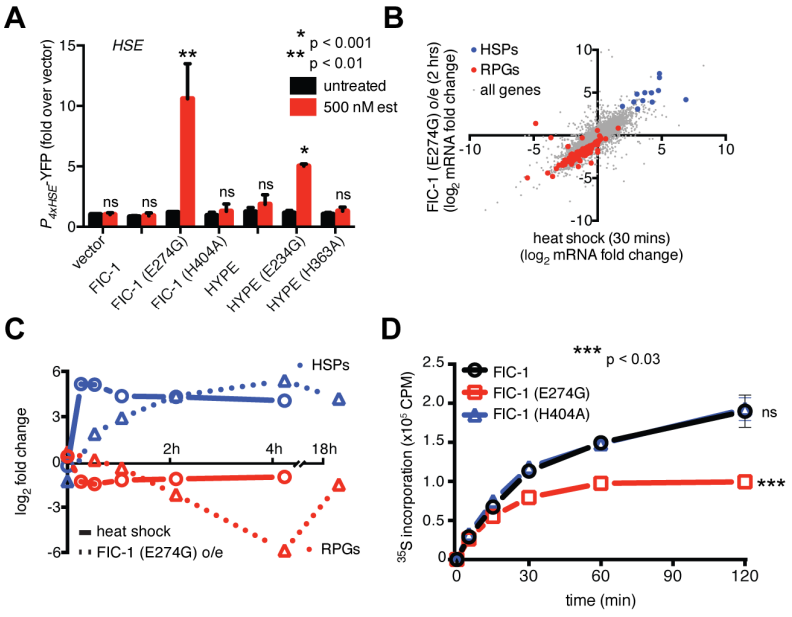

Figure 5

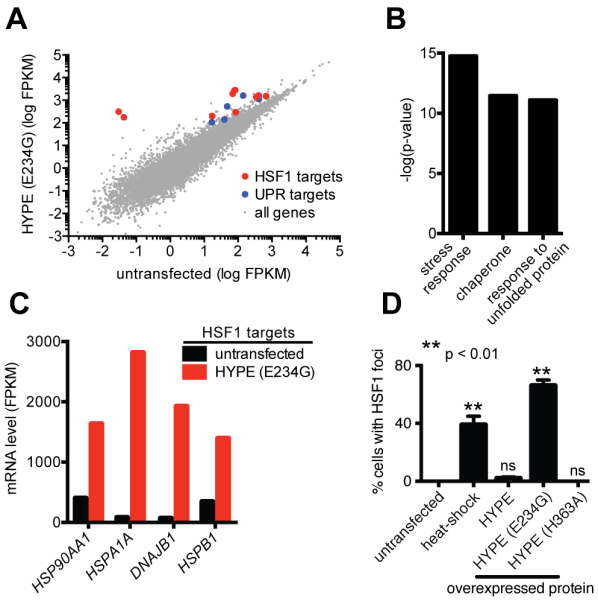

Figure 6

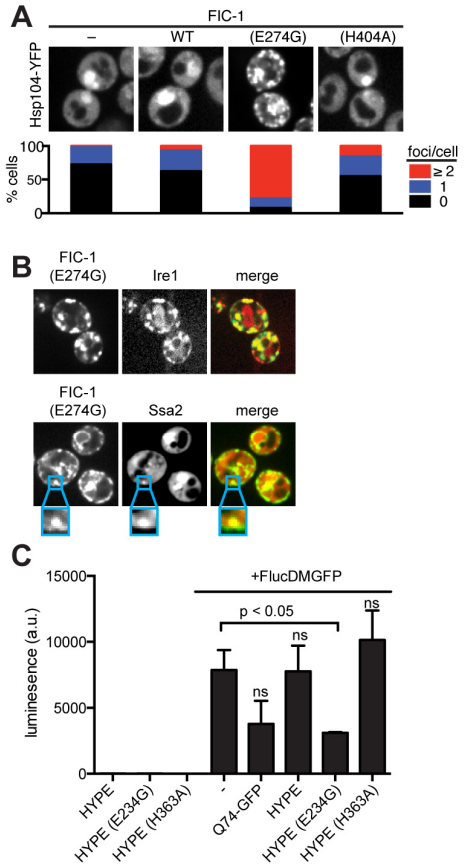

Figure 7

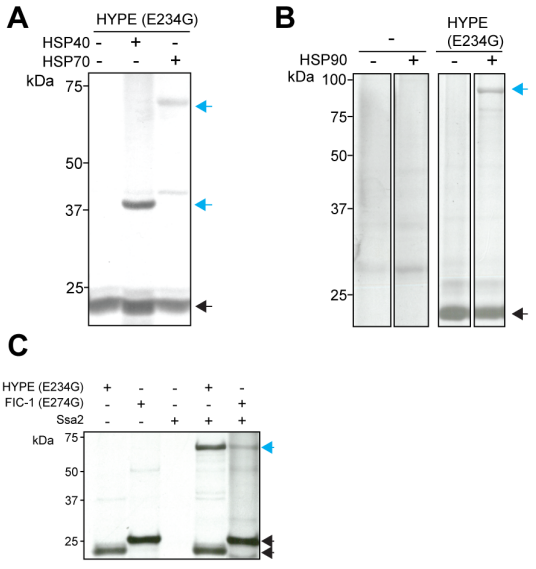

Figure 8

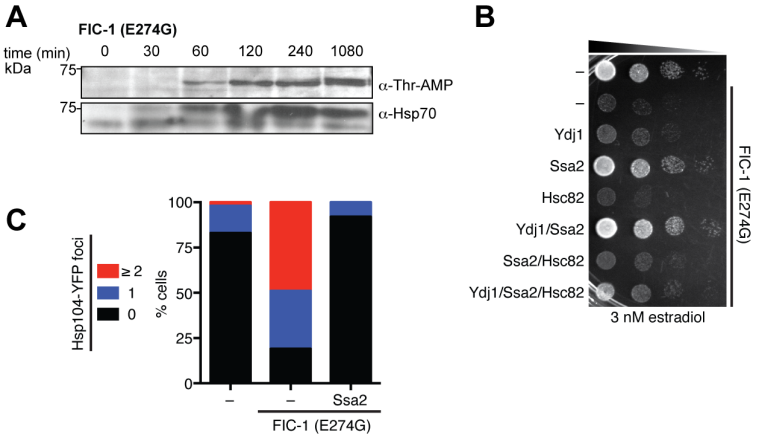

Figure 9

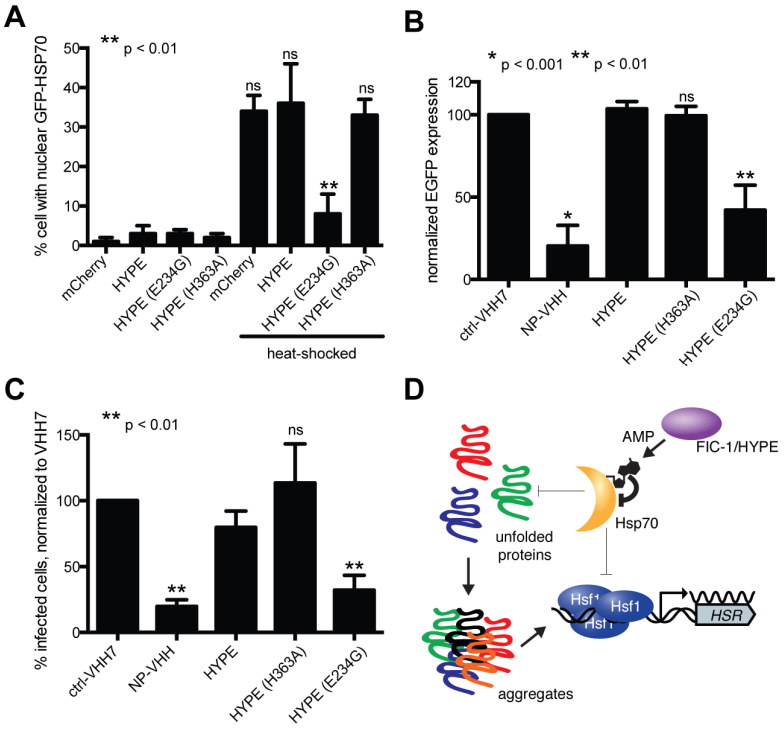
A
** p < 0.01
% cell with nuclear GFP-HSP70
mCherry
HYPE
HYPE (E234G)
HYPE (H363A)
mCherry
HYPE
HYPE (E234G)
HYPE (H363A)
heat-shocked
B
* p < 0.001 ** p < 0.01
normalized EGFP expression
ctrl-VHH7
NP-VHH
HYPE
HYPE (H363A)
HYPE (E234G)
C
** p < 0.01
% infected cells, normalized to VHH7
ctrl-VHH7
NP-VHH
HYPE
HYPE (H363A)
HYPE (E234G)
D
AMP
FIC-1/HYPE
Hsp70
unfolded proteins
Hsf1
HSR
aggregates

Appendix

Nederlandstalige Samenvatting

Virussen beschikken over het algemeen over een compact genoom hetwelk de informatie voor een beperkt aantal genprodukten bevat. Het succes van virussen is gebaseerd op een complex netwerk van essentiele interacties met eiwitten van de gastheer. Ten einde deze interacties nader te identificeren en nieuwe zwakke plekken te vinden om in te grijpen in de virale levenscyclus heb ik gebruik gemaakt van de intracellulaire expressie van variabele domeinen afkomstig van de zware keten antistoffen ofwel VHHs ("variable region of heavy chain only"), opgewekt in alpacas. De door mij ontwikkelde VHHs hebben als doelwit de intracellulaire eiwitten van vesicular stomatitis virus (VSV) en influenza A (IAV). In tegenstelling tot conventionele antistoffen of daarvan afgeleide fragmenten herkennen de "heavy chain only" antistoffen van de *camelidae* hun doelwit uitsluitend via het variabele domein van de zware keten. De daarvan afgeleide fragmenten, met name het ~15 kDa variabele domein, binden met hoge affiniteit en specificiteit, zijn goed water-oplosbaar en voor het merendeel niet afhankelijk van disulfide bruggen. Dit maakt het mogelijk VHHs in het cytosol van zoogdiercellen tot expressie te brengen.

Hoofdstuk 1 is de introductie van dit proefschrift. Ik geef een overzicht van antivirale VHHs en hun toepassingen in de diagnostiek, in de kliniek en in fundamenteel onderzoek. Ik leg de nadruk op het gebuik van intracellulair tot expressie gebrachte VHHs die virus infecties remmen. In hoofdstuk 2 beschrijf ik het opwekken van VHHs die IAV nucleoprotein (NP) herkennen, alsmede hun karakterisatie. Gebruik makend van een testsysteem gebaseerd op competitie in een immunoprecipitatie experiment kon ik aantonen dat de 6 door mij geidentificeerde VHHs tenminste 3 verschillende NP epitopen herkennen. Wanneer deze VHHs intracellulair tot expressie worden gebracht beschermen ze de gastheercel tegen infectie met IAV, omdat ze de import van de virale ribonucleoproteine partikels (vRNPs) naar de kern verhinderen. Deze import van vRNPs naar de kern is essentieel voor virale transcriptie en replicatie. Naast de remming van vRNP import is er tenminste één VHH (αNP-VHH1) die ook transcriptie en replicatie van IAV in de kern blokkeert, een conclusie die gebaseerd is op transfectie van een polymerase-afhankelijk reconstitutie test systeem. Om beter inzicht te verkrijgen in het onderliggende mechanisme heb ik de binding van αNP-VHH1aan NP onderzocht met behulp van Röntgendiffractie (hoofdstuk 3). De door mij geidentificeerde plaats van binding vertoont overlap met die van het antivirale eiwit Mx. Een superpositie van

de bindingsplaats met de gerapporteerde structuurmodellen van vRNPs laat zien dat binding van αNP-VHH1interfereert met de herkenning van een nucleair localisatie signaal (NLS) op een naburige NP subeenheid . Naar alle waarschijnlijkheid blokkeert dit de interactie van vRNPs met eiwitten van de α-importin familie en verhindert zo de import van vRNPs naar de kern. Mijn bevindingen verschaffen dus ook een mogelijke verklaring voor het mechanisme van werking van de cytosolaire Mx eiwitten. Nadat vRNPs in de kern zijn aangekomen wordt alleen de productie van langere transcripten geremd door αNP-VHH1. Dit mechanisme vertoont wederom een frappante parallel met de inhibitoire rol van Mx eiwitten in de kern. Hoe precies de occlusie van de bindingsplaats op NP door αNP-VHH1 dit phenotype veroorzaakt is nog niet geheel duidelijk, maar wellicht verhindert αNP-VHH1 conformationele veranderingen die essentieel zijn voor transcriptie.

In Hoofdstuk 4 beschrijf ik een nieuwe screeningsaanpak voor de identificatie van antivirale VHHs. Deze method is gebaseerd op de phenotypes opgewekt door de intracellualire expressie van VHHs, in mijn geval: bescherming tegen het lethale/lytische effect van een virus infectie in weefselkweek. Met behulp van lentivirale transductie heb ik een diverse collectie van VHHs geintroduceerd in de A549 cel lijn, zodanig dat gemiddeld een enkele cel slechts één VHH tot expressie brengt. Deze collectie A549 transductanten werd vervolgens blootgesteld aan een lytische dosis van hetzij IAV, hetzij VSV. De overlevende cellen werden vervolgens geoogst en geanalyseerd. Dit resulteerde in de isolatie van 15 VHHs die beschermden tegen IAV, en 4 die beschermden tegen VSV. Alle geidentificeerde VHHs herkennen ofwel NP in het geval van IAV ofwel N in het geval van VSV. Dit laat ten minste zien dat de virale nucleiproteines een geschikt doelwit kunnen zijn voor antivirale therapie. De anti-IAV NP VHHs waren tot op zekere hoogte verwant aan de al geidentificeerde VHHs (Hoofdstuk 2), maar leverden verschillende VHHs op die een epitoop herkenden dat geen overlap vertoonde met wat ik rapporteerde in Hoofdstuk 2. De VSV-specifieke VHHs herkenden allen een uniek epitoop. In hoofdstuk 5 beschrijf ik de kristalstructuur van twee van de vier VHHs in complex met VSV N, en voor een derde VHH identificeer ik het herkende epitoop met behulp van “escape” mutanten. Voor VHH 1307 kon ik vaststellen dat de bindingsplaats directe overlap vertoont met de bindingsplaats van co-factor P, een enzymatisch inactief eiwit dat evenwel essentieel is voor de activiteit van het L eiwit, het VSV RNA polymerase. Dit verklaart uiteraard waarom VHH 1307 een anti-viraal effect heeft. Een tweede VHH, VHH 1004 remt waarschijnlijk wel VSV replicatie maar niet VSV transcriptie; het bindt aan een functioneel slecht gekarakteriseerd deel van het N eiwit, het N-terminale segment. Voor VHHH 1001 kon ik de bindingsplaats identificeren met behulp van escape mutanten; de mutaties waren gelocaliseerd in een nucleocapsid-specifiek contact gelocaliseerd in het C-terminale deel van het N eiwit. Ik

veronderstel dat VHH 1001 virale transcriptie en replicatie remt door stabilisatie van de capside structuur, en zo het RNA-N eiwit complex ontoegankelijk maakt voor transciptie.

Een beter begrip van de levenscyclus van virussen, ongeacht hun herkomst, heeft baat bij het ontwikkelen van nieuwe technieken. Methodes die het mogelijk maken de localisatie en expressie niveaus van virale eiwitten te volgen en te beinvloeden, hun interacties met andere eiwitten in kaart te brengen en te verstoren blijven hoog op het verlanglijstje staan. Mijn werk laat zien dat VHHs hierbij een nuttig hulpmiddel kunnen zijn, en het mogelijk maken zowel structurele als functionele informatie te verkrijgen. Ik concludeer dan ook dat VHHs een interessante toevoeging zijn aan het instrumentarium van de viroloog.

List of Publications

Hanke L, Morin B, Knockenhauer KE, Schmidt FI, Whelan SPJ, Schwartz TU, Ploegh HL, Single-Domain Antibody Fragments that Target the Vesicular Stomatitis Nucleoprotein Inhibit Virus Replication (Chapter 5). Accepted for publication in *EMBO reports.*

Truttmann MC, Zheng X, **Hanke L**, Damon JR, Grootveld M, Krakowiak J, Pincus D, Ploegh HL 2016 Unrestrained AMPylation targets cytosolic chaperones and activates the heat shock response. *Proceedings of the National Academy of Sciences of the United States of America* (PNAS) 114: 201619234. (Addendum 1)

Hanke L, Knockenhauer KE, Brewer R, van Diest E, Schmidt FI, Schwartz TU, Ploegh HL. 2016. The Antiviral Mechanism of an Influenza A Virus Nucleoprotein-Specific Single-Domain Antibody Fragment. *MBio* **7**: 1–11. (Chapter 3)

Duarte JN, Cragnolini JJ, Swee LK, Bilate AM, Bader J, Ingram JR, Rashidfarrokhi A, Fang T, Schiepers A, **Hanke L**, Ploegh HL. 2016. Generation of Immunity against Pathogens via Single-Domain Antibody-Antigen Constructs. The *Journal of Immunology* 197: 4838–4847.

Schmidt FI, **Hanke L**, Morin B, Brewer R, Brusic V, Whelan SPJ, Ploegh HL. 2016. Phenotypic Lentivirus Screens to Identify Functional Single-Domain Antibodies. *Nature Microbiology* 1**:**16080. (Chapter 4)

Ashour J, Schmidt FI, **Hanke L**, Cragnolini J, Cavallari M, Altenburg A, Brewer R, Ingram J, Shoemaker C, Ploegh HL. 2015. Intracellular Expression of Camelid Single-Domain Antibodies Specific for Influenza Virus Nucleoprotein Uncovers Distinct Features of Its Nuclear Localization. *Journal of Virology* 89:2792–2800. (Chapter 2)

Acknowledgements

Science is a group effort. Many individuals have contributed to the findings described in this thesis and have helped to shape my scientific expertise. I am very thankful to all of them.

I am especially thankful to Hidde Ploegh for offering me research opportunities in his laboratory and for guidance during my time at the Whitehead Institute. His thirst for knowledge and advancing our understanding of biological processes is truly inspiring.

I thank Thomas Schwartz at MIT for his guidance in protein biochemistry and X-ray crystallography, and for helping me to solve the protein structures presented in this thesis.

I am thankful to the committee members for reading my thesis at record speed, and especially to Emmanuel Wiertz for his help with the thesis and for putting together the thesis defense.

I am grateful to my students Rebeccah Camille Brewer and Eline van Diest for all their hard work and all the fun times in the laboratory.

I would like to thank Jessica Ingram, Florian Schmidt, Matthias Truttmann Joseph Ashour and Andrew Woodham. With their experience and kindness, they have helped me tremendously during my time at the Whitehead Institute.

I thank Kevin Knockenhauer for an outstanding collaboration and for teaching me the tricks of crystal growth and structural biology.

I would like to thank Sean Whelan and Benji Morin at Harvard Medical School for excellent collaboration on the VSV project.

Curriculum Vitae

Leo Paul Hartmut Hanke was born on October 16th, 1985 in Göttingen, Germany. He attended the Jakob-Grimm Schule gymnasium in Rotenburg an der Fulda, Germany, where he did his Abitur in 2005. Afterwards, Leo traveled the world for a year and visited Asia and New Zealand. During his travels, he worked on construction sites, on farms and as a sales person for Persian rugs. In 2007, he started his undergraduate studies in biological sciences at the University of Konstanz, Konstanz, Germany. In 2010, he conducted his bachelor's thesis research in the group of Jan Hoeijmakers and Gijsbertus van der Horst at the Erasmus University Medical Center, Rotterdam, The Netherlands, where he studied the DNA repair enzyme DNA photolyase. For his master's degree, he returned to the University of Konstanz but also took the opportunity to learn about tropical disease at a summer course of the Department of Tropical Medicine at the Mahidol University in Bangkok, Thailand. For his master's thesis research, he joined Hidde Ploegh's group at the Whitehead Institute for Biomedical Research, Massachusetts Institute of Technology, Cambridge, MA, USA, where he used alpaca derived, single-domain antibodies to manipulate cellular signaling. After receiving his master's degree from the University of Konstanz in 2012, he returned to Hidde Ploegh's laboratory for his doctoral research, focusing on the manipulation of RNA viruses using single-domain antibodies. The defense of this doctoral thesis, entitled "Single-Domain Antibodies as Tools to Perturb and Study RNA Viruses", will take place on April 24th, 2017. In May he will start his postdoctoral research in the group of Gerald McInerney at Karolinska Institutet in Stockholm, Sweden.